Laura Ramaseder, BSc

Comparison of different sensor placement algorithms for model-based leak localization in a real world case study (Hart close to Graz)

MASTER'S THESIS

to achieve the university degree of

Diplom-Ingenieur

Master's degree programme: Civil Engineering, Environment and Transportation

submitted to

Graz University of Technology

Supervisor:

Assoc.Prof. Dipl.-Ing. Dr.techn. Daniela Fuchs-Hanusch

Institute of Urban Water Management and Landscape Water Engineering

Assisting adviser:

Dipl.-Ing. Stefan Krakow

Graz, October 2016

Contact:

Laura Ramaseder

laura.ramaseder@student.tugraz.at

EIDESSTATTLICHE ERKLÄRUNG

AFFIDAVIT

I declare that I have authored this thesis independently, that I have not used anything other than the declared sources/resources, and that I have explicitly indicated all material which has been quoted either literally or contextually from the sources used. The text document uploaded to TUGRAZonline is identical to the present master's thesis.

Ich erkläre an Eides statt, dass ich die vorliegende Arbeit selbstständig verfasst, andere als die angegebenen Quellen/Hilfsmittel nicht benutzt, und die den benutzten Quellen wörtlich und inhaltlich entnommenen Stellen als solche kenntlich gemacht habe. Das in TUGRAZonline hochgeladene Textdokument ist mit der vorliegenden Masterarbeit identisch.

_____	_____
Date	Signature

Acknowledgement

At this point I would like to thank all people who contributed a part to my thesis.

First I would like to thank my thesis supervisor Assoc.Prof. Dipl.-Ing. Dr.techn. Daniela Fuchs-Hanusch of the Institute of Urban Water Management and Landscape Water Engineering at Graz University of Technology for the guidance as well as her support on the way.

I would also like to acknowledge my assisting advisor Dipl.-Ing. Stefan Krakow who was always ready to listen to my questions and made helpful comments and remarks.

Additionally, I would like to thank Dipl.-Ing. Markus Günther and Dipl.-Ing. David Steffelbauer for sharing their knowledge on this topic with me and helping me with the literature research.

Every result in this thesis was also accomplished with the help and support of Lorenz Günther Kaufmann, Dipl.-Ing. David Steffelbauer and David Camhy. They supported this work with their programming skills. With their participation and input they made the leakage localization tool easy to use, so that the calculations could be performed.

Furthermore, I would also want to thank my sister Lisa Ramaseder and my friend Christoph Schwarz for spending their time to proofread this thesis and providing helpful suggestions for modification.

Finally I want to express my gratitude to my family, especially my mum, and my friends for their encouragements and support throughout my whole studies and my thesis. Without their support it would not have been able to complete my thesis that successfully.

Abstract

Leaks in water distribution networks cause a loss of drinking water and energy, and can impose a risk to public health due to contamination. Additionally, they lead to an economical loss in form of damage to the pipe network. Therefore, water system operators are motivated to implement regular leakage detection surveys. Early leak detection helps to save water, prevent water contamination and damage on the surrounding environment.

A reduction of water losses from water distribution systems (WDS) can be achieved through active leakage control (ALC). ALC aims to locate non-visible leaks and their efficient repair through qualified staff using adequate technical equipment. To support ALC model-based leak localization is recently in focus of research. One central point of this method is the optimal placement of sensors. In this thesis six different sensor placement methods were compared on basis of a real world case study in Hart, close to Graz/ Ragnitz.

Twelve sensors were placed in the water distribution system according to the ideal positions found by the six placement algorithms. The leaks were simulated by systematically opening selected hydrants. Model-based leakage localization was conducted with flow and pressure data from the sensors, a hydraulic model and a mathematical algorithm for solving the optimization problem of minimizing the discrepancy between the calculated and the measured pressures. The calculations were conducted with an uncalibrated hydraulic model and with calibrated models. The results were compared with the aim to derive differences in leak localization accuracy related to differently placed sensors. The results from the calculation consist of leak plots, leak-, distance- and outflow histograms. The leak plot shows the real leak and the location where the simulated leak was found.

The results of the calculations have shown that in some cases a minimal distance of 500 m to the real leak could be achieved but in other cases the simulated leak was found on the opposite side of the search area. At bigger leaks the search area could be narrowed down to smaller radiuses which makes later pinpointing easier.

No significant difference between the different sensor placement methods could be derived. The topology-based methods provide suboptimal results compared to the sensitivity-based algorithms. But also for the sensitivity-based algorithms the algorithm could not narrow down the area around the real leaks in all cases precisely. The calibration of the WDS in terms of changing roughness values only had a minor influence on the localization accuracy.

Keywords: Water distribution system, genetic algorithm, differential evolution, optimization, sensor placement, leakage localization

Kurzfassung

Leckagen in Trinkwasserverteilungssystemen verursachen einen Trinkwasser- und Energieverlust und stellen ein öffentliches Gesundheitsrisiko aufgrund von eindringenden Verschmutzungen dar. Zusätzlich führen sie zu einem finanziellen Verlust in Form von Schäden an Leitungen im Netz. Aus diesen Gründen sind Wasserversorger daran interessiert, regelmäßige Untersuchungen im Bereich der Leckagedetektion durchzuführen. Die Früherkennung von Leckagen hilft Trinkwasser zu sparen und verhindert eine Wasserkontamination und Schäden an der umliegenden Umgebung.

Eine Reduktion der Wasserverluste in Trinkwasserverteilungssystemen kann durch aktive Leckkontrolle (ALC) erreicht werden. ALC zielt darauf ab nicht sichtbare Schäden zu orten und deren rasche Reparatur durch gut geschultes und erfahrenes Personal zu veranlassen unter Verwendung spezieller technischer Ausrüstung. Um die ALC zu unterstützen, steht Modell-basierte Leckage Lokalisierung kürzlich im Fokus der Forschung. Einer der zentralen Punkte dabei ist die optimale Platzierung von Sensoren im System. Im Rahmen dieser Diplomarbeit wurden sechs verschiedene Sensorplatzierungsmethoden auf Basis einer Fallstudie in Hart bei Graz/ Ragnitz miteinander verglichen.

Zwölf Sensoren wurden entsprechend der durch die sechs Platzierungsmethoden idealen gefundenen Positionen im Wasserversorgungsnetz platziert. Die Leckagen wurden durch systematisches Aufdrehen ausgewählter Hydranten simuliert. Die Modell-basierte Leckage Lokalisierung wurde mit Druck- und Durchflussmessungen von den Sensoren, einem hydraulischen Modell und einem mathematischen Algorithmus durchgeführt, um ein Optimierungsproblem zu lösen, bei es darum geht, die Diskrepanz zwischen den berechneten und den gemessenen Drücken zu minimieren.

Die Berechnungen wurden mit einem unkalibrierten Modell und anschließend mit kalibrierten Modellen durchgeführt. Die Ergebnisse wurden mit dem Ziel Unterschiede in der Genauigkeit der Leckage Lokalisierung in Bezug auf unterschiedlich platzierte Sensoren abzuleiten, miteinander verglichen. Die Ergebnisse der Berechnungen bestehen aus Lageplänen, Leckage-, Distanz- und Durchflusshistogrammen. Die Lagepläne geben eine Übersicht über die reale und gefundene Leckage.

Die Ergebnisse der Berechnungen haben gezeigt, dass in manchen Fällen eine minimale Distanz von 500 m erreicht werden konnte, in anderen jedoch konnte gar keine Eingrenzung erzielt werden. Größere Leckagen konnten leichter eingrenzt werden als kleinere. Es konnte kein wesentlicher Unterschied zwischen den Ergebnissen der verschiedenen Sensorplatzierungsmethoden abgeleitet werden. Die Topologie-basierten Algorithmen erzielten jedoch im Vergleich zu den Sensitivitäts-basierten Methoden weniger gute Ergebnisse. Aber auch die Sensitivitäts-basierten Algorithmen konnten das Gebiet um die reale Leckage nicht in allen Fällen gut eingrenzen. Die Kalibrierung des Wasserversorgungsnetzes durch Änderung der Rauhigkeitswerte hatte nur geringen Einfluss auf die Genauigkeit der Ergebnisse.

Table of Contents

List of Abbreviations

AL	Acoustic logging
ALC	Active Leak Control
CARL	Current Annual Real Losses
DE	Differential evolution
DMA	District metered area
ELL	Economic Level of Leakage
GA	Genetic algorithm
GPR	Ground penetrating radar
ILI	Infrastructure Leakage Index
IWA	International Water Association
LNC	Leak noise correlator
MNF	Minimum Night Flow
NL	Noise logging
NRW	Non-revenue water
PM	Pressure management
SCADA	Supervisory control and data acquisition
TGT	Tracer gas technique
UARL	Unavoidable Annual Real Losses
WDS	Water distribution system

1 Introduction

Water distribution systems (WDS), especially the pipes, are exposed to several inadequately predictable influences which can cause damage on single parts of the network. Even in the best maintained distribution systems an absolute dense network is not possible due to technical and economic reasons. Therefore, leakages exist in every WDS. The resulting leakages of drinking water should be kept as small as possible. A leakage describes the loss of water which arises due to damages of pipes, joints, service reservoirs or tanks.

Water utilities and municipalities are conducting investigations and estimations of the water balance in water supply systems. Therefore, the International Water Association (IWA) Water Loss Task Force presented the standard international water balance structure and terminology which is widely used.

System Input Volume (corrected for known errors)	Authorised Consumption	Billed Authorised Consumption	Billed Metered Consumption (including water exported)	Revenue Water
			Billed Unmetered Consumption	
		Unbilled Authorised Consumption	Unbilled Metered Consumption	Non-Revenue Water (NRW)
			Unbilled Unmetered Consumption	
	Water Losses	Apparent Losses	Unauthorised Consumption	
			Customer Metering Inaccuracies	
		Real Losses	Leakage on Transmission and/or Distribution Mains	
			Leakage and Overflows at Utility's Storage Tanks	
			Leakage on Service Connections up to point of Customer metering	

Figure 1.1: IWA "best practice" water balance

Figure 1.1 provides an overview of the water usage in a water supply system. The water balance is based on the measurement of water produced, imported, exported, consumed and lost (Farley, 2003).

The amount of water which is applied to the WDS by the source (tank) and is billed to the customer represents the revenue water. Using the example of the water consumption of Austria (Figure 1.2) the revenue water accounts for 84% where 70% are consumed by private households and 14% are used by public facilities and enterprises. The non-revenue water (NRW) is the difference between the system input volume and the billed authorized consumption.

In the example of Austria 16% of the water consumption consists of NRW.
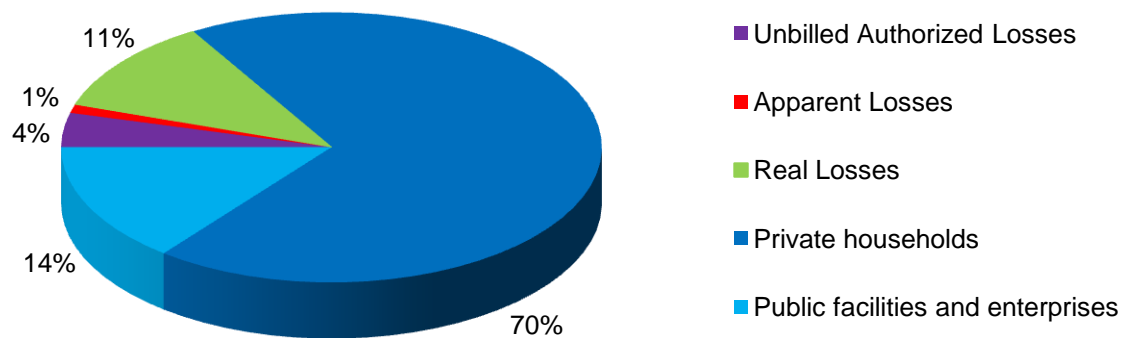
Figure 1.2: Water consumption of Austria (ÖVGW 2004 and 2007, BMLFUW 2012)

According to the standard international water balance structure and terminology of the IWA the NRW consists of three components: Unbilled authorized consumption, apparent losses, and real losses (physical losses) (Farley, et al., 2008). Unbilled authorized consumption includes water used for firefighting and street cleaning and for watering of public areas. Apparent losses are caused by customer metering inaccuracies, data handling errors, meter discrepancies, and water theft. Real losses are the annual volumes lost from bursts and all types of leaks at tanks, reservoirs, pipes, and overflows. (Farley, 2003). Apparent- and real losses form the amount of water which is supplied to the system by the source but does not reach the ultimate consumer. The water gets lost somewhere in the system through leaks that occur from damages in the pipework system.

The individual components of the real annual losses and the components of the night minimum flow can be calculated according to the Background and Burst Estimates (BABE) concept which was developed by Lambert (1993).
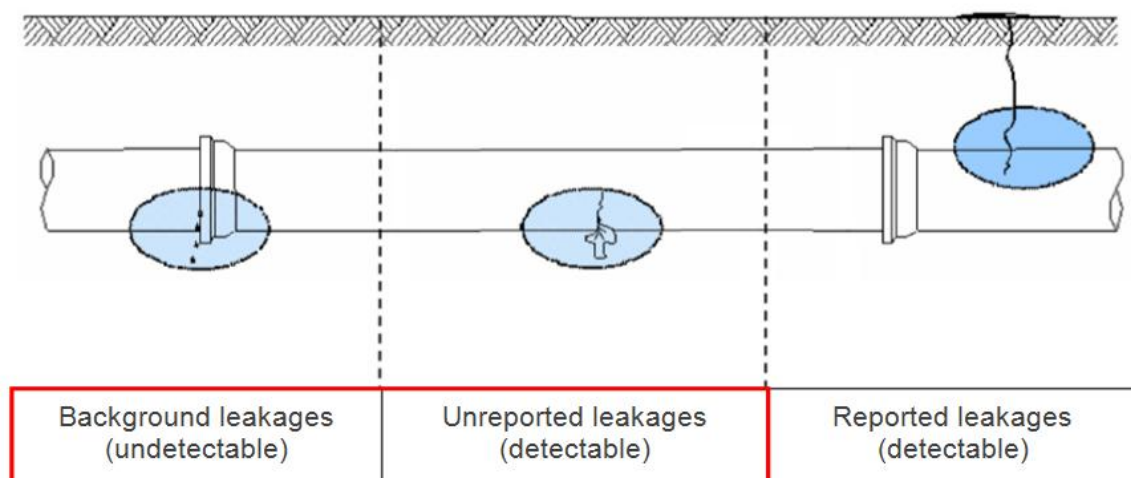
Figure 1.3: Components of real losses according to the BABE-concept (Lambert, 1993)

According to Lambert (1993) real losses can be classified into background leakages, reported leakages and unreported leakages. Background leakages are small non-visible, inaudible leaks at joints, cracks or fittings with small flow rates. Due to the fact that they cannot be detected they have a long run time which leads to a great amount of water loss. Background leakages are often unavoidable. A small part can be eliminated by reducing the system pressure or renewal of pipes. Unreported leaks increase gradually and have moderate flow rates. These leakages can be found by active leakage control (ALC). The life span of unreported leaks depends on the method and the intensity of the ALC. Reported leaks and bursts have typically high flow rate but only short run times (Fanner, et al., March 2009). The water comes to the surface and is reported by the general public or by the staff of the water supply companies.

For developing a leakage management strategy it is important to get an understanding of the reasons for losses and their influencing factors. There are several factors that can cause real losses in water distribution systems for example poor pipe connections, internal or external pipe corrosion, mechanical damage, ground movement, high system pressure, damage due to excavation, pipe age, freezing in winter, defects in pipes, ground conditions, and also poor installation (Puust, et al., 2010).

There are several reasons why leakages in a WDS should be kept as small as possible. The most important are the ecological aspects. Water is a fundamental resource which should be saved because it is essential for life. Additionally, higher CO_2-emissions are produced harming the environment due to the greater effort and energy demand for pumps and processing installations. Further, the risk of infiltration of polluted water into the pipe exists in case of a pressure drop. From the economical view leakages increase the daily operation hours of pumps and processing installation in a WDS and lead to higher operation and maintenance costs due to the additional energy consumption. Moreover, a great amount of leakage water can cause damage to property and persons. The intentional delay of the repair of known leakages can lead to penal consequences. High water losses cause a pressure drop in the WDS and can further result in complaints from the consumers. The fulfillment of demand can potentially no longer be guaranteed in peak periods and the capacity of the pumps is reached earlier (Schrotter, 2010).

Early leakage detection is very import not only because of the economical loss but also because it can be harmful to the environment and leaks can cause damage on the surrounding infrastructure. Earlier leak detection can save a great amount of water and prevent small leaks to enlarge and turn into bursts (RLE Technologies).

Leakage management is of great interest for researchers and practitioners since leakage affects water companies and their customers worldwide (Puust, et al., 2010). The number of new leaks each year is influenced by long-term leakage management

(Farley, et al., 2003). The state-of-the-art in leakage management is presented in the following section.

1.1   State-of-the-art in leakage management

The whole process from becoming aware of the leak existence to controlling the level of leakage in the system is referred to as leakage management process (Puust, et al., 2010).

The four basic components of managing real losses are pressure management, speed and quality of repairs, pipe materials management (infrastructure management), and active leakage control (ALC).

Figure 1.4 shows the four basic leakage management strategies according to Lambert (May 2000). The small square depicts the Unavoidable Annual Real Losses (UARL) which cannot be eliminated totally even in a well-maintained network. The large box represents the volume of the Current Annual Real Losses (CARL) these are the potentially avoidable real annual losses. The difference between the UARL and the CARL is the infrastructure leakage index (ILI) (Fanner, et al., 2007). The ILI is an indicator of how effectively the infrastructure activities (repairs, ALC, and pipeline management) are managed at the current pressure (Farley, et al., 2003).
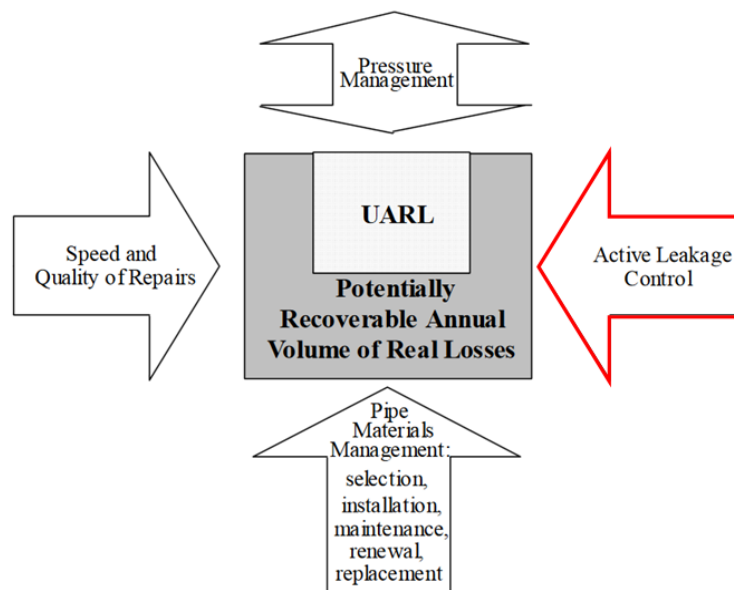
Figure 1.4: Four basic leakage management activities which constrain annual real losses (Lambert, May 2000)

The potentially avoidable annual real losses can be reduced by the four methods shown in Figure 1.4.

Pressure measurement (PM) is one of the fundamental factors of an efficient leakage management because it can influence the frequency of new leaks, and the flow rates of leaks and bursts (Farley, et al., 2003). If the supply pressure increases also the

4

leakages increase and vice versa. Thus, if pressure can be reduced, this leads to an immediate positive impact on the water lost (Frauendorfer, et al., 2010). PM is more sustainable than ALC but requires continuous monitoring and maintaining pressure reducing valves and pump controls (European Union, 2015).

Leaks have to be repaired as soon as possible to keep the average duration of the leak low (Frauendorfer, et al., 2010). The quality of the repair should be supervised to minimize the probability of a reoccurring leak (European Union, 2015). Interruptions of the water supply for the consumers should be kept as short as possible. The level of leakage depends on the flow rate and the run time. The run time includes the awareness time, the location time, and the repair time (Figure 1.5). The awareness time is the time used for the water supply company to be aware of a leak or burst.
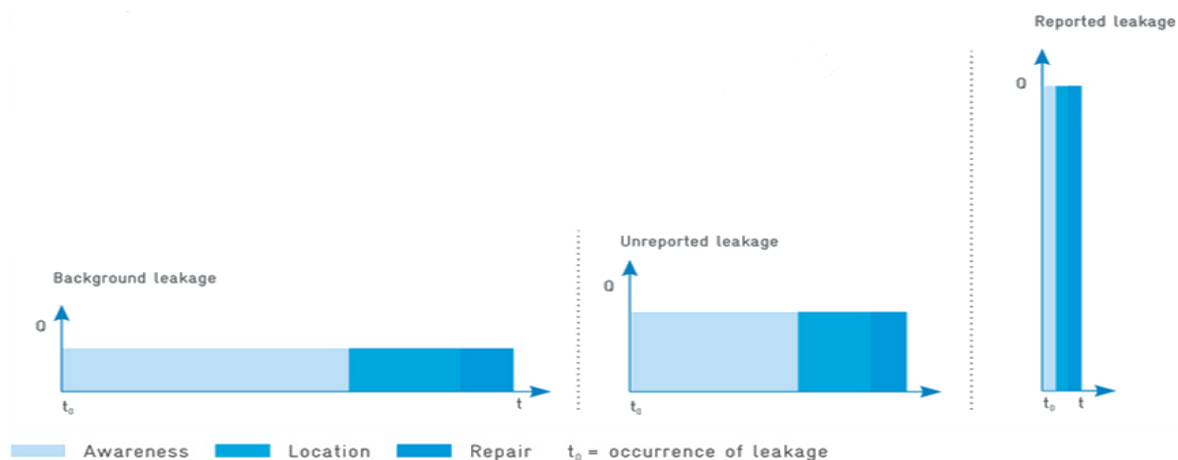
Figure 1.5: Relationship between leakage run time and flow rate (Farley, 2001), (Thornton, et al., 2008)

The infrastructure management includes the renewal or replacement of pipes while using solid quality materials and installation in the long term (Frauendorfer, et al., 2010). Compared to ALC and PM infrastructure management is an expensive method to reduce leakage (European Union, 2015).

According to Farley (Farley, 2003) leakage management can be divided into passive (reactive) and active leakage control.

1.1.1 Passive (reactive) leakage control

Using the traditional, passive leakage approach the water supply company waits until a customer reports the leakage. This is the case if the leak appears on the surface. Not all leaks become apparent and this leads to unreported leaks and higher costs. A passive leak control is often practiced in less developed WDS with a very low leakage level. This is the first step for improvement (Farley, 2003).

1.1.2 Active leakage control (ALC)

The ALC is an on-going process of detecting, locating, and repairing leaks (European Union, 2015). The ALC controls how long the unreported leaks run until they are located (Farley, et al., 2003). ALC means that the water company supply system is ac-

tively looking for unreported leaks and bursts and pinpointing these leaks. The active control methods, for example acoustic loggers, are very time consuming and expensive (Puust, et al., 2010). Using these methods, a large number of sensors is needed.

Every WDS has a level of leakage at which any further activities would not be cost effective. This point is referred to as economic level of leakage (ELL) (Farley, 2003). Figure 1.6 shows a typical analysis of the ELL.
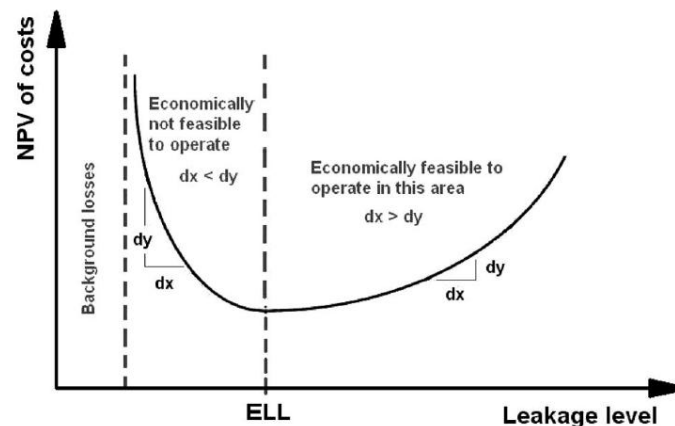
Figure 1.6: Economic level of leakage (Puust, et al., 2010)

According to the European Union (2015) ALC can be categorized into two stages: Leak monitoring and localization, and leak location and pinpointing. In the following the terms of the European Union are used. Table 1-1 shows frequently used methods for leak localization and pinpointing which are partially presented in the following sections.

Table 1-1: Commonly used techniques for leak localization and pinpointing

Leak monitoring and localization	Leak location and pinpointing
Visual survey	Ground microphones
Minimum night flow measurements	Listening sticks
Step test	Leak noise correlator
Ground penetrating radar	Tracer gas technique
Acoustic logger	Pig-mounted acoustic systems

1.1.2.1 Leakage monitoring and localization

The aim of this phase is to narrow down the area where leakage is occurring in order to make later pinpointing easier. A traditional approach is to divide the network into so-called district metered areas (DMAs). DMAs are discrete areas of the WDS and are created by closing boundary valves or by permanently disconnecting pipes to other areas so that it remains flexible to changing demands (European Union, 2015). Leakage monitoring requires the installation of flow meters and pressure sensors at

specific points in the DMS (Pilcher, et al., March 2007). The water flowing into and out of the DMA is metered and flows are periodically analyzed in order to monitor the level of leakage. Figure 1.7 shows an example of the division of a network into DMAs and sub-DMAs.

Figure 1.7: Dividing a network into DMAs (Pilcher, et al., March 2007)

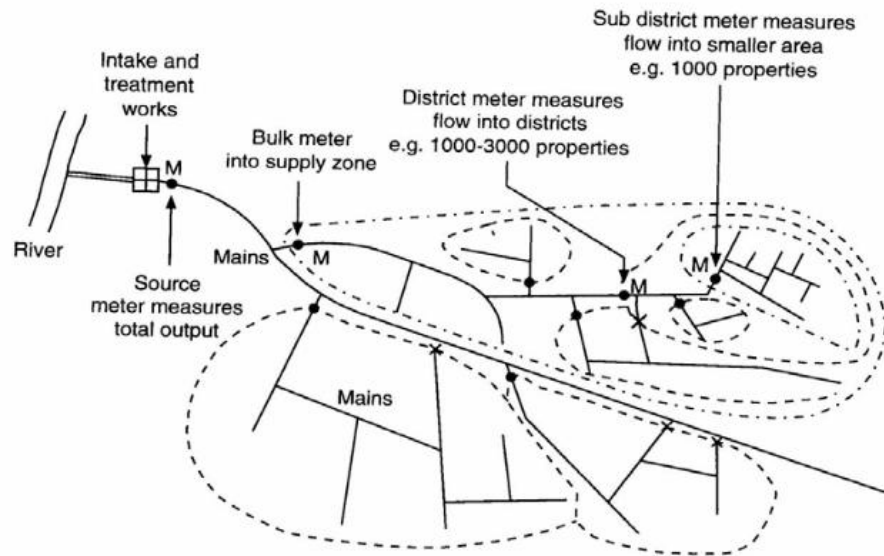In WDS where it is not practical to install DMAs other leak localization methods such as acoustic data loggers can be used (European Union, 2015). Other common techniques are step testing, ground motion sensors, and ground penetrating radars which are used to identify and prioritize the area of leakage. These methods make it easier to pinpoint the leak later but do not provide any information of the exact location yet (Puust, et al., 2010).

According to Puust, et al. step testing is the most effective method for leak localization (2010). It is carried out during the period of the minimum night flow (MNF). A possible disadvantage can be the infiltration of ground water and some parts of the network can temporarily be without any water.

Leak signals can be measured with vibration sensors or hydrophones which are temporarily or permanently attached to the pipe fittings directly. Hunaidi, et al. (Hunaidi, et al., 2004) referred to this method directly as noise logging (NL) or acoustic logging (AL). NL works well for surveying large areas but not for pinpointing leaks. The sensors can be mounted at hydrants, pipe fittings, and valves being 200 and 500 meters apart. Data is usually collected during the MNF period between 02:00 and 04:00 am and is statistically analyzed for the detection of leak signals (Hunaidi, et al., 2004). Small leaks are more difficult to locate especially when using acoustic logging (noise logging) for plastic pipes. The method works well for iron or steel pipes but not for PVC (polyvinyl chloride) and PE (polyethylene) pipes. The application in large WDS is very expensive and time-consuming (Puust, et al., 2010).

7

The ground penetrating radar (GPR) is a non-destructive geophysical method which can be used to locate leaks in buried water pipes. Hereby, voids in the soil created by leaking water, or by detecting anomalies in the pipe depth are detected by radar. The GPR waves are partially reflected back to the surface when they encounter an anomaly. The time difference between the transmitted and reflected waves is an indicator for the depth of the reflecting object (Hunaidi, et al., 2004). Anomalies like metal objects in the ground can lead to false conclusions. GPR is not usable in cold climates. Some GPR can be used for calculations up to two meters into the ground. The GPR provides good results for non-metallic pipes and pipes with a large diameter but in general any pipe can be analyzed (Puust, et al., 2010).

Figure 1.8: Ground penetrating radar (GPR) (Worksmart, Inc., 2012)

These leakage localization methods are expensive and require a lot of manpower. An additional possibility to the methods mentioned above is to install permanent flow meters and connect them with a supervisory control and data acquisition (SCADA) system. The SCADA detects unusual increase in flow pattern which signifies a leakage (Puust, et al., 2010).

If a leak has been localized it can be located and pinpointed using various methods. Some of them are introduced in the following section.

1.1.2.2 Leakage location and pinpointing

Location and pinpointing methods are used for unreported as well as for reported leaks and include acoustic and non-acoustic techniques. Acoustic methods are basic listening stick, electronic listening stick, leak noise correlator, noise loggers, multi acoustic sensor strip, and in-pipe sounding. Gas injection, ground penetrating radar, infrared photography, and in-pipe hydraulic plug are non-acoustic techniques (European Union, 2015).

Leak noise correlators (LNC) are comparing the noise detected at two different points of the pipe (Hamilton, et al., 2013). Therefore, two microphones are located in contact with the pipe at the same time, with one microphone on each side of the leak to correlate the sound from a leak (Stenberg, 1982), (Grunwell, et al., 1981). The sensors can be up to 3000 meters away from each other, depending on the pipe materi-

al. The sound is compared with the correlator which calculates the time difference for the sound to reach the correlator. With the knowledge of the speed of sound in the pipe, the distance to the leak can easily be computed. The most accurate LNC can locate a leak within one meter of the actual leak in most pipe sizes. The LNC work best with clean, small-diameter, metallic pipes in high water pressure areas (Puust, et al., 2010).
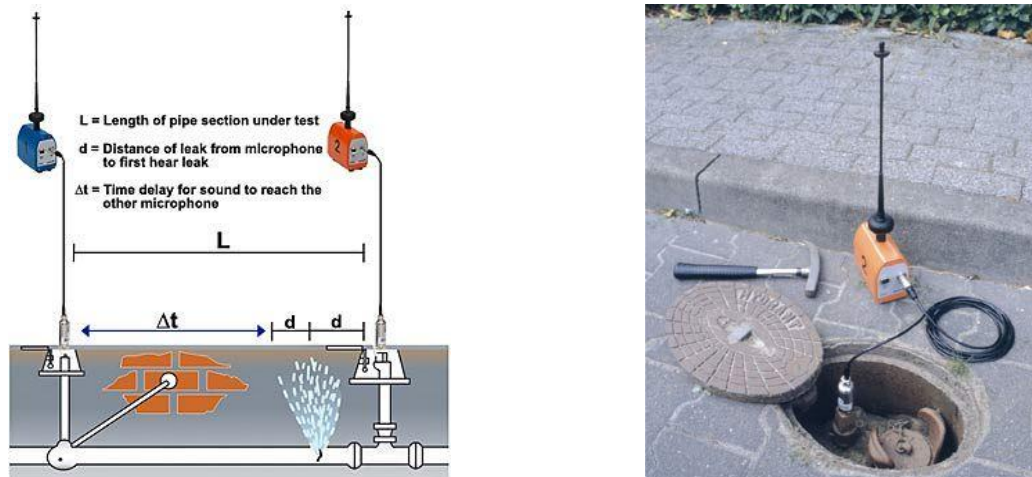
Figure 1.9: Leak noise correlator (SeCorrPhon AC 06) (SEWERIN)

The gas injection method uses a tracer gas which is non-toxic, water-insoluble, and lighter than air. Due to the low costs and viscosity hydrogen is used. The gas is injected into an isolated section of a pipe. This tracer gas technique (TGT) can be practiced in pipes from 75 to 1000 mm diameter (Hamilton, et al., 2013). After the injection the ground is scanned by a highly sensitive gas detector, which identifies any traces of escaped gas from the leak point. Using this method multiple leak locations can be found in a single pipe section where other techniques fail. The disadvantages are the high costs and that leaks cannot be found if they are under water at the bottom of the pipe (Puust, et al., 2010).

Examples for in-pipe sounding methods are free swimming systems. These systems are inserted into a pipeline and are floating along the pipe due to the water velocity. The sound is continuously recorded. At the end of the inspection a capture device is

Figure 1.10: Smart Ball® Injection Process (Pure Technologies)

used to extract the system from the pipe. These systems are combined with an above-ground tracking device, which tracks the progress of the sensor through the pipe. (Hamilton, et al., 2013)

The leakage pinpointing methods are the most precise technologies that are currently available. Because of the high equipment costs and the man-hours needed, pinpointing methods should be used in combination with localization methods (Puust, et al., 2010).

The whole process only using the methods mentioned above could take weeks or months with an important volume of water wasted before the leak is found. Additionally, these techniques are very time- and labor-consuming. To avoid these inconveniences, model-based leakage localization can be used. Techniques to locate leaks based on pressure monitoring devices make pinpointing in the field more effective and less expensive (Rosich, et al., 2013). The principle of model-based leakage localization is to compare the real-world measurement with the data obtained from the hydraulic model. One central point of model-based leakage localization is finding the ideal position of sensors. To reduce the costs it is aimed to use a minimum number of sensors.

In section 2 the state-of-the-art in model-based leakage localization and sensor placement is introduced more detailed.

1.2 Objective and research questions

The aim of this research is to compare sensor placement methods regarding the effect of leakage localization accuracy. Therefore, a model-based leakage localization algorithm is used which was developed at the Institute of Urban Water Management and Landscape Water Engineering at Graz University of Technology. Additionally, pressure and flow measurements were performed in a WDS in Hart close to Graz/ Ragnitz and leakages were simulated by opening hydrants. The algorithm was applied to the measured data from the different sensors. The results obtained from the calculations are evaluated according to the distance between the leakage position found by the algorithm and the real leakage. These analyses are performed for the different sensor placements and leak sizes. The results are analyzed regarding the following questions:

- *Which sensor placement method is the most accurate in finding the actual leak?*
- *Can the sensor placement algorithms be compared with each other?*
- *Is it possible to narrow down the area where the leak could be with the different sensor placement methods?*
- *Does it affect the results calculating with small (0.25 l/s) or bigger (1.0 l/s) leakages?*
- *How big is the pressure drop at a leakage with 0.25/ 0.5/ 0.7 and 1.0 l/s?*

2 State-of-the-art in the field of model based leakage localization

Model-based leakage localization represents an alternative to the traditional methods mentioned in the previous section. It should not be seen as a replacement for pin-pointing methods. Model-based leakage localization only provides an approach. Real time monitoring is using real time sensor data to detect abnormalities in these to find faults or abnormal situations in the system. If it is used together with hydraulic/ mathematical models it is referred to as model-based techniques.

Several studies have been published on leak detection and isolation methods for water distribution systems.

Leakage detection by solving an inverse steady-state problem was first introduced by Pudar and Liggett (1992). They observed state variables like pressure and flow and assumed that leaks only occur at nodes. A sensitivity matrix was used to decide where to place the measuring sensors. Pudar and Liggett (1992) depict that the location and size of the leaks are sensitive to the quality and quantity of the pressure measurements and to the knowledge of the pipe friction parameters.

The use of pressure and flow measurements in combination with hydraulic models is a suitable approach for on-line monitoring of the water balance (Wu, et al., 2006), (Almandoz, et al., 2005).

Ragot and Maquin (2006) proposed a methodology based on fuzzy analysis of the residuals. The method calculates the residuals between measurements with leaks and the ones without leaks. The researchers used analytical redundancy to detect and isolate faults on sensors.

Mashford, et al. (2009) developed a methodology to locate leaks using support vector machines (SVMs) which act as pattern recognizers. The SVMs are trained and tested on simulation data from a hydraulic EPANET model. Mashford proved in his study that leak size and location can be predicted with reasonable degree of accuracy.

Alternatively, Pérez, et al. (2011) proposed a method based on pressure measurements and pressure sensitivity analysis of nodes in a network. Pérez, et al. (2011) analyzed the residuals (differences between the real measurements and the simulations of the hydraulic model) regarding a given threshold with respect to model uncertainty and noise. If the residuals reach the threshold they are compared against the leak sensitivity matrix to find out which leak is present.

Another methodology for leakage detection and localization in DMAs based on pressure sensors is developed by Pérez, et al. (2013). The approach uses residual fault sensitivity analysis.

Quevedo, et al. (2011) extended the method of Pérez, et al. (2011) to work with non-binary fault signatures. This method is based on measuring the additional head loss which is caused by the leakage.

Meseguer, et al. (2015) described an integrated monitoring framework for leakage localization using a hydraulic model of the network. This methodology is based on the use of pressure and flow sensors at the DMA inlets and a limited number of pressure sensors inside the DMA. The results of the model-based leakage localization depend on the choice of the number of sensors and their positions. Due to the budget the number of sensors installed is usually limited. The sensor devices have to be properly located in order to improve the real-time leakage localization. Therefore, a methodology to optimize the number and placement of sensors is required. The leak localization method is very sensitive to the number of sensors and their placements. Meseguer, et at. (2015) claimed that sensor placement and leakage localization should always be considered together.

The main idea of model-based leakage localization is to use real-time measurements of pressure and/ or flow in a water distribution system and compare them with simulation results generated by a well-calibrated hydraulic model. By analyzing the discrepancies of the measurements leakages can be detected. In this research differential evolution, a special genetic algorithm, is used for leakage localization.

The problem can mathematically be described by

$$f(\vec{x}) = \frac{1}{n} \sum_{i=1}^{n} \left(m_i - \widetilde{m_i}(\vec{x}) \right)^2 \rightarrow \min_{\vec{x}} f(\vec{x}) \tag{1}$$

where n is the number of used sensors, m_i represents the measurement data obtained from the sensors installed in the field, and $\widetilde{m_i}(\vec{x})$ describes the values from the hydraulic simulation model.

The parameter $\vec{x}$ is changed in the hydraulic model in a way that the simulated values fit again with the real measured values. The vector $\vec{x}$ describes the leakage in the hydraulic system and is declared by the equation

$$\vec{x} = \begin{pmatrix} c_e \\ L_p \end{pmatrix} \tag{2}$$

where c_e represents the emitter coefficient, and L_p represents the position of the leak in the WDS. This location is given by the node in the hydraulic model (Steffelbauer, et al., 2016).

The emitter coefficient or discharge coefficient c_e characterises the flow and pressure loss behaviour of nozzles in fluid systems. The c_e-value can be calculated through the leakage outflow power law equation provided by EPANET (Rossman, 2000)

$$Q = c_e * p^{e_e} \tag{3}$$

12

where Q represents the flow rate, p the pressure at the leak position, and e_e the pressure exponent. For steady state simulations, e_e can be set to a value of 0.5. The leakage outflow is dependent on the emitter coefficient and the pressure, which is calculated by the hydraulic solver. Due to the fact that the c_e-value can be chosen to get the desired flow rate, c_e describes the size of the leak.

The parameter $\vec{x}$ is calculated in a way that the fitness function $f(\vec{x})$ is minimized. For solving this so-called optimization problem often stochastic algorithms (e.g. genetic algorithms) are used because gradient based algorithm may fail due to the many local minima the fitness function may have (Steffelbauer, et al., 2016). Multiple local minima can arise due to the topology of the supply network, because the system is under-determined or by reason of the order of the L_p-axis. The aim is to find the global minimum which is searched by the differential evolution (DE). For better understanding principles of genetic algorithms (GA) and DE are explained in the next section in detail.

2.1 Genetic algorithm

A genetic algorithm is a search method that is based on the principles of genetics and natural selection. The GA imitates natural evolution by taking a population of strings, which encodes possible solutions, and combines them based on a fitness function to produce individuals that are fitter than previous ones.

GA was first developed by John Henry Holland (in the 1960s), who was supported by his students and colleagues from the University of Michigan. Later, David E. Goldberg successfully refined the GA by trying to solve several optimization problems (Goldberg, 1989). Genetic algorithm is a subfield of evolutionary algorithm which is based on Darwin´s principals of reproduction and survival of the fittest (Darwin, November 1859). Darwin´s theory of evolution describes that some organisms in nature differ from others. Some of these differences are inherited. There are a lot of organisms that produce more children than can survive and many of the survivors do not reproduce themselves. Due to the fact that more organisms are produced than can survive, the individuals have to compete for resources. Every single individual has different advantages and disadvantages in the struggle of survival. That fact of natural selection causes them to change over time (Mitchell, 1996).

The reasons why GAs are used is because they provide near-optimal solutions in a short amount of time. It is faster and additionally more efficient compared to traditional methods. Using GA there is always an answer to the problem, which gets better over time. Furthermore, GA offers many solid solutions and not just a single one.

Figure 2.1 shows the iterative process of the genetic algorithm. After a coding is chosen to define the genetic algorithm problem, the first step is to initialize a random population of individuals. In the context of sensor placements in water distribution systems an individual corresponds to the possible presence or absence of a sensor

at a node. A good population size consists of about 20 to 30 individuals (Grefenstette, 1986). The population within each iteration is called generation. Each individual of the population has a set of n traits, where n is the number of sensors. In the following research five sensors were used for each sensor placement. The traits are encoded as bit strings. The individuals represent suitable solutions for the problem. In the next step, the fitness of each individual in the population is evaluated. This fitness value is calculated from the fitness function. It provides information about how fit an individual is compared to the others within the population. Fitter individuals have a greater chance to survive and be reproduced according to Darwin´s Theory of "Survival of the Fittest". A new population is created by repeating the following steps of selection, crossover and mutation until the new population is complete. Afterwards, the fitness of the new population is evaluated. If the termination criterion is reached, the iterative process is terminated. If not, the individuals are evaluated again and the process starts over again.
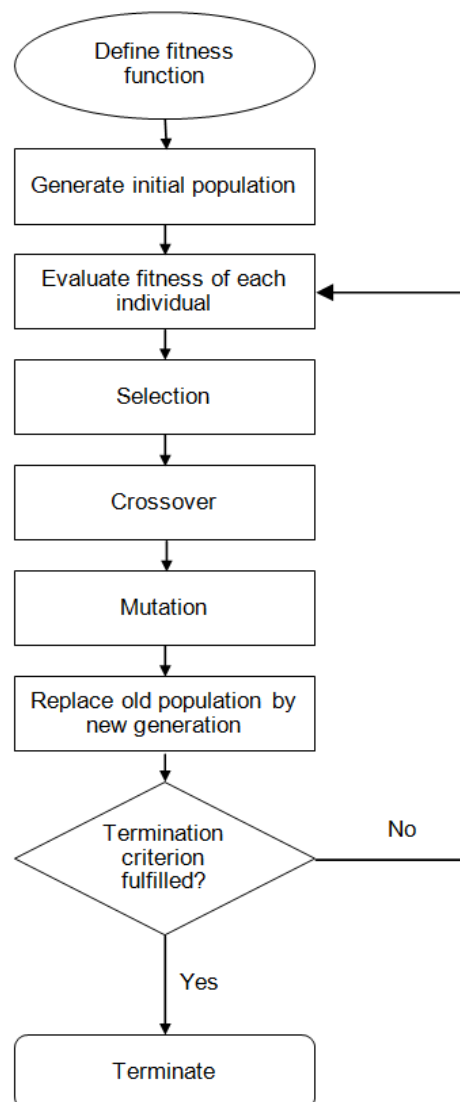

Figure 2.1: Genetic algorithm - flow chart (Malhotra, et al., March 2011)

2.1.1 Optimization problem

GA is used as a method to solve an optimization problem. For GA it is possible to find a global optimum even though many local optima exist. Optimization means to find input values in a way to get the best output values. The problem consists of minimizing the fitness function by systematically choosing input values and computing the value of the function.

2.1.2 Encoding

When starting the algorithm the individuals first have to be encoded. There are many ways to encode the individuals. The used method depends on the problem and the number of instances of the problem. The most common way is the binary encoding, where every individual is a string of bits with 0 and 1. Another method is the permutation encoding, which is mostly used in ordering problems. Here, every individual consists of a string of numbers that forms a sequence. During the value encoding the individuals consist of a string of values, which can be numbers as well as words or letters. In the tree encoding the individuals are trees of objects. This type of encoding is mainly used for program development (Malhotra, et al., March 2011).

Figure 2.2 shows some encoding types mentioned above.

Binary encoding		0	0	1	1	0	1	0	0	1	0
Permutation encoding		8	5	3	2	4	7	9	6	1	0
Value encoding		A	F	E	Z	P	S	C	L	K	B

Figure 2.2: GA - binary encoding, permutation encoding and value encoding

2.1.3 Fitness function

The fitness is usually the value of the function which is solved in the optimization problem. The fitness function is defined by the equation (1).

The aim of this calculation is to minimize the discrepancy between the real-world measurements (pressure and flow) and the results obtained by hydraulic simulations.

2.1.4 Selection

Individuals are selected from the population to crossover. The aim is to select the best individuals to survive and to create the offspring. There are many different methods to select the best individuals, e.g. the roulette wheel selection, the rank selection, the tournament selection, and the stochastic universal sampling. In the roulette wheel selection (RWS) two individuals are selected from the population to reproduce according to their fitness $f(c_i)$. The probability of being chosen $p(c_i)$ is based on the fitness value according to the function

$$p(c_i) = \frac{f(c_i)}{\sum_{j=1}^{n} f(c_j)} \tag{4}$$

where n is the number of individuals in the population (Razali, et al., July 6-8, 2011).

The better the individuals are, the more chances they have to be selected. In Figure 2.3 the roulette wheel selection is illustrated. All individuals of a population are placed in an imaginary roulette wheel. The area of each individual corresponds to its fitness value. The wheel is turning and the ball circles around the wheel. The individual where the ball stops is the one to be selected. The selection point is a random point on the wheel (Razali, et al., July 6-8, 2011).
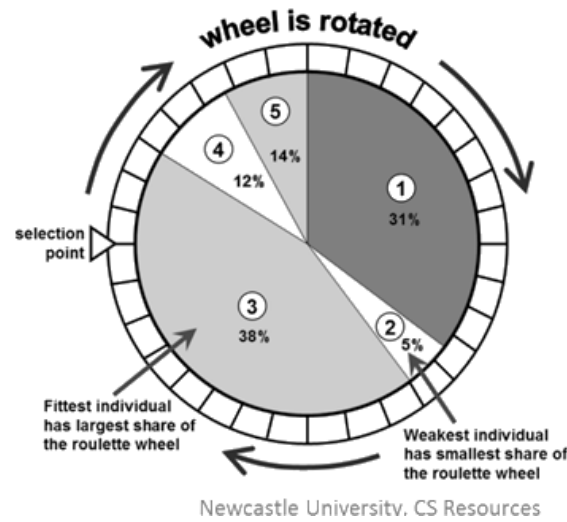

Figure 2.3: GA - roulette wheel selection (Dalton, 2007)

Some GAs also work with elitist selection, which means that a special number of the best individuals are chosen to pass the next generation without crossover or mutation. This guarantees that the individuals with good traits are not eliminated by crossover or mutation operators. Elitism is used to speed up the convergence of a GA (Bodendorfer, 2003).

The selection operation guarantees that the individuals of the offspring are better or at least equally good than in the previous generation ().

$$f_n(\vec{x}) \geq f_{n+1}(\vec{x}). \tag{5}$$

2.1.5 Crossover

Once the individuals are selected from the population they will be recombined. During crossover new fitter individuals are created by combining certain traits of the selected individuals. The crossover is a process of combining more than one parent individual and producing two new individuals, their children. The typical crossover rate should be high, between 75 and 95% (Grefenstette, 1986).

There are many methods for crossover e.g. single-point crossover (SPC), two-point crossover (TPC), cut and slice, uniform crossover, and arithmetic crossover. When

using SPC one single crossover point is selected randomly from both parent individuals (chromosomes). The offspring is created by adding the first part of the first parent to the second part of the second parent and vice versa. Often more than one crossover point is involved. At the TPC two crossing points are selected on the parent strings. Every trait between the two points is swapped between the parent individuals to produce new children for the next generation. At the uniform crossover traits are copied from the parents using a fixed mixing ratio between them. The same crossover points are selected randomly on both parent strings. The typical ratio is 0.5 where the children are created from 50% of the traits of each parent. In the arithmetic crossover the weighted arithmetic mean of the parents' traits is calculated to create new offspring (Kaya, et al., 2011).

Figure 2.4 shows the single-point crossover, the two point crossover and the uniform crossover process.
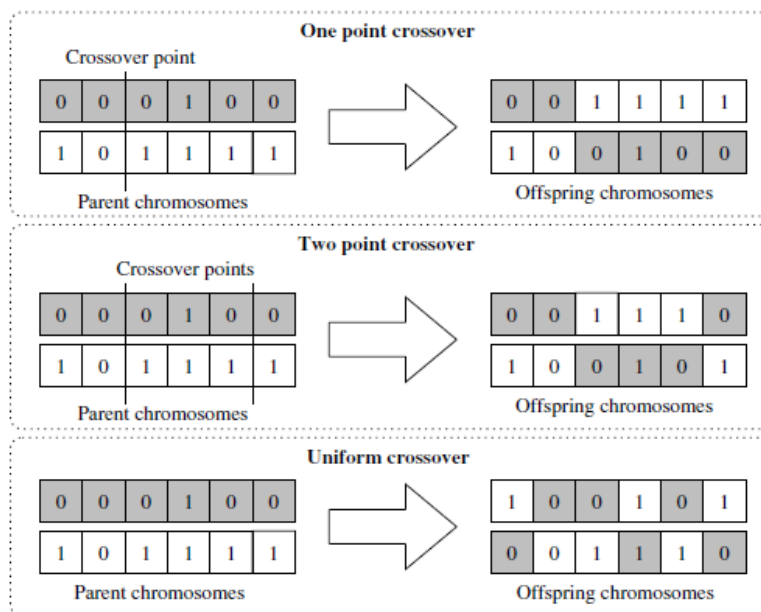

Figure 2.4: GA – single-point crossover, two-point crossover and uniform crossover (Sastry, et al., 2002)

2.1.6 Mutation

In the mutation process following the crossover operation random traits are changed to create new individuals. Mutation is used to maintain and introduce diversity in the population. Otherwise a local maximum environment would be reached eventually. The mutation probability p_m signifies whether a trait of an individual is mutated or not. Usually this mutation rate should be very low, between 0.5 and 1 % (Grefenstette, 1986).

The most commonly used mutation operators are the bit flip mutation, the swap mutation, the scramble mutation, and the inversion mutation. Figure 2.5 depicts the before mentioned mutation operators.

In the bit flip mutation one or more bits are selected and flipped. In the swap mutation two bits of the individual are chosen randomly and swapped. In the scramble mutation a set of traits is chosen from the individual and the values are shuffled randomly. Also, in the inverse mutation a set of traits is chosen but the whole string in the set is inverted (Tutorialspoint).
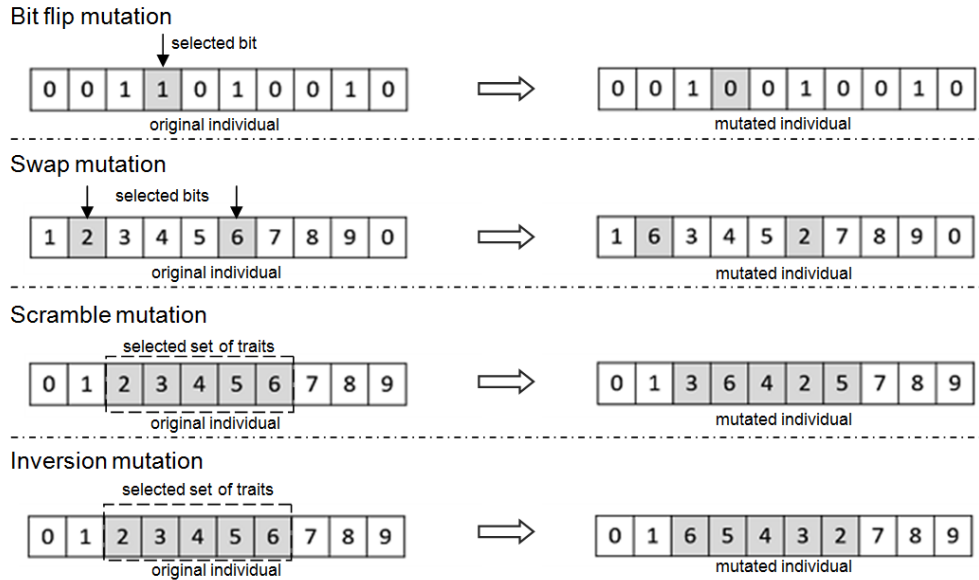

Figure 2.5: GA – bit flip mutation, swap mutation, scramble mutation and inversion mutation (Tutorialspoint)

Following the mutation the new offspring is placed in a new population. This new generated population is now used for another run of the genetic algorithm. If the termination condition is fulfilled, it stops and the best solution is returned to the population. The algorithm starts again with the evaluation of the fitness of each individual.

2.1.7 Termination criterion

The iterative process of the GA is repeated until the final condition is reached. This could be the case if a solution is found that fulfills the minimum criteria or if a fixed number of generations is reached. The process could also be terminated if the computation time is over or if the highest ranking solution is reached.

GAs have been increasingly applied to various research and optimization problems in the recent past. GAs have been proved to be a suitable approach for solving the optimization problem by selecting the potential sensor positions (Meseguer, et al., 2015). GAs are used in four of the sensor placement methods mentioned in this study.

For the leakage localization used in this study differential evolution (DE), a special genetic algorithm, is used. Therefore, DE is briefly explained in the next section.

2.2 Differential evolution

DE is an evolutionary technique that is used to solve global optimization problems. DE is a parallel direct search method which was invented by Kenneth Price and Rainer Storn (1997). DE is similar to GA except that the candidate solutions are considered as real vectors instead of binary strings ($\vec{x} = \begin{pmatrix} c_e \\ L_p \end{pmatrix}$). DE uses NP (population size) D-dimensional parameter vectors as a population for each generation. The initial vector population is chosen randomly. DE starts with the mutation, followed by the crossover and ends with the selection. At the mutation operation new parameter vectors are generated by adding the weighted difference between two population vectors (F) to a third vector ($\vec{x_1}$).
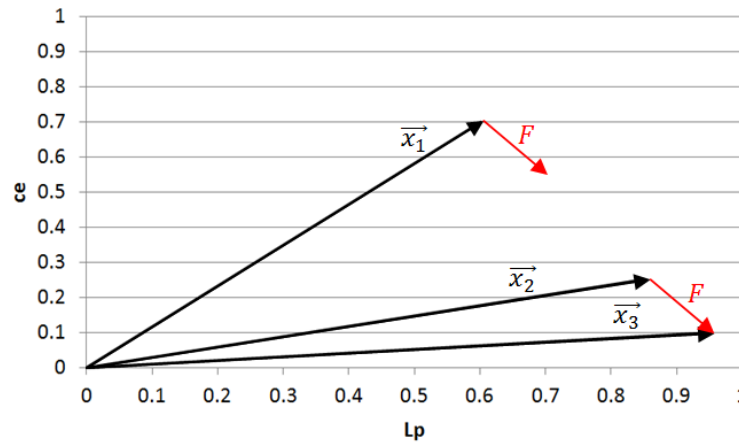

Figure 2.6: DE - mutation operation

In order to increase the diversity the mutated vector´s parameters are then mixed with the parameters of another vector (target vector) to receive the trial vector. This process is called crossover. In the selection process it will be decided whether the vector becomes a member of the new generation or not. Therefore, the trial vector is compared with the target vector. If it is a better solution it is replaced in the population. Otherwise, the target vector remains unchanged (Storn, et al., 1997).

After the crossover and mutation the solutions which best describe the problem are selected. Therefore, the vector $\vec{x}$ is evaluated according to the fitness function (1).

The algorithm starts the hydraulic EPANET model and $\vec{x}$ is imported with a certain ratio so than it can be compared to the measurements.

Dong, et at (2012) found out with their case studies that the DE technique has better convergence properties than the GA. DE is able to locate the current best solution with a higher frequency than the GA in all their case studies. They proved that DE is robust which means that DE is able to reproduce the same results over many trials, whereas GA performance is more dependent on the randomized initialization of the individual parameters (Dong, et al., 2012).

In this study DE is used as a method to solve the optimization problem. DE shows a great rate of convergence and computation time in the WDS can be saved significantly. The problem consists of minimizing the fitness function by systematically choosing input values and computing the value of the function.

Before the leakage localization the near-optimal positions of a minimum number of sensors in the WDS have to be computed. These calculations are done with different sensor placement methods which are presented in the following section.

2.3 Sensor placement methods

In this study six different sensor placement methods (Casillas, Pérez, SPuDU, Shannon entropy, Shortest Path 1 and Shortest Path 2) are compared to establish a model-based leakage localization in a real-world case study. In the following sections 2.3.1 to 2.3.3 the background of the six different sensor placement methods that are used in this research are described further.

2.3.1 Sensor placement – Casillas

Casillas proposes a new approach to place sensors for leak localization in district metered areas. The water flowing into and out of the DMA is metered and flows are periodically analyzed in order to monitor the level of leakage.

Casillas uses a non-binarized leak sensitivity matrix and a projection based leak isolation approach. This leads to an optimization problem which is solved by GA. The aim is to minimize the number of non-isolable leaks. Casillas compared his results with a semi-exhaustive search method with a higher computation effort to prove that it is also possible to get near-optimal solutions using GA in an efficient way. To support his method Casillas conducted experiments with two networks.

The aim of the leak location approach used in this method is to detect and isolate leaks in a DMA. The leak detection is based on the computation of the residuals, which represent the differences between the pressure measurements and their estimations in a hydraulic network. For the leak isolation method it is important to analyze the residual vector using sensitivity analysis in order to determine which node has the highest probability of presenting a leak.

Casillas wants to develop an approach to place a given number of sensors in a DMA in a WDS to get a sensor configuration with maximized leak isolability.

Casillas proposed three ways of improving the robustness of the GA-based sensor placement using time horizon analysis, distance-based scoring and the consideration of different leak sizes. To prove the different methods experiments were performed on two hydraulic networks (Casillas, et al., 2013).

2.3.2 Sensor placement – Pérez

The objective of the sensor placement algorithm from Pérez is to develop an efficient model to detect and to locate leaks in a water distribution network. He presents a methodology to locate pressure sensors to optimize leakage detection by using a minimum number of sensors. The base of his work is to analyse the pressure variation produced by a leak. Therefore, Pérez analyses the difference between the measurements and their estimation using the hydraulic model regarding a given threshold that takes the model uncertainty into account.

Pérez characterized consumers for the model calibration and DMAs. In order to test his methodology sensors were installed in three DMAs within the Barcelona network and leakages were simulated as case studies.

In previous experiments Pérez wanted to find out the behaviour of pressure in case of a leakage. First he studied how the pressure in a node varies depending on the distance of the leak. He recognized that a sensor which is placed in a node is not equally sensitive to all leakages. In another experiment he examined the pressure difference in all nodes for a fixed leakage depending on the distance to the leak. Pérez realized that there are nodes which are especially sensitive to any leakage although they are far away.

His methodology for the sensor placement uses the sensitivity matrix to evaluate the effect of a leakage on the pressure in a node. As some sensors are more sensitive than others the sensitivity matrix has to be normalized.

The evaluation of the residuals (differences between measured and computed results) is the basis of leakage detection. The leaks signature is the value of the residuals in case of a leak in the network. All signatures build the leak signature matrix (FSM). Pérez wanted to create the FSM for the Normalized Sensitivity Matrix. A binarization was performed by the use of a threshold. Through the normalization it is possible to use only one threshold for all sensors but the selection of this threshold is significant. If it comes close to one, the perfect localization of the leakage is reached but all sensors are required.

Sensor placement obviously describes an optimization problem. The aim is to find an efficient leakage detection method and at the same time use the least amount of sensors. Due to the fact that this problem is very difficult to solve and time-consuming Pérez used genetic algorithms to generate the solutions (Pérez, et al., 2009).

2.3.3 Sensor placement – SPuDU

This sensor placement method was developed by the Institute of Urban Water Management and Landscape Water Engineering at Graz University of Technology in 2014.

SPuDU (Sensor Placement under Demand Uncertainties) is a methodology that considers the effects of uncertain hydraulic model parameters on solving problems of optimal sensor placement. The aim is to find optimal sensor positions by using a minimum number of sensors. The quality of a hydraulic model relies on the model input parameters which are fraught with uncertainties. Uncertainties in hydraulic models, e.g. fluctuation in demands, can cause pressure differences within a system.

SPuDU uses a non-binarized sensitivity matrix. The sensitivity matrices and the residuals are calculated using hydraulic simulations. The leakage localization is based on the computation of the residuals, which are the differences between the field measurements and the measurements from the simulated hydraulic model. The hydraulic simulation model is also used to calculate the effects of uncertain hydraulic input parameter on the output of the hydraulic model. These are called model output uncertainty (MOU). This is done by Monte Carlo simulations (MCS). The output parameters received from the MCS are put in the sensor placement algorithm of Casillas (Casillas, et al., 2013) by extending to punish measurement points with high uncertainties.

A quality parameter is calculated for the best sensor positions found by the GA that represents the requirements for leakage localization. This parameter is computed for different numbers of sensors and is considering different intensities of uncertainty. Out of these calculations cost-benefit functions are generated which illustrate the relation between the quality of leakage localization and the number of sensors. If the quality meets the requirements the optimization problem is solved for the number of sensors used.

Due to the fact that the number of possible solutions for optimal sensor positions grows exponentially with the number of sensors placed in the WDS, DE is used to solve the problem of leakage localization by saving computation time. DE is chosen due to its good rate of convergence and is not only used for sensor placements but also for leakage localization.

This sensor placement method was tested on two different hydraulic systems. The calculations showed that points which are sensitive to demand variations might also be sensitive to leakages. Thus, these points are less ideal to place sensors on (Steffelbauer, et al., 2014).

2.3.4 Sensor placement – Shannon entropy

The concept of the Shannon entropy function was introduced by Claude E. Shannon in his paper "A Mathematical Theory of Communication" in 1948. His mathematical equation of measuring uncertainty was

$$S(p) = -\sum_{j=1}^{m} p_j \ln p_j \tag{6}$$

where S is the entropy function and p = (p$_1$,...,p$_j$,...,p$_m$) is a probability distribution.

The Shannon entropy function allows to estimate the best possible average of bits (units of entropy) to encode an information source.

This method identifies the monitoring points by maximizing a sensitivity function and the Shannon entropy function. The sensitivity function shows how sensitive the pressure at node n reacts by changing the roughness coefficient in pipe m. The sensitivity matrix $n \times m$ is built with the values of each of the two functions.

The objective of the Shannon entropy method is to use genetic algorithm search methods and maximize the Shannon entropy function (S) to find the optimal set of monitoring points.

Genetic algorithm (GA) is based on evolutionary ideas of genetics and natural selection to solve complex optimization problems. The basic idea is to simulate processes in natural systems which are necessary for evolution, meaning the fitter individuals are dominating over the weaker ones over successive generations. The GA evolves toward an optimal solution with the three main genetic operators of selection, crossover and mutation. The GA is explained in section 2.1 in more detail.

De Schaetzen conducted field tests to show the results of all three different methods he has presented and compared them to an expert choice. Therefore, pressure and flow were recorded at the monitoring locations of a water distribution system (De Schaetzen, et al., 2000).

2.3.5 Sensor placement – Shortest Path 1

This sensor placement method uses shortest path algorithm to identify good monitoring point locations. The shortest path from the tank to every node in the network depending on the pipe length is calculated at each repetition. The node which is furthest from the tank is chosen to be the monitoring point.

In the shortest path 1 method a zero-length-pipe which links the tank to the node mentioned above has to be added. This iteration is repeated until the total number of monitoring points is reached.

This algorithm sets priority in locating the pressure measurements near the inner network (De Schaetzen, et al., 2000).

2.3.6 Sensor placement – Shortest Path 2

The shortest path 2 method also uses the shortest path algorithm similar to the method in section 2.3.5.

However, in this method all pipes along the shortest path from the tank to the node furthest are set to a length of zero at the beginning. This iteration is repeated until the total number of monitoring points is reached. The first selected node is the same as in method "Shortest Path 1".

This algorithm sets priority in locating the pressure measurements at the outskirts of the network (De Schaetzen, et al., 2000).

In section 3.2 the application of the sensor placement methods on the WDS of Hart is described.

3 Methodology

The measurements, which are relevant for this work, were made from April 12th to May 18th, 2016. In the following the investigation area, the used soft- and hardware and the measuring procedure are described in detail.

3.1 Investigation area

The field tests for this research took place at the border between Hart close to Graz and Graz-Ragnitz, which are municipalities in the district of Graz-Umgebung in Styria, Austria. Hart close to Graz is located between Graz and Laßnitzhöhe and covers an area of 11.1 km^2. In January 2015, the community had about 4,538 residents. Ragnitz is a local part of the municipaly of Kainbach, which counts about 2,732 residents (Das Land Steiermark, 2015).

The red square in Figure 3.1 highlights the area where the measurements took place.

Figure 3.1: Overview maps (sources:
[1] http://www.austrianmap.at/amap/index.php?SKN=1&XPX=637&YPX=492, 29 09 2016;
[2] https://www.google.at/maps, 30 08 2016)

3.1.1 Overview

An overview of the area Hart close to Graz/ Ragnitz is shown in Figure 3.2. The WDS of interest is a very small one with a length of approximately 9.55 km. The pressure loggers are installed on twelve different nodes in the system. The seven underground hydrants are marked in green and the five above-ground hydrants are marked in red. The tank "HB Koppenhof" is marked in blue. The different colours of the pipes indicate their diameters. The pipes which connect the tank to the distribution system have the largest diameter of 125 mm. The three hydrants where the leakages for the measurements were simulated are marked in blue. These artificial leaks are described in section 3.3.
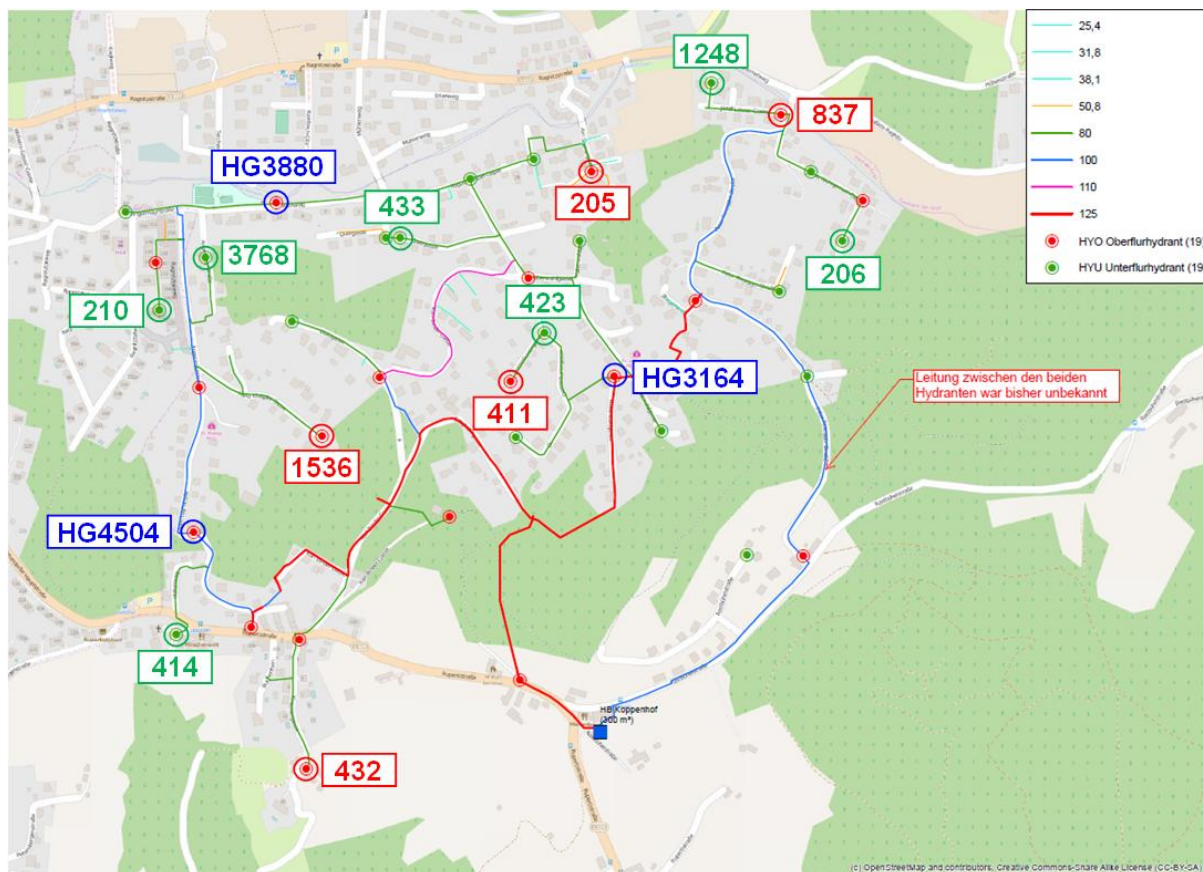
Figure 3.2: Overview map of the area (Hart close to Graz/ Ragnitz) (Institute of Urban Water Management and Landscape Water Engineering/ Graz University of Technology - adapted, 2015)

Institute of Urban Water Management and Landscape Water Engineering, which is part of the Faculty of Civil Engineering at Graz University of Technology in Austria

Table 3-1 shows the classification of the different notations of the hydrants with the pressure loggers. In the EPANET model the nodes are named after their hydrant number and in the readout data from the sensors they are called by their plan number. In the following the sensors are always named with the plan number.

Table 3-1: List of hydrants

hydrant number (node number)	plan number	hydrant number (node number)	plan number
HG3420	423	HG4215	1248
HG3445	411	HG4339b	210
HG3835	433	HG4383	3768
HG3933	205	HG4540	1536
HG4150	206	HG4576	414
HG4162	837	HG4744	432

3.1.2 EPANET model

The water distribution network was modelled with EPANET 2 (see Figure 3.3), which is a public domain water distribution system modelling software package developed by the United States Environmental Protection Agency´s (EPA) Water Supply and Water Resources Division (Rossman, 2000). EPANET 2 software is freely available on the EPA´s website (EPA US Environmental Protection Agency). The EPANET model consists of 212 nodes plus the tank "HB Koppenhof" and 216 pipes with a total length of approximately 9.55 km. Figure 3.3 shows the used EPANET model. There are 39 pipes with a diameter of less than 80 mm (blue), 100 pipes of 80 mm (cyan), 33 pipes of 100 mm (green), 7 pipes of 110 mm (yellow), and 37 pipes of 125 mm (red). In a pre-project of 2015 the average base demand for each household was calculated according to the yearly consumption data of the study area from the period 2010 to 2014 (Landuyt, 2015).
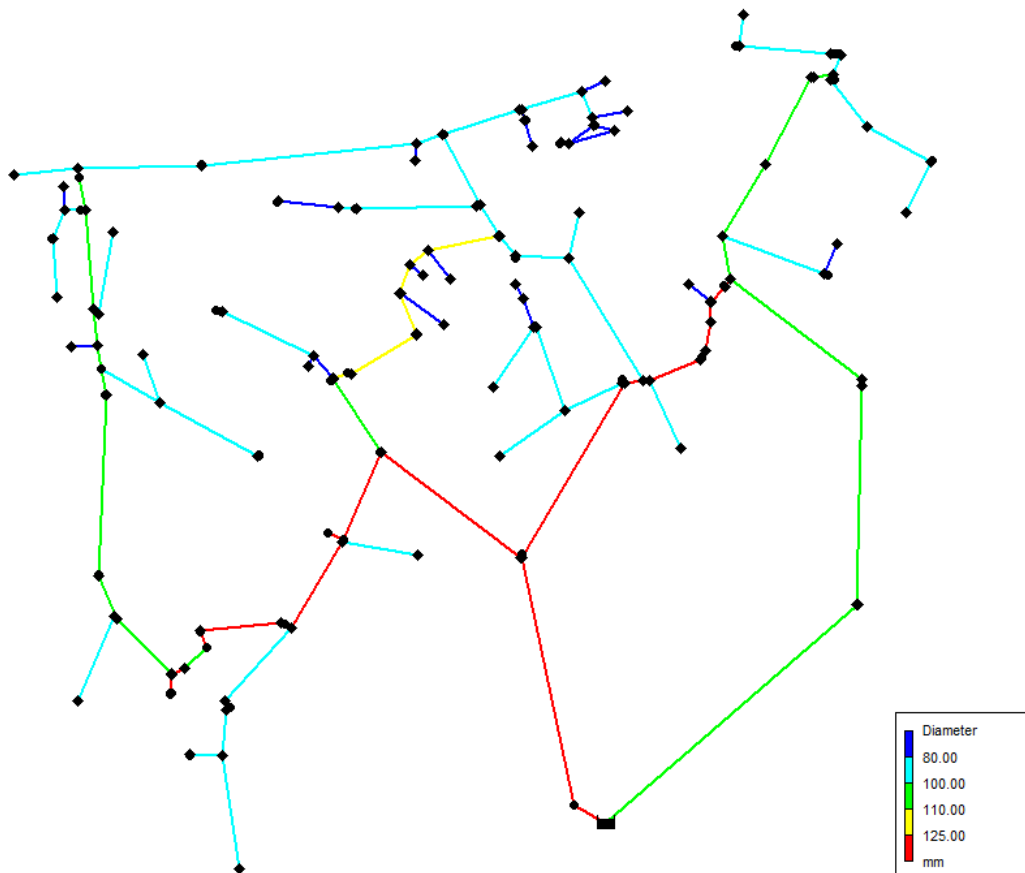

Figure 3.3: EPANET model

The positions of the pressure sensors which can be seen in Figure 3.2 are calculated using different sensor placement algorithms. Their application on the WDS of Hart is described in the following section 3.2 in detail.

3.2 Sensor placement scenarios

Before the field test and the calculations start the sensor placement already took place according to the six methods that were mentioned in section 2.3. In the whole water distribution network there were twelve pressure loggers installed.

The following sections 3.2.1 to 3.2.6 explain which sensors are relevant for the particular sensor placement method. For each approach five nodes are used. In the following tables on the right, next to the figures the hydrant number and the plan number of the used hydrants are listed.

3.2.1 Sensor placement by Casillas

Casillas used a non-binarized sensitivity matrix to minimize the number of non-isolable leaks. He used a simple GA to solve the optimization problem and to find near-optimal solutions for pressure sensor placement. This method is not dependent in the selected isolation method (Casillas, et al., 2013).

The result of this method shows that the above-ground hydrant 205 (marked in red) and the underground hydrants 423, 433, 1248 and 3768 (highlighted in green) are the best nodes for leakage localization (see Figure 3.4).
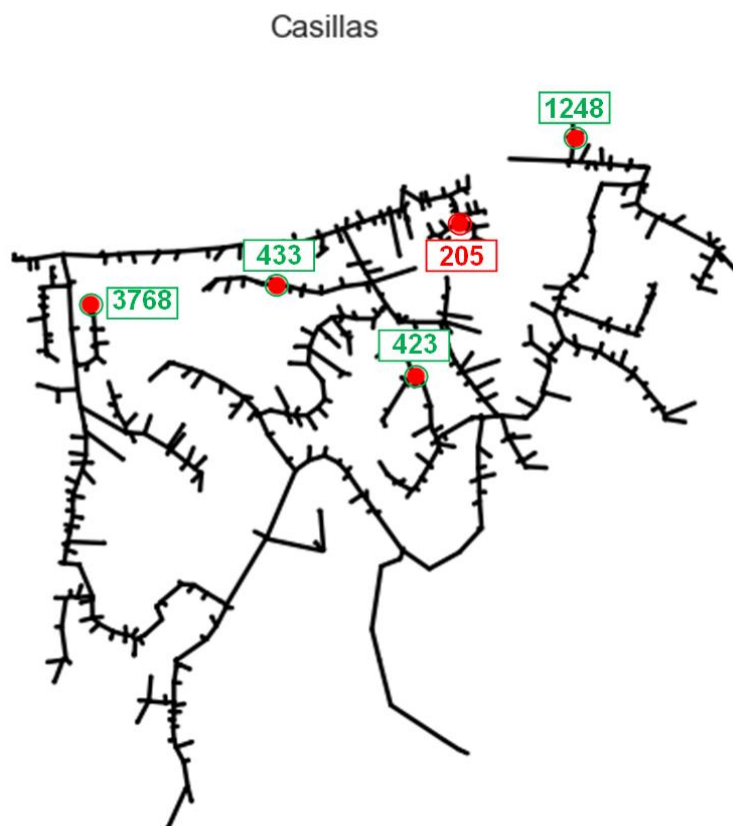

Table 3-2: Hydrant list Casillas

hydrant no.	plan no.
HG3420	423
HG3835	433
HG3933	205
HG4215	1248
HG4383	3768

Figure 3.4: Sensor placement Casillas (Casillas, et al., 2013)

3.2.2 Sensor placement by Pérez

Pérez introduced another method to detect leaks in the WDS by binarization of the pressure sensitivity matrix. This way, the nodes which are most sensitive to leakages can be identified (Pérez, et al., 2009).

The Pérez´ method indicates that the above-ground hydrants 205 and 1536 (marked in red) and the underground hydrants 210, 1248 and 3768 (highlighted in green) are the most sensitive nodes for leakage localization (see Figure 3.5).
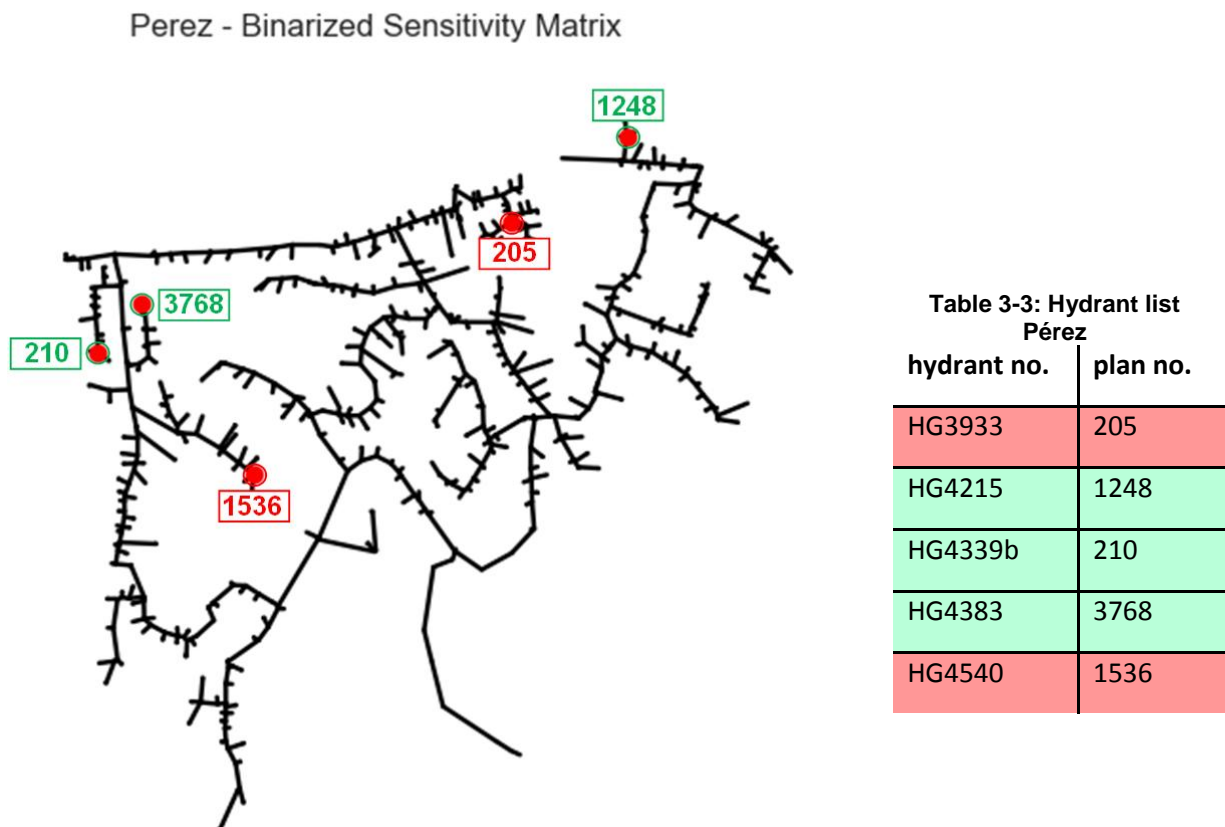
Perez - Binarized Sensitivity Matrix

Table 3-3: Hydrant list Pérez	
hydrant no.	plan no.
HG3933	205
HG4215	1248
HG4339b	210
HG4383	3768
HG4540	1536

Figure 3.5: Sensor placement Pérez (Pérez, et al., 2009)

3.2.3 Sensor placement by SPuDU

SPuDU enables an efficient sensor placement of flow meters and pressure sensors through a non-binarized sensitivity matrix with a projection-based leak isolation approach. This method considers uncertainties in the hydraulic model such as fluctuations in demand which can cause differences in the system pressure. SPuDU uses differential evolution to find out the optimal positions (Steffelbauer, et al., 2014).

The above-ground hydrants 205 and 837 (marked in red) and the underground hydrants 423, 1248 and 3768 (highlighted in green) resulted in being the best nodes for leakage localization using SPuDU (see Figure 3.6).
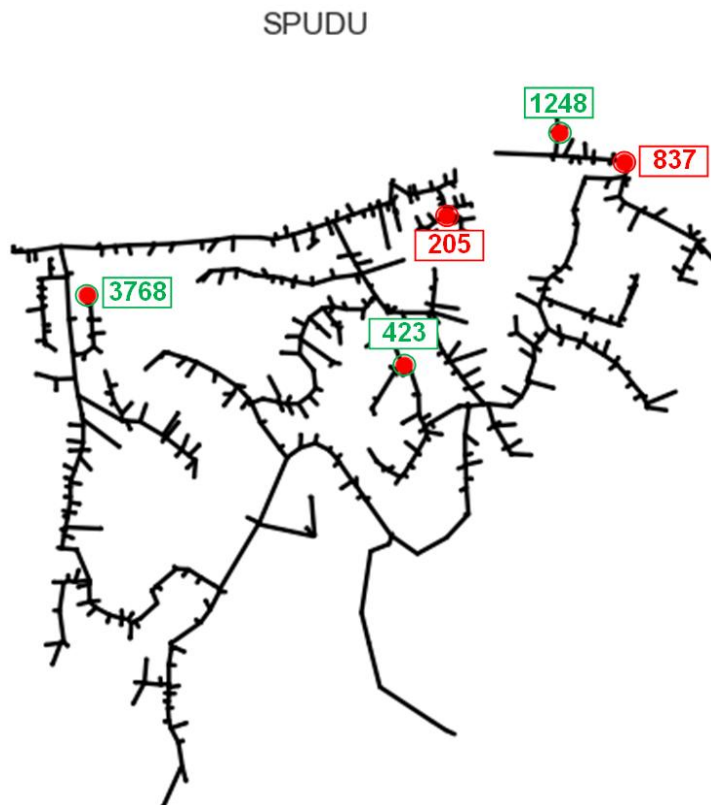
SPUDU

Table 3-4: Hydrant list SPuDU

hydrant no.	plan no.
HG3420	423
HG3933	205
HG4162	837
HG4215	1248
HG4383	3768

Figure 3.6: Sensor placement SPuDU (Steffelbauer, et al., 2014)
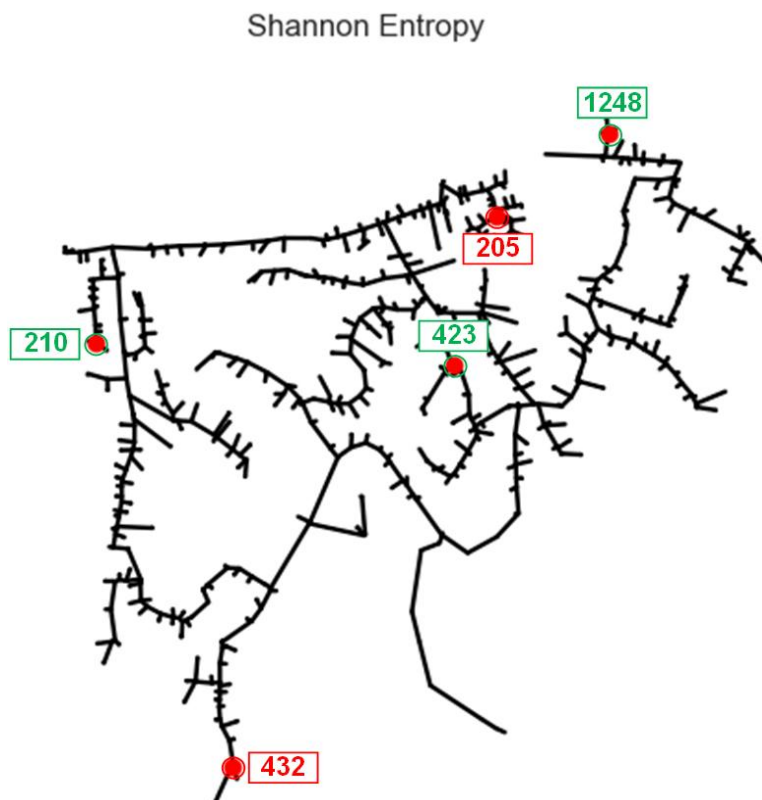
3.2.4 Sensor placement by Shannon entropy

Shannon Entropy

Table 3-5: Hydrant list Shannon Entropy

hydrant no.	plan no.
HG3420	423
HG3933	205
HG4215	1248
HG4339b	210
HG4744	432

Figure 3.7: Sensor placement Shannon entropy (De Schaetzen, et al., 2000)

This method tries to identify the optimal sensor positions by maximizing a sensitivity function and the Shannon entropy function using a GA search method (De Schaetzen, et al., 2000).

The result of this method shows the above-ground hydrants 205 and 432 (marked in red) and the underground hydrants 210, 423 and 1248 (highlighted in green) as the best nodes for leakage localization (see Figure 3.7).
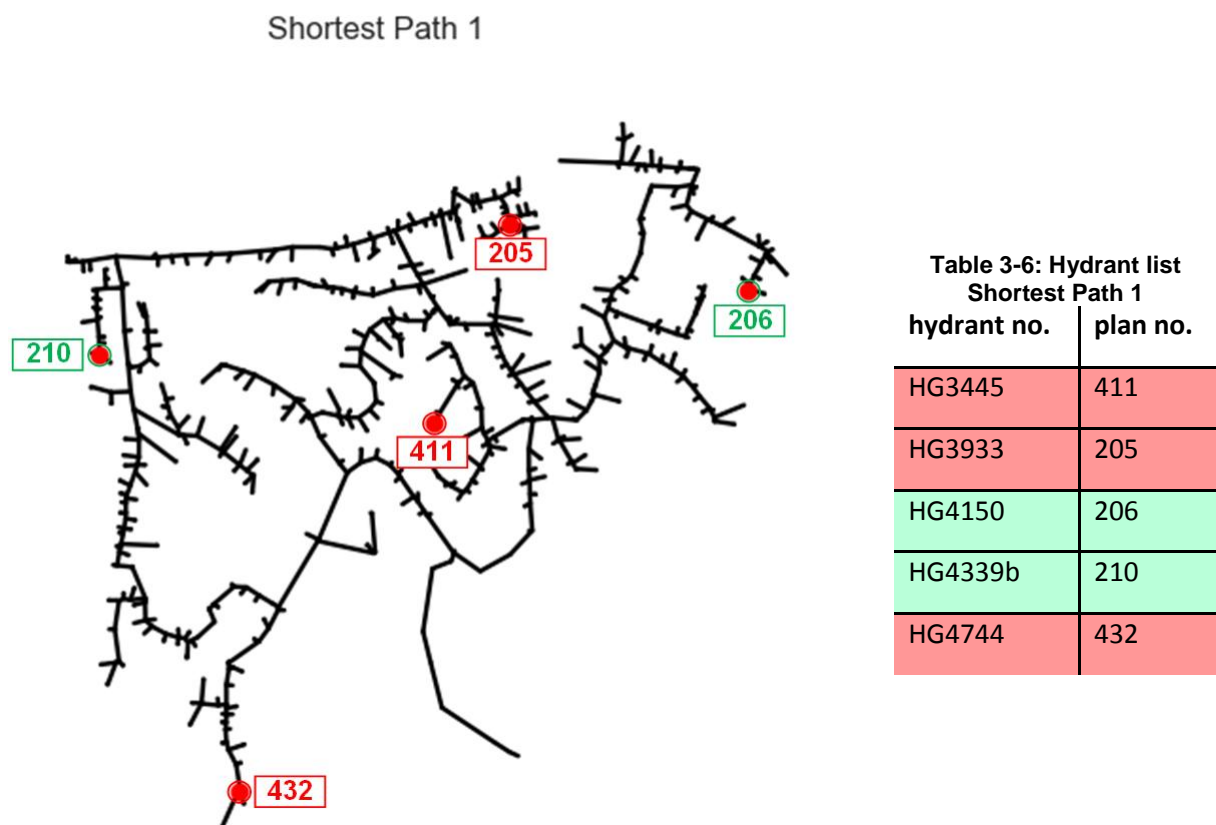
3.2.5 Sensor placement by Shortest Path 1

Shortest Path 1

Table 3-6: Hydrant list Shortest Path 1	
hydrant no.	plan no.
HG3445	411
HG3933	205
HG4150	206
HG4339b	210
HG4744	432

Figure 3.8: Sensor placement Shortest Path 1 (De Schaetzen, et al., 2000)

Shortest Path 1 method uses a topology-based algorithm to identify optimal sensor positions. It calculates the shortest path from the tank to every node in the network depending on the pipe length. The pressure measurements are located near the inner network (De Schaetzen, et al., 2000).

Using this method, the above-ground hydrants 205, 411 and 432 (marked in red) as well as the underground hydrants 206 and 210 (highlighted in green) resulted in being the best nodes for leakage localization (see Figure 3.8).

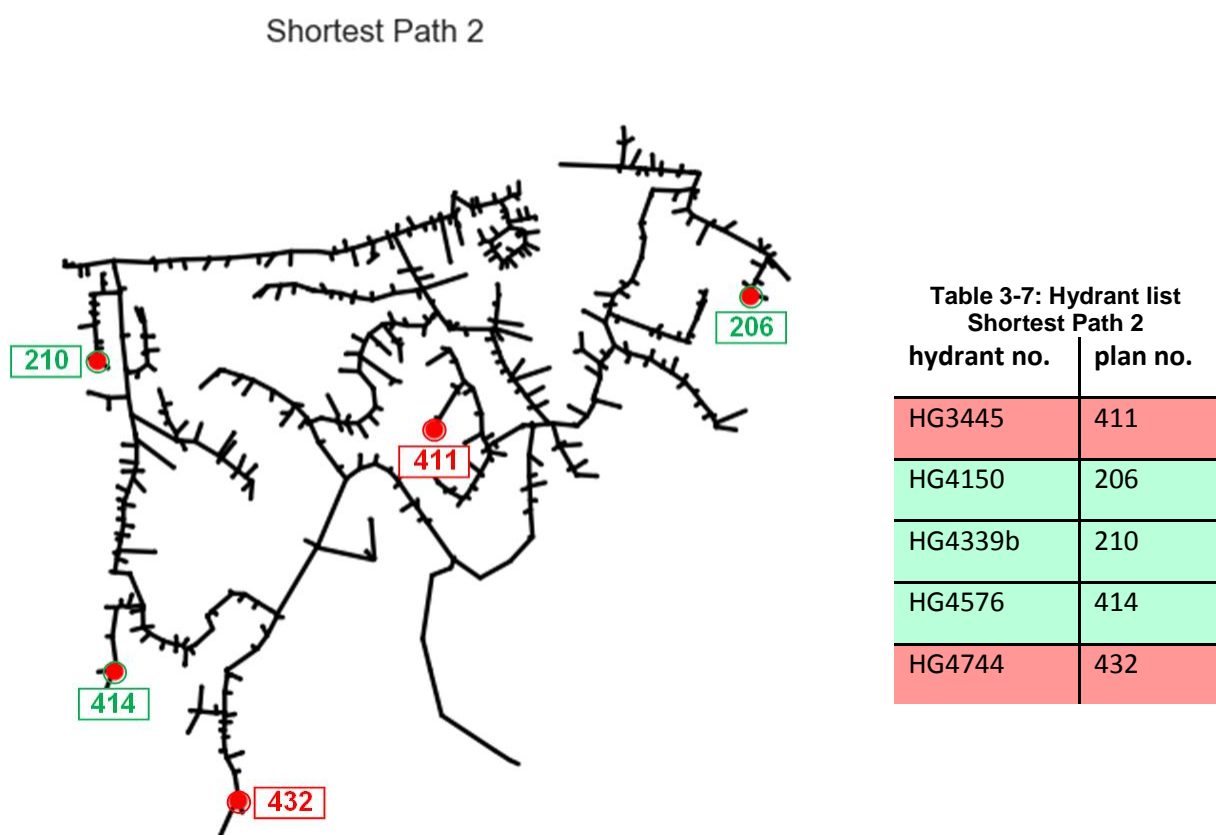### 3.2.6 Sensor placement by Shortest Path 2

The shortest path 2 method also uses the shortest path algorithm that calculates the shortest path from the tank to every node in the network depending on the pipe length. Additionally, all pipes along the shortest path from the tank to the node furthest away are set to a length of zero. The pressure measurements are located at the outskirts of the network (De Schaetzen, et al., 2000).

Here, the above-ground hydrants 411 and 432 (marked in red) and the underground hydrants 206, 210 and 414 (highlighted in green) were calculated to be the best nodes for leakage localization (see Figure 3.9).

Figure 3.9: Sensor placement Shortest Path 2 (De Schaetzen, et al., 2000)

Table 3-7: Hydrant list Shortest Path 2

hydrant no.	plan no.
HG3445	411
HG4150	206
HG4339b	210
HG4576	414
HG4744	432

Besides the pressure measurement also artificial leaks are generated in the WDS of Hart. The general build-up and the measuring process are presented in the following section.

3.3 Artificial leaks

During the measurements three leaks were simulated at different hydrants and different times in the WDS by opening selected hydrants. Each leakage was simulated for nine days. After three days the leak size (0.25 l/s, 0.5 l/s and 0.7 l/s or 1.0 l/s) was changed.

At the selected above-ground hydrants a fire hose with a length of 15 to 20 m was mounted. The fire hose was connected through a pipe coupling with a PE-pipe whose external diameter was 32 mm. At this PE-pipe there were clamp-on sensors installed which were linked with a measuring kit, a portable, ultrasonic flow measuring system "Prosonic Flow 92". This device was temporary metering the velocity of the fluid in order to calculate the volume flow by acoustic discharge measurement using the transit time principle (see also section 3.4.1). The clamp-on sensors are fixed to the piping from the outside. One measuring sensor is sending an ultrasonic signal which reflects on the other side of the pipe to the other sensor. The ultrasonic signal is sent alternating in flow direction and against. Due to the fact the water is propagating with a certain velocity the transit time of the signal in flow direction is shorter than the transit time against flow direction. This transit time difference Δt is a reference value for the average velocity v ($v \sim \Delta t$). According to the equation $Q = v * A$ where Q stands for the flow rate and A for the pipe cross-sectional area, the device calculates the flow from the measuring values. The "Prosonic Flow 92" has a built-in data logger with a capacity of 40,000 measuring values.
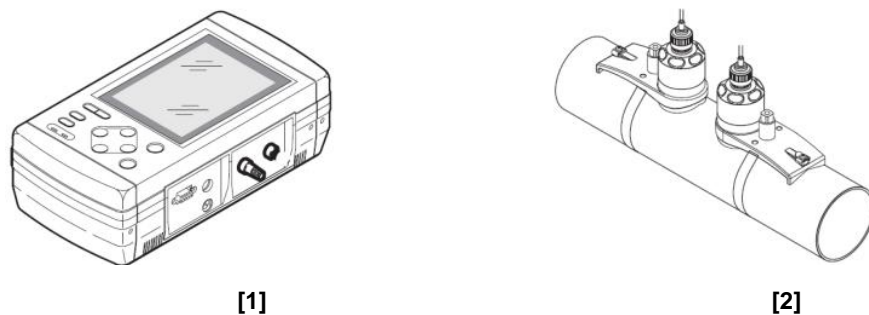

[1]   [2]

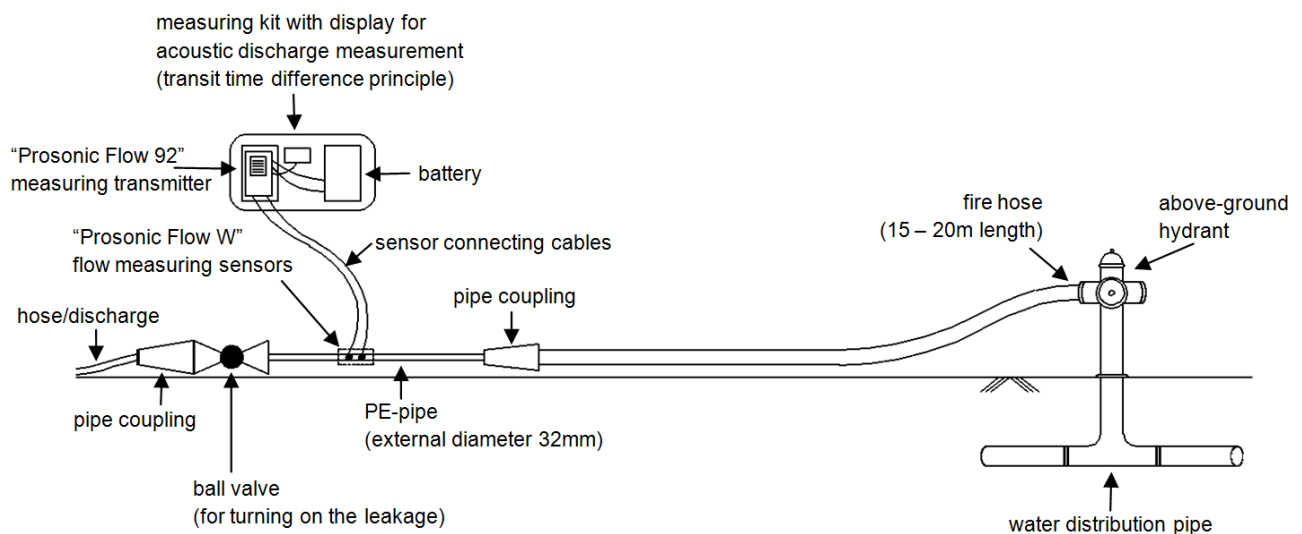**Figure 3.10: [1] "Prosonic Flow 92" measuring Transmitter; [2] "Prosonic Flow W" flow measuring sensors (Endress + Hauser)**
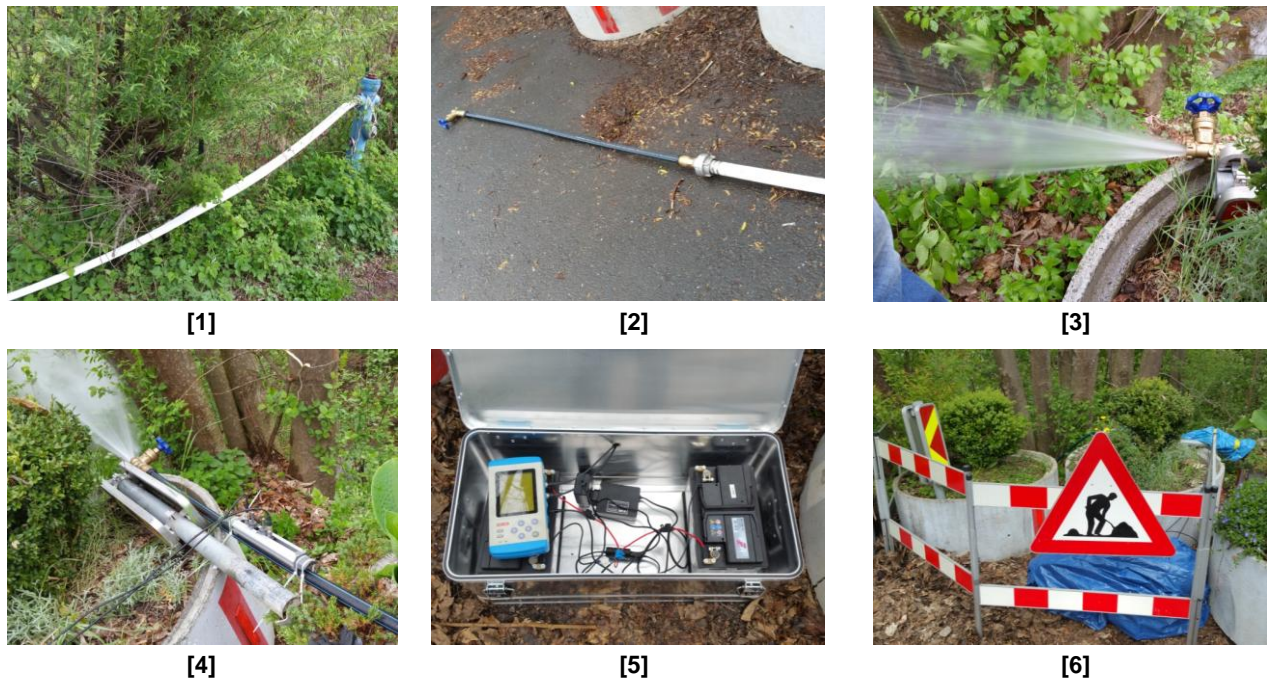

Figure 3.11: General build-up of the artificial leakage

33

Figure 3.12: Artificial leakage
[1] Above-ground hydrant with connected fire hose; [2] PE-pipe with closed ball valve;
[3] Opened ball valve; [4] "Prosonic Flow W" with flow measuring sensors;
[5] Measuring kit with "Prosonic Flow 92" measuring transmitter; [6] Closed-off area

The "Prosonic Flow 92" measuring transmitter, the power adapter and the battery were put in a metal case covered with a protection sheet to prevent the devices from rain and other influences.

The data gained of the measurements of the artificial leaks is visualized in Figure 4.2 to Figure 4.4.

3.4 Collecting the data

In this section the devices used to collect the measuring data from the flow meter and the pressure loggers are introduced and the procedure used is explained.

3.4.1 Ultrasonic flow meter at tank "HB Koppenhof"

The flow rate was measured at the tank "Koppenhof" with the FLUXUS ADM 6725, a portable, ultrasonic flow meter from the company FLEXIM. The clamp-on transducers are mounted directly on the pipe and the water supply must not be interrupted (non-invasive). The advantage of this flow meter is that the measurements do not cause any pressure drop. The transducers automatically send the data to the instrument upon connection. Only the pipe and fluid parameters have to be entered. The FLUXUS ADM 6725 has an internal database which contains many common pipe materials and fluids (FLEXIM GmbH, 2006).

In order to measure the flow of the medium the transit time difference correlation principle is used. Two transducers are mounted on the same side of the pipe. Ultra-

sonic signals are sent by one transducer, reflected by the opposite side of the pipe and received from the second transducer, alternating with and against the flow direction. As there is a flowing medium in the pipe, the transit time of the signals in flow direction is shorter than against the flow direction. This transit time difference Δt is measured and the average flow velocity can be calculated. The signals are checked for their usefulness and plausibility while the whole measurement process is controlled by integrated microprocessors to eliminate interfering signals. To read out the flow data the FLUXUS ADM 6725 is connected via a supplied cable to the PC and the data can be exported to Microsoft Excel.

Path of the ultrasonic signal

Transit time difference Δt

[1] [2] [3]

[4] [5]
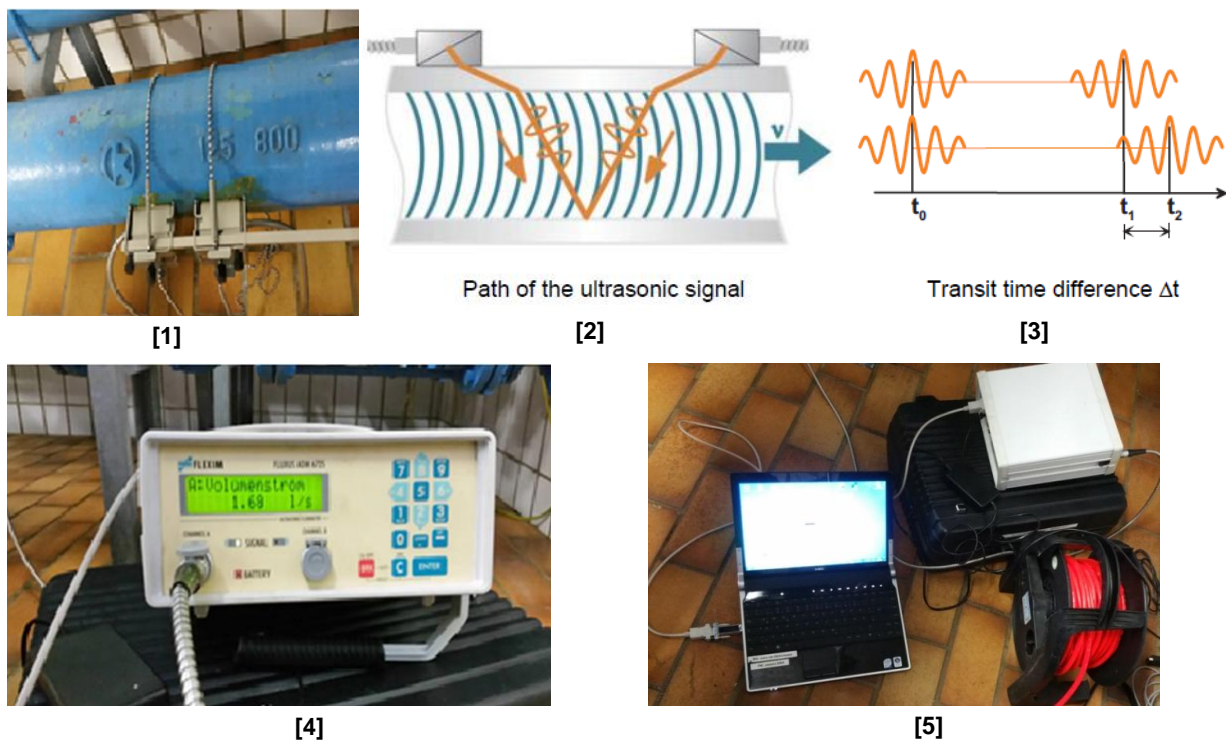
Figure 3.13: Flow meter FLEXIM FLUXUS ADM 6725
[1] 2 transducers mounted in reflex mode; [2] transit time difference correlation principle (FLEXIM GmbH, 2008); [3] transit time difference (FLEXIM GmbH, 2008) [4] FLUXUS ADM 6725; [5] Downloading the data from the flow meter

To read out the data from the flow meter FLUXUS ADM 6725 a PC has to be connected to it via cable. The installed software "FluxData" has to be opened. "FluxData" software enables to change measurements and parameters between the PC and the flow meter, gives a graphical presentation and statistical analysis of the results, and is able to convert the data files into other formats (FLEXIM GmbH). "COM4" has to be selected at Options/serial interface. The button "Connect" will start the download the data. After finishing the data transfer the user has to click on "<" to save the measured data. Then the measurements have to be deleted from the device´s memory. The measurement can be started again and the device is showing the actual flow rate.
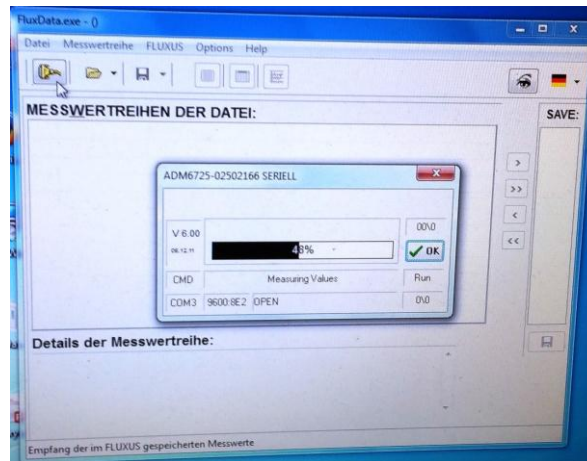
Figure 3.14: "FluxData" software

3.4.2 Pressure measurements in the field

For the measurements twelve pressure loggers named SEWAD 30 which are high precision, microprocessor-controlled manometers with digital display combined with a comprehensive data acquisition system, were installed. Five models were mounted directly onto above-ground hydrants and seven onto underground hydrants. The manometer works with a signal processor with a programmable analogue-to-digital converter. The SEWAD 30 has a pressure measuring range from 0 - 30 bar with 10 mbar resolution and an accuracy of ±0.2 %. The SEWAD 30 is able to record data periodically at intervals of 1, 5, 10, 15, 30 seconds or 1, 2, 5, 10, 30, 60 or 90 minutes. The used loggers were programmed to read out the data every minute with a PC using a supplied cable. The logger also displays the time and date for each pressure value. The storage capacity of the SEWAD 30 consists of 28,000 or 56,000 spaces depending on the interval (SETEC Engineering). Therefore, the data had to be read out once a week and later only biweekly. The data can be directly exported to Microsoft Excel for further evaluation.

The pictures below (Figure 3.15) show how the SEWAD 30 pressure loggers were mounted on the hydrants and how the data was collected. On rainy days some of the underground hydrants were filled with water, so it had to be pumped down before reading out the data. Hydrant 206 was continuously filled with water due to a broken draining. In Figure 3.2 it can be seen where exactly the pressure loggers were installed.
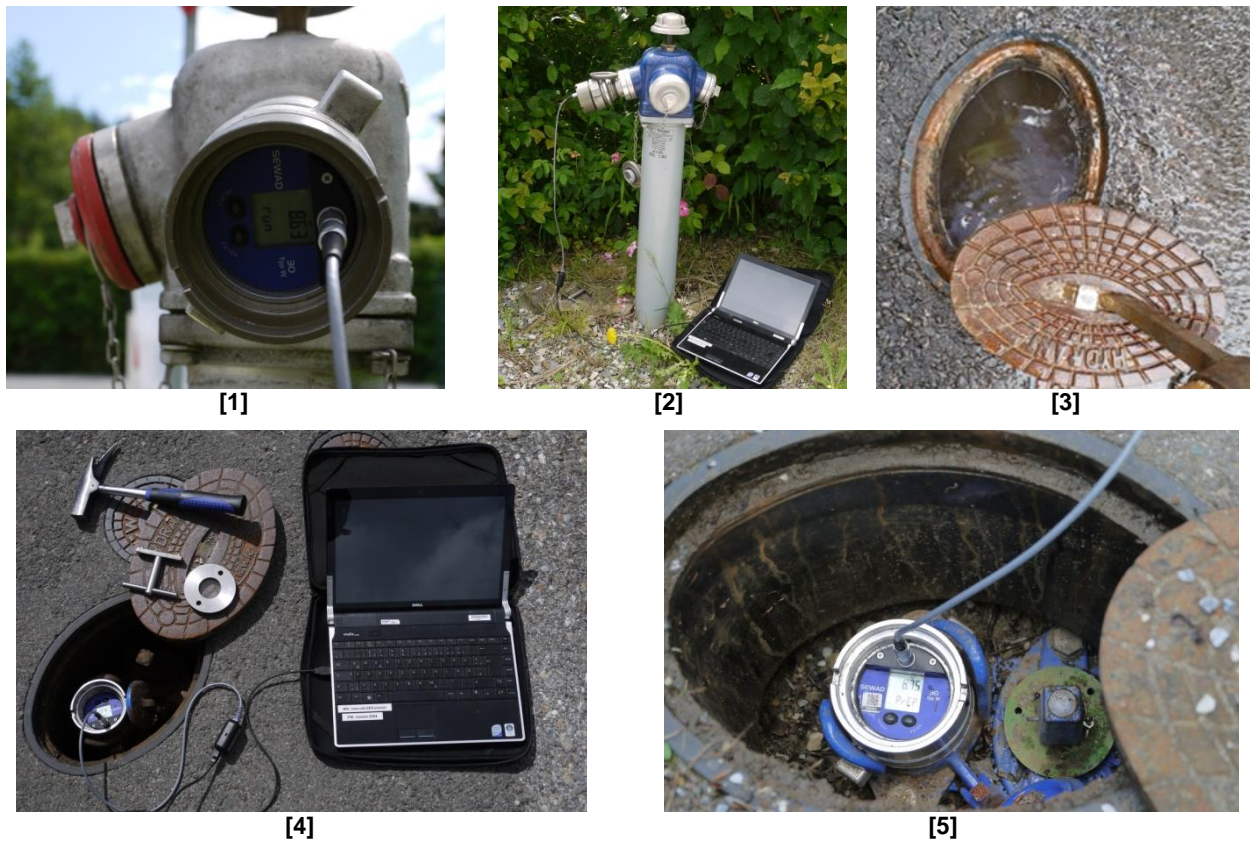
Figure 3.15: Pressure logger SEWAD 30
[1] and [2] Above-ground hydrants with pressure loggers; [3] Underground hydrant under water (206);
[4] Downloading data from pressure logger; [5] Underground hydrant with pressure sensor

First, the cover panel of the pressure logger at the hydrant has to be opened and any dust or sand on the sensor has to be cleaned carefully before opening the device. To read out the data from the logger the cable with the K 104-A converter has to be connected to the sensor (red dots) and the USB has to be linked to the PC. The program "Logger 5.2" has to be started. The "Logger 5.2" software is used for reading data from a logger device, configuration and programming, chart visualization, graphical chart viewer, printing reports, exporting data in different formats, and calculating water levels (Keller AG für Druckmesstechnik, 2014). In Figure 3.16 the main windows of the program are visualized.

In the program´s "Wizard" the operator has to click first on the button "Reading Data from Device" and then "Read Newest Record". Afterwards proceed with "CSV_1". The user has to click on "Export", then choose "CSV_1" and "UTF-8" and click on "Convert". The data can now be exported and the .csv-file can be renamed. After closing this window the operator has to click on "Programming" to adjust the record interval. The buttons "Endless", "Immediately when writing configuration" and "Use PC time", only if the time is correct, have to be chosen. The user has to check whether the event data record is enabled and then clicks on "Write configuration" and "OK". When the sensor displays "Run", the program can be closed and the cable can
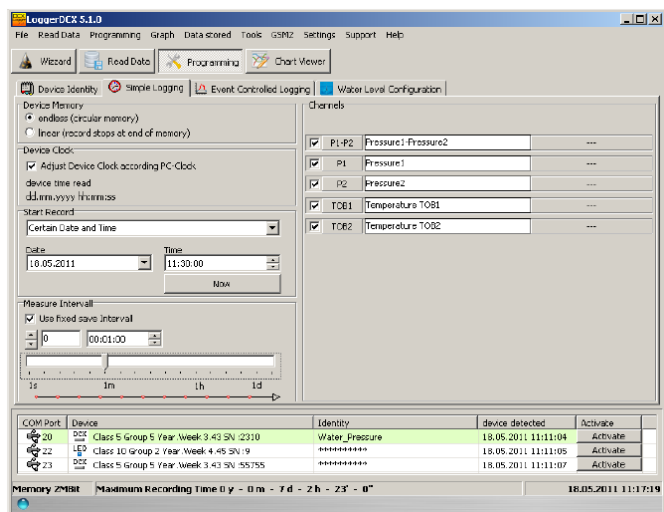
37

be disconnected from the pressure logger. Finally, the cover panel of the hydrant has to be closed again.
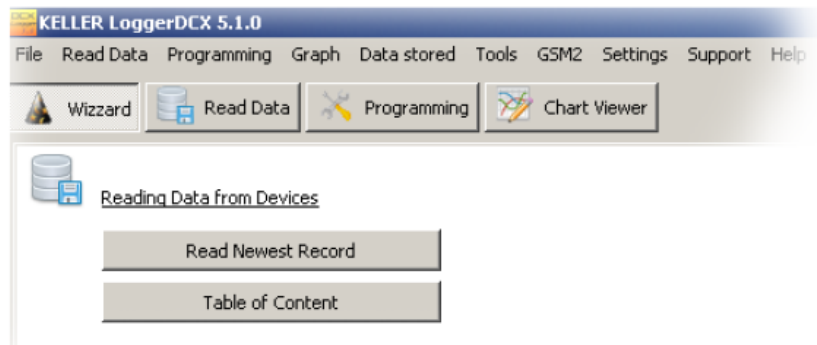
[1]
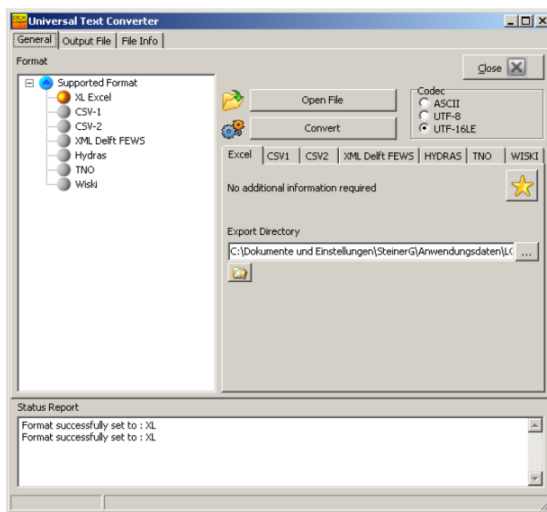
[2]   [3]

Figure 3.16: "Logger 5.2" software [1] Wizard; [2] Converter; [3] Programming

3.5 Preparation for evaluation

First of all, it is important to process the measuring data in order to be able to evaluate the results. Additionally to the artificial leaks night measurements were conducted. These measurements are used for the calibration of the hydraulic EPANET model which was performed by Kapala (2016). Although the model calibration was not part of this study the approach of the night measurements is briefly described in the following because the data is used to test the leakage localization.

3.5.1 Night measurements

The calibration measurements were conducted during the night of April 11th, 2016. For these night measurements the record interval was set to one second. These measurements were done by opening selected hydrants in the water distribution network to reach a specific flow in a set time.

The amount of water [l/s] taken from each hydrant corresponds to the values in Table 3-8. After the first round, a leakage of one l/s was simulated at node HG3880 for about 15 minutes. Then, a leakage of one l/s was simulated at node HG3537 for approximately 15 minutes. After the second round of the hydrant opening a leakage of one l/s was simulated at node HG3302 for about ten minutes.

Table 3-8: Calibration measurements ([1] first round; [2] second round)

Time [min]	HG3880 [l/s]	HG3409 [l/s]	HG4118 [l/s]	Time [min]	HG4504 [l/s]	HG3537 [l/s]	HG3302 [l/s]
5	15	0	0	5	10	0	0
10	8	8	0	10	6	6	0
15	5	5	5	15	5	5	5
20	0	16	0	20	0	16	0
25	0	7	7	25	0	6	6
30	0	0	12	30	6	0	6
35	7	0	7	35	0	0	9
		[1]				[2]	

The mean values of the inflow, the leakage outflow and the pressures were calculated for the three leaks of 1.0 l/s and for one leak of 9.0 l/s during the night measurements. For the 1.0 l/s leak the average of a ten-minute period was calculated ending at the last peak of the leak. For the 9.0 l/s leak the values of only three minutes were taken. In Figure 3.17 these periods are marked in red.
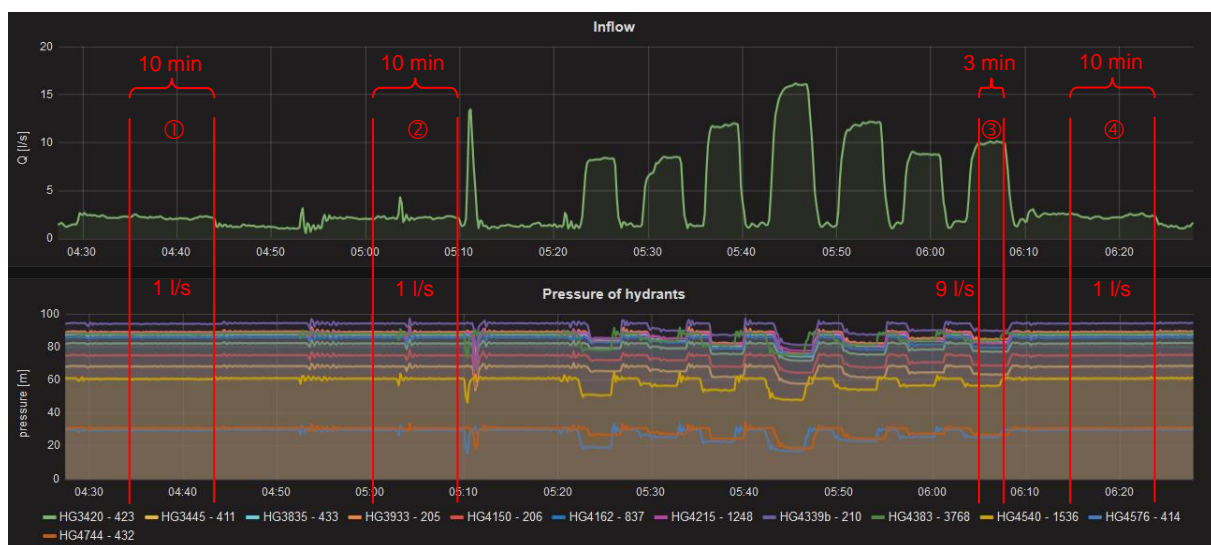

Figure 3.17: Evaluation of the night measurements

The average pressure values were ordered by the different sensor placements which have been introduced in section 2.3. Table 3-9 presents the average pressure values calculated with the sensor placement methods Casillas and SPuDU.

Table 3-9: Mean values of the night measurements

	hydrant ID	③	④	②	①
leakage [l/s]	Q_HG3302	9.079235713	1.054610344		
	Q_HG3537			1.051664146	
	Q_HG3880				1.023957428
inflow [l/s]	Q_LHG2461a	9.975248619	2.349617304	2.224126456	2.202778702
period		3min	10min	10min	10min

Sensor place-ment method	hydrant ID	Ø pressure [mWC]	Ø pressure [mWC]	Ø pressure [mWC]	Ø pressure [mWC]
Casillas	HG3420	77.12068530	81.99683078	81.96451156	82.02476679
	HG3835	82.84484541	87.28976276	87.18027719	87.20015398
	HG3933	84.64095171	89.09540038	88.99161792	88.95101612
	HG4215	82.05859122	88.09999705	88.11921564	88.18179825
	HG4383	83.61330801	88.02977704	87.91336140	87.75672534
SPuDU	HG3420	77.12068530	81.99683078	81.96451156	82.02476679
	HG3933	84.64095171	89.09540038	88.99161792	88.95101612
	HG4162	79.49921492	85.55562923	85.54823597	85.63162564
	HG4215	82.05859122	88.09999705	88.11921564	88.18179825
	HG4383	83.61330801	88.02977704	87.91336140	87.75672534

The data shown in Table 3-9 was put separately for each sensor placement method and each leakage scenario into files in a toml-format. During the night measurements 24 toml-files which were used as input files for the access software "Jenkins" were generated. This program will be introduced in section 3.6.

3.5.2 Measurements at hydrants

Figure 3.18 shows the evaluation of the leakages using the example of the first leak at hydrant HG3880. For each size of the leak (0.7 l/s, 0.25 l/s, and 0.5 l/s) the mean values were generated for the significant time period from 01:00 to 04:00 am. For the purpose of leak localization the minimum night consumption is of interest, since at that time customers demand is low and the leak component is at its largest percentage. In Figure 3.18 these periods are marked in red.

From the individual average values of each leak size a new mean value was generated. This was done with all leaks at the three hydrants and all sizes.

Figure 3.18: Evaluation of the leak measurement at hydrant HG3880

In Table 3-10 the mean values of the leak measurements are presented in an extract of the leak simulation at hydrant HG3880 and the sensor placement SPuDU. The mean values which were used for further calculations in the program "Jenkins" are highlighted in grey. The complete table with the mean values of all sensor placements of the leakage at HG3880 is presented in Table 4-2and Table 4-3.

Table 3-10: Mean values of the leak measurements (example: HG3880 - SPuDU)

leak 1 – HG3880					
period	01:00 - 04:00				
date			18.04.2016	19.04.2016	20.04.2016
			0.7 l/s		
leakage [l/s]			0.71425	0.68918	0.67326
mean [l/s]				0.69222939	
inflow [l/s]			1.71930	1.64954	1.65937
mean [l/s]				1.67606901	
	hydrant ID		**Ø pressure [mWC]**		
	HG3420	423	82.17515	82.29633	82.46404
				82.31184249	
	HG3933	205	89.19217	89.32188	89.50220
				89.33875354	
SPUDU	HG4162	837	85.80798	85.92101	86.07456
				85.93451854	
	HG4215	1248	88.35352	88.44954	88.61276
				88.47194004	
	HG4383	3768	88.07471	88.25811	88.42454
				88.25245319	

41

After calculating these mean values input files for the access software "Jenkins" were generated for each sensor placement method and each leakage scenario. For these leak measurements 56 input files were created. One example of such an input file is depicted in Figure 3.19. The parameters which vary between the files are marked in red.

```
[Epanet]
Name = "Ragnitz_Simple.inp"
Sensor_Placement = "SPUDU"
Leak = "HG3880"
Leakage_Outflow = 0.69222939
Precision_Flow = 3
Precision_Pressure = 2

[Flow]
M171 = 1.67606901

[Pressure]
HG3420 = 82.31184249
HG3933 = 89.33875354
HG4162 = 85.93451854
HG4215 = 88.47194004
HG4383 = 88.25245319

[Genetic_Algorithm]
Population = 30
Generations = 100
Variables = 2
CR = 0.7
F = 0.5
CE_Min = 0.0
CE_Max = 1.0
Similarity_Measure = "euclidean"
Similarity_Attributes = "None"
Weighting_Factor_Flow = 1
```

Figure 3.19: "Jenkins" input file (example: 0.7 l/s leak at HG3880, SPuDU)

The name "Ragnitz_Simple.inp" is the name of the uncalibrated EPANET model of the WDS. This model was modified during this study several times to improve the results. Further, the input file consists of the name of the sensor placement method and the average values of inflow, leakage and pressure. The algorithm (DE) which was used in this calculation is presented in section 2.2.

For the leakage localization in this study the mutation factor F was set to 0.5 and the crossover ratio c_R equalled 0.7 for every simulation (Steffelbauer, et al., 2016). The limits of the emitter coefficient was set to $c_{e\_MAX} = 1.0$ and $c_{e\_MIN} = 0.0$. For these calculations a population of 30 was used and the process of DE terminated when a number of 100 generations is reached. Due to the fact that each iteration provided one possible solution the process was repeated 100 times.

3.6 Jenkins – access software to Python/ EPANET

"Jenkins" is an open source tool written in Java which provides continuous integration and continuous delivery of projects. Continuous integration is a development practice where developers are able to integrate code into a shared storage at regular intervals. "Jenkins" is a server-based system which can be integrated with a number of testing and development technologies. The program is installed on a server where the central build takes place.

"Jenkins" was used in combination with EPANET and Python. The EPANET model was integrated through the EPANET Programmer´s Toolkit by the programming language Python. Python is a high-level, general-purpose, freely available, interpreted, and dynamic programming language (Python, 2016). Figure 3.20 displays the surface of "Jenkins". In order to start the calculation the arrow to the right of "sww_azm_leakage_localization" has to be selected.
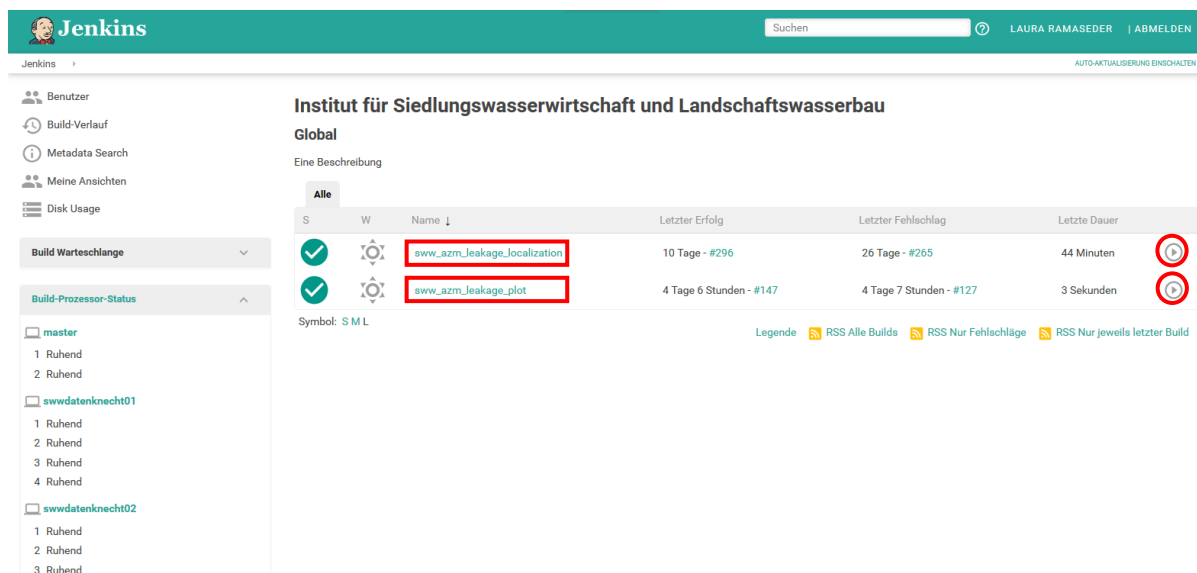

Figure 3.20: Jenkins - leakage localization

Afterwards, the window shown in Figure 3.21 will open. The input files are uploaded here by clicking on "Durchsuchen". When the file is selected the build will start by pushing the button "Build". This process was repeated with all generated input files. The results of the calculation are output files with a txt-format. An example of such an output file will be presented in section 4. The calculation with a single input file takes about 45 minutes.

Afterwards, the output files were exported to Microsoft Excel and the evaluation was done manually. Histograms which show the results depending on the found nodes for the leakage were created. These also display the distance from the found leak to the real leak. The leak plot was also generated manually for the first results of the calculations. It illustrates the real leakage and shows how often a node was found as leak by the algorithm.

The code of "Jenkins" was modified, so it was possible to plot the results by clicking on the arrow right of "sww_azm_leakage_plot" (highlighted in red in Figure 3.20). In the opening window (Figure 3.21) the toml-input file and the appropriate txt-output file can be uploaded. The plotting will start by pushing the button "Build".
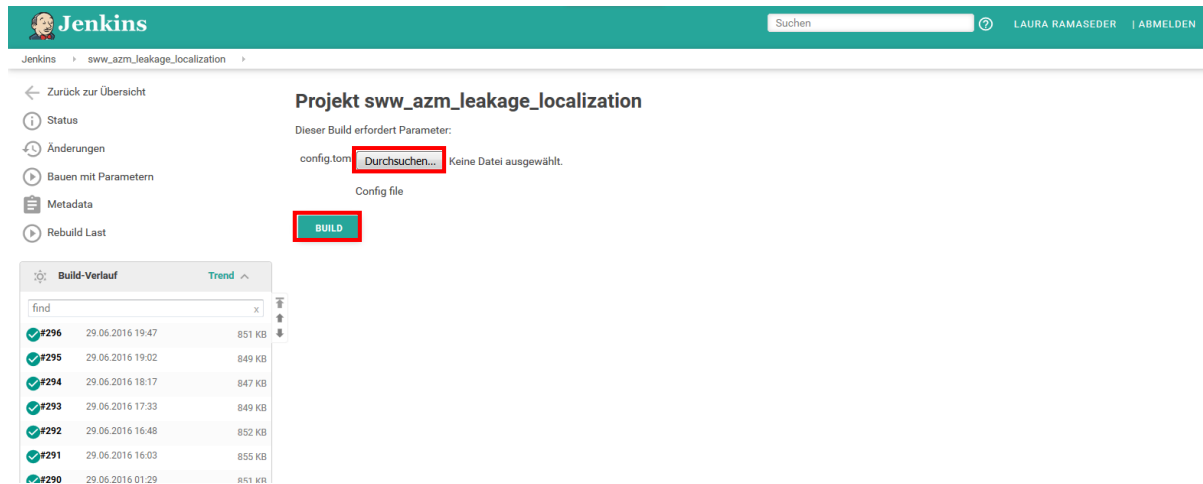
Figure 3.21: Jenkins - upload of the input file (.toml-file)

The output files of this build are the leak plot and histograms of the nodes where the leakage was found, the distance from the found leak to the real leak, and the outflow. The plotting only takes a few seconds.

In Table 3-11 an output file by "Jenkins", is presented with an example of a 0.7 l/s leakage at the hydrant HG3880 calculated on the basis of the sensor placement method SPuDU.

Table 3-11: Output file (example: 0.7 l/s leak at hydrant HG3880, SPuDU)

	leak measured	leakage outflow simulated [l/s]	distance to leak [m]	leak simulated [l/s]	fitness value	leakage outflow measured [l/s]
0	HG3880	0.72	491.669137	HG4383	0.243226550	0.69222939
1	HG3880	0.72	491.669137	HG4383	0.243226550	0.69222939
2	HG3880	0.63	360.535348	K1_62	0.265734575	0.69222939
3	HG3880	0.72	491.669137	HG4383	0.243226550	0.69222939
4	HG3880	0.72	491.669137	HG4383	0.243226550	0.69222939
5	HG3880	0.63	581.382822	K1_97	0.271647511	0.69222939
6	HG3880	0.63	581.382822	K1_97	0.271647511	0.69222939
7	HG3880	0.63	301.023108	K1_11	0.271647511	0.69222939
8	HG3880	0.72	491.669137	HG4383	0.243226550	0.69222939
9	HG3880	0.63	360.535348	K1_62	0.265734575	0.69222939
10	HG3880	0.72	491.669137	HG4383	0.243226550	0.69222939
11	HG3880	0.63	581.382822	K1_97	0.271647511	0.69222939
12	HG3880	0.64	491.669137	HG4383	0.244082830	0.69222939
13	HG3880	.	.	.	.	.
14	HG3880	.	.	.	.	.
15	HG3880	.	.	.	.	.

44

The values from the columns "leakage measured" and "leakage outflow measured" are parameters from the input file. The column "leakage simulated" shows the nodes where the leakage is found in the EPANET model and the distance from the measured leakage to the simulated leakage is calculated in meters (m). The fitness value in conjunction with the term "GA" are explained in section 2.1.

As set in the input file each calculation was conducted 100 times with 100 generations. Therefore, each output file consists of 100 lines of possible solutions. The results of these output files are demonstrated in leak plots and histograms in the following section 4.

3.7 Calculation scenarios

In each scenario the calculations in "Jenkins" in combination with EPANET and Python were performed with the measuring data which were received from the field measurements, but the EPANET model of the WDS was slightly modified to improve the results. Three different hydraulic models were analyzed: the uncalibrated model, the calibrated model and the recalibrated model.

3.7.1 Uncalibrated model

At the beginning, the builds were calculated using an uncalibrated EPANET model named "Ragnitz_simple". In this model the roughness values of the pipes are generally set at 0.1 mm (Figure 3.22).
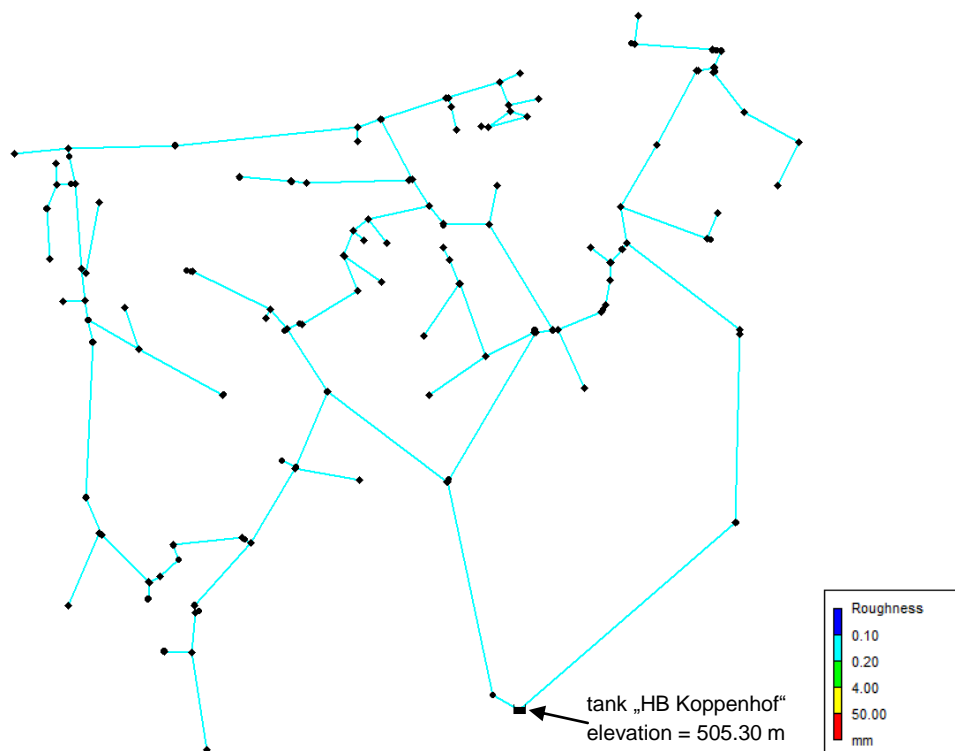
Figure 3.22: Uncalibrated EPANET model (roughness = 0.1 mm)

3.7.2 Calibrated model

Afterwards, the calculations were done with a calibrated EPANET model. The file names had to be changed in the toml-input files from "Ragnitz_simple" to "Ragnitz_calibrated". The hydraulic model (Ragnitz_simple) was calibrated in terms of pipe roughness. Therefore, calibration measurements which are mentioned in section 3.5.1 were conducted during the night of April 11th, 2016.

A programmed calibration algorithm calculated the roughness for each pipe. The EPANET model with the adjusted roughness values is displayed in Figure 3.23.
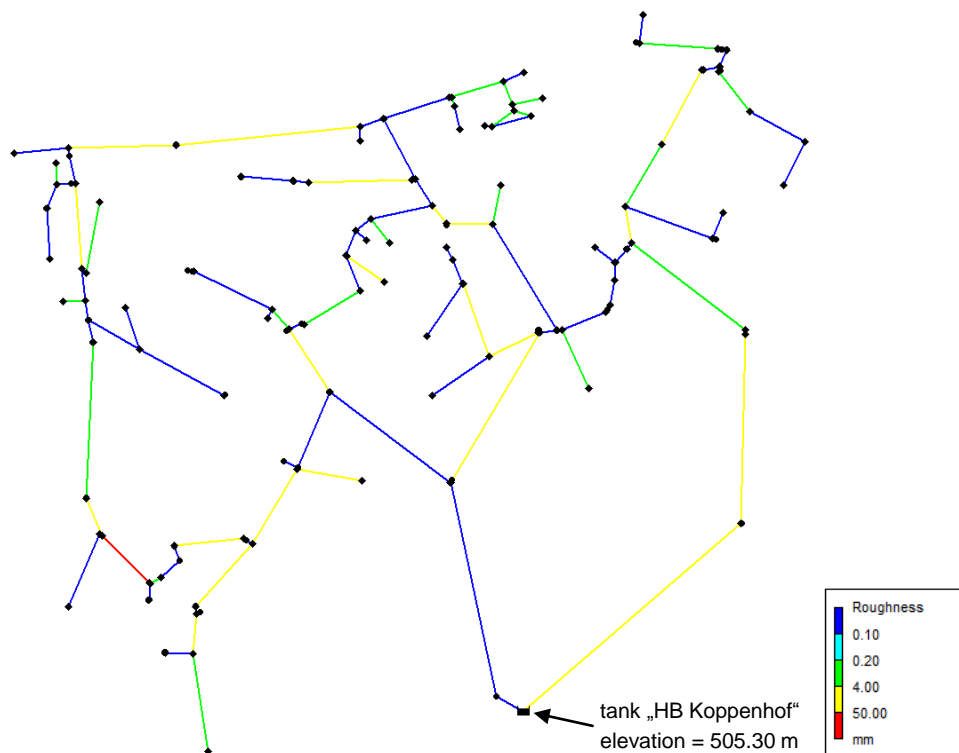
Figure 3.23: Calibrated EPANET model (adjusted roughness values)

3.7.3 Recalibrated model

Similar to the results of the calculation with the previous calibrated model (Ragnitz_calibrated) the results of the recalibrated model were not as precise as expected. Thus, some changes have been made to improve the calibration of the model and the elevation of the tank was reduced by a height of 2.5 m. The new input file was named "Ragnitz_Simple_Recalibrated.inp". The EPANET model with the adjusted roughness values and the change of the tank elevation is displayed in Figure 3.24.
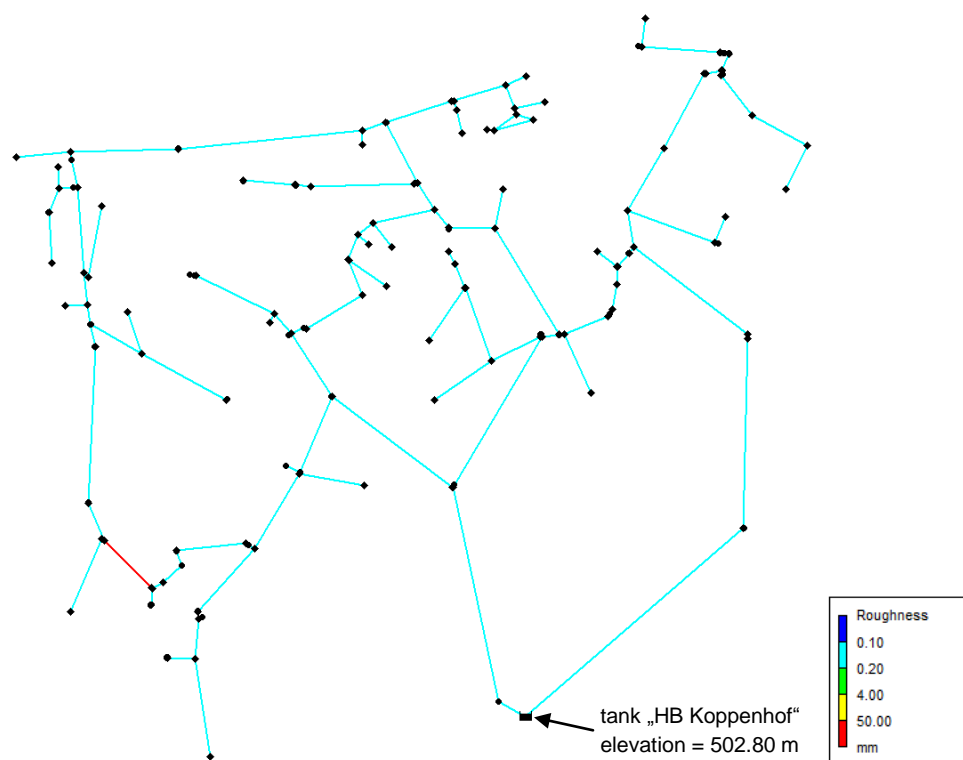
Figure 3.24: Recalibrated EPANET model (adjusted roughness values, change of tank elevation)

4 Representation of the results

In this section the results of the measurements from the described case study which were calculated using the simulated model of the WDS in EPANET are presented.

After collecting the data from the flow meter, the pressure loggers, and the artificial leaks, the data can be visualized with the data management system "Grafana". This program depicts time series data and features pluggable graph panels with many visualization options. "Grafana" is connected to a server at TU Graz where the data of all measurements are stored and "Grafana" can access them. In Figure 4.1 an example of the calibration measurement is shown. In the first panel the flow can be seen. The x-axis represents the time in 10-minute-intervals and the y-axis indicates the outflow in l/s. In the second panel the pressure of all twelve hydrants with pressure loggers is shown. The y-axis displays the pressure in m, the x-axis is identical to the graph above. It is visible that if there is an outflow the pressure in the network decreases. The greater the outflow the greater the pressure loss (see Figure 4.1). If the outflow is one l/s or less the pressure drop is not clearly recognizable. Normally, the pressure loss happens at the same time as the hydrant is opened. When looking at the Figure 4.1 more deeply a small time delay is visible. This arises because the times at the pressure sensors and the flow meter were not well aligned with each other.

Figure 4.1: Night measurements

4.1.1 Leakage measurements

The first leak was simulated at hydrant HG3880 from April 17th to April 25th, 2016. The first panel of Figure 4.2 shows the inflow which was measured at the "HB Koppenhof". The typical diurnal variations of the water consumption of the residents with peaks in the morning and evening are visible. The second panel illustrates the flow rate of the opened hydrant. At first, the outflow of the hydrant was adjusted to ap-

proximately 0.7 l/s for three days. Afterwards, the outflow was set to 0.25 l/s. In Figure 4.2 the second panel shows a small increase of outflow from 0.25 l/s to 0.33 l/s. This probably happened because a resident of the area turned up the ball valve a little bit.
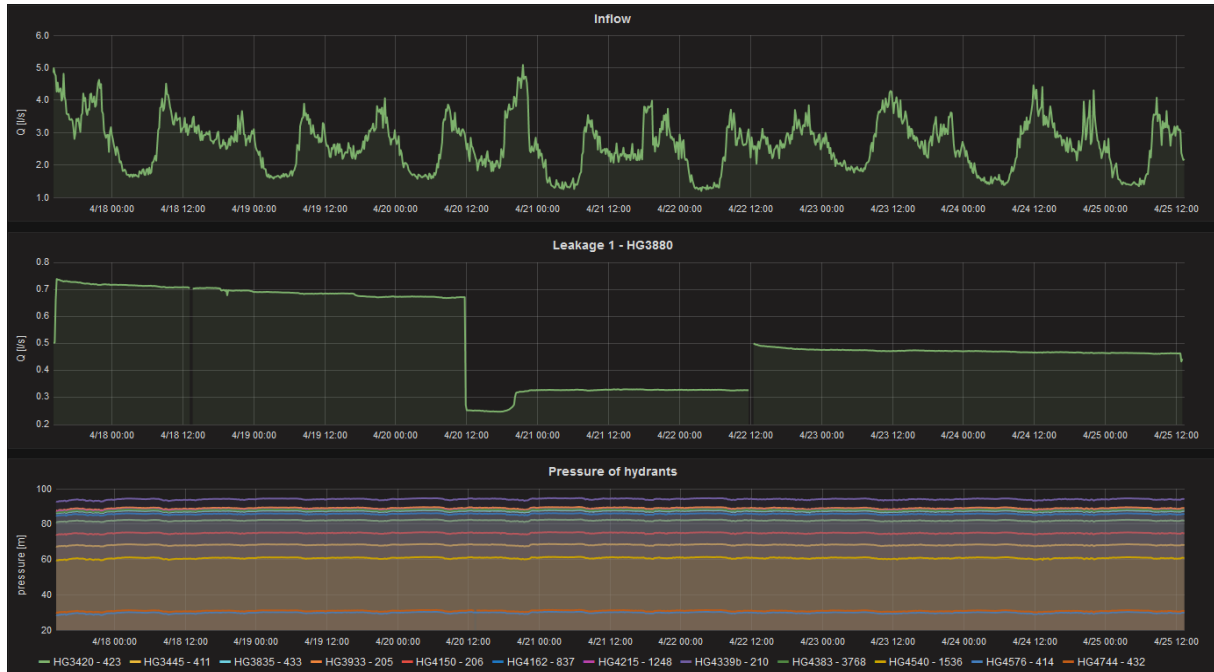

Figure 4.2: Leakage measurements HG3880

Then the outflow of the hydrant was set to about 0.5 l/s. The third panel represents the pressure of all twelve selected hydrants. In reality there was a pressure drop caused by the outflow but due to the fact that the outflow was small it is not visible in the diagram. When looking at Figure 4.1 for example, the decrease in pressure in case of a leak can be noticed when the hydrant was opened with a flow rate of 15.0 l/s.

For the second leak the hydrant HG4504 was opened from April 25th to May 4th, 2016. First, the outflow was set at 0.25 l/s, then at 0.5 l/s, and finally at 0.7 l/s (Figure 4.3).
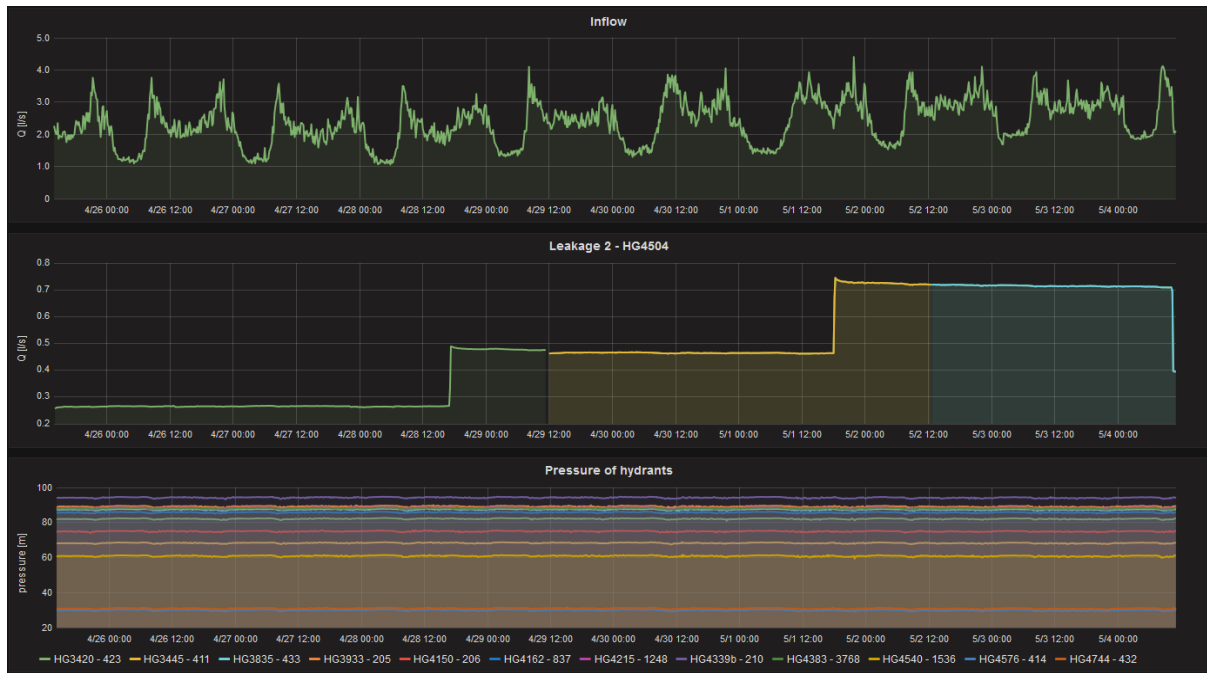
Figure 4.3: Leakage measurements HG4504

The third leak was simulated at hydrant HG3164 from May 9th to May 18th, 2016. At the beginning the outflow amounted to 0.5 l/s. After three days it has risen to 0.7 l/s and finally the flow rate was 0.25 l/s (Figure 4.4).
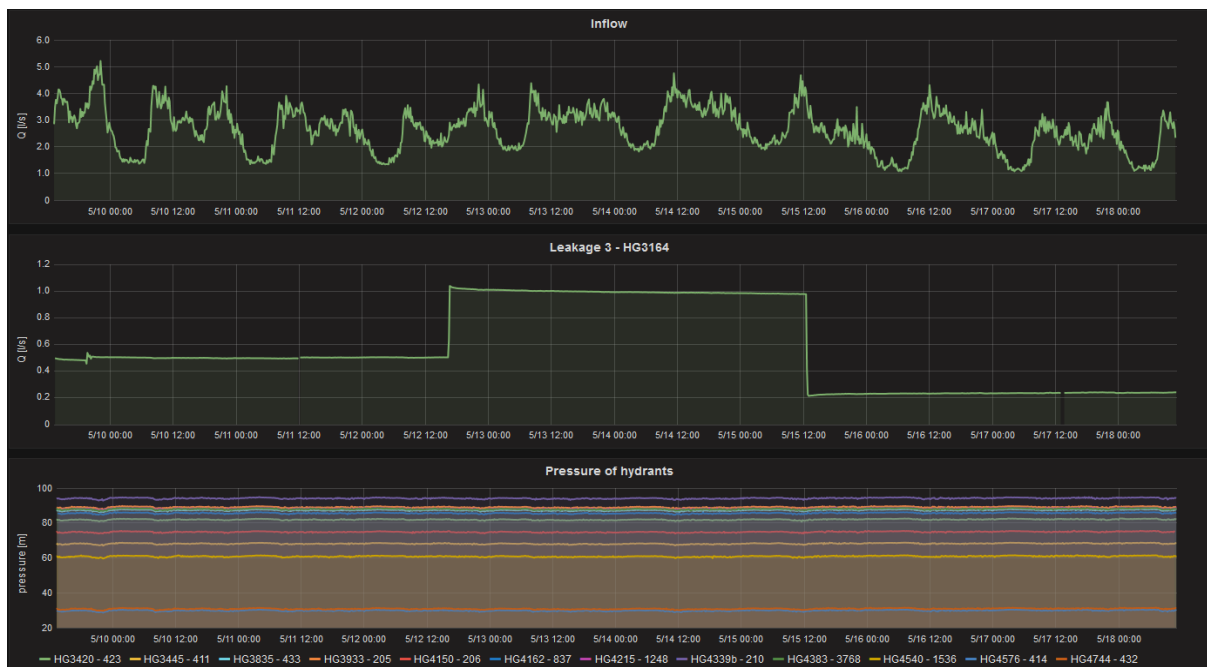
Figure 4.4: Leakage measurements HG3164

When looking at Figure 4.2 to Figure 4.4 it can be noticed that the outflow of the leak was decreasing bit by bit. The reason for this was the inconsistency of the PE-pipe´s diameter.

Therefore, the external diameter of the pipe was measured at four different days (under pressure and pressureless) during the leakage measurements. The results of these measurements are presented in the following section.

4.2 Varying diameter of PE-pipe

The external diameter of the PE-pipe was measured three times on April 25th, 2016 during the simulating of the first leak at hydrant HG3880, twice while the pipe was under pressure and once pressureless. During the second leak at hydrant HG4504 the diameter was metered on April 26th and 28th and on May1[st], 2016 every time under pressure. Figure 4.5 illustrates an example of the 1.0 l/s leakage measurement at HG3164.

Leckage measurement at HG3164
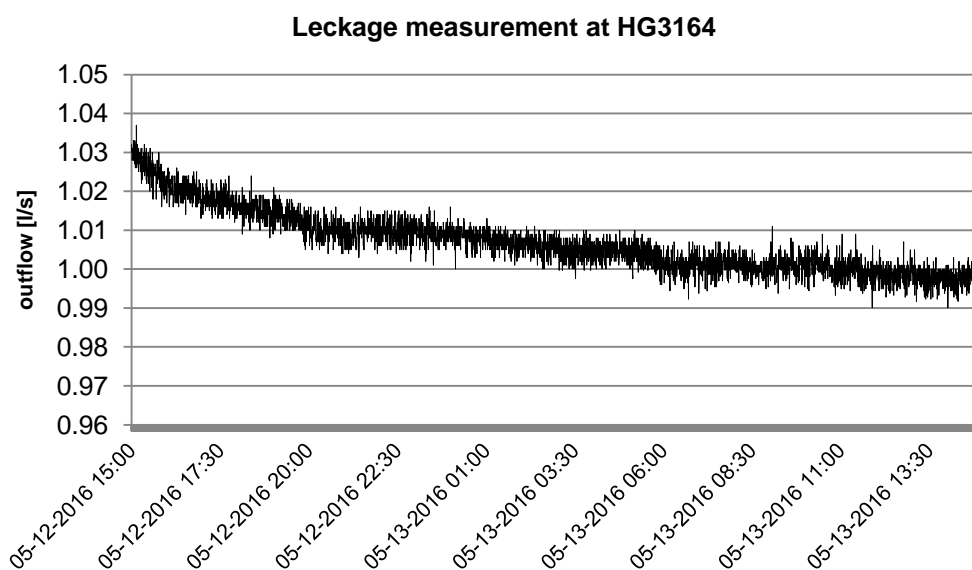
Figure 4.5: Leakagemeasurement at HG3164

At the measuring device the diameter was adjusted to 32 mm. The diameter slightly varies depending on the working pressure. According to the equation $Q = v * A$, assuming that the velocity is constant, if the diameter increases, the cross-sectional area also increases while the outflow decreases. The measuring device can not react to the variation of the diameter, so the graph shows that the outflow is decreasing although Q is constant in reality. Table 4-1 shows the measurements of the external diameter of the PE-pipe. UP represents that the pipe is under pressure, PL means the status of the pipe is pressureless.

51

Table 4-1: PE-pipe measuring section - external diameter
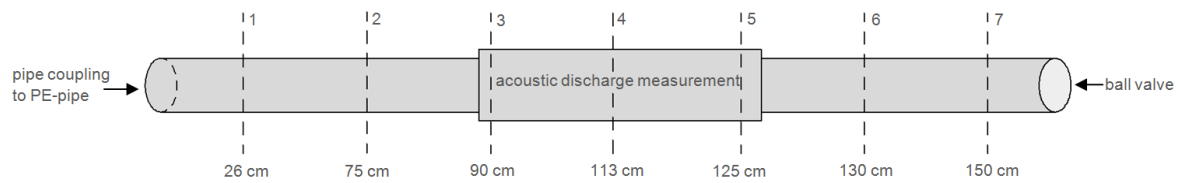
date	nr.	1 [mm]	2 [mm]	3 [mm]	4 [mm]	5 [mm]	6 [mm]	7 [mm]	status	outflow [l/s]
	1	32.40		32.35	32.40	32.40			UP	0.44
25.04.2016	2	32.40		32.30	32.40	32.60		32.70	PL	0
	3	32.60		32.60	32.70			32.70	UP	0.25
26.04.2016	1	32.70	32.70				32.85	32.85	UP	0.25
28.04.2016	1	32.70	32.90	32.80	32.70	32.70	32.45	32.80	UP	0.48
01.05.2016	1	32.70	32.70	32.30	32.30	32.70	32.70	32.70	UP	0.75

As already described in section 3.5 the mean values of the inflow, the leakage, and the pressures were generated for the night time period. This was done for each size of leak (0.7 l/s, 0.25 l/s, and 0.5 l/s).

4.3 Mean values

Table 4-2 shows the results from the calculations of the mean values of leakage, in-flow and pressure calculated with the sensor placement methods by Pérez, Casillas and SPuDU from the leakage simulation at the hydrant HG3880. For each leak size the average values were computed for the significant time period from 01:00 to 04:00 am. Leakage and inflow rate are indicated in l/s and the pressure in mWC. The mean values from the leakage simulation at the hydrants HG4504 and HG3164 can be found in the appendix (A.1).

Table 4-2: Results from the calculations of the mean values of leakage, inflow and pressures with respect to the different sensor placements (Pérez, Casillas, SPuDU) at HG3880

			leak 1 - HG3880							
period	01:00 - 04:00									
date			21.04.2016	22.04.2016	23.04.2016	24.04.2016	25.04.2016	18.04.2016	19.04.2016	20.04.2016
			0.25/0.33		0.5			0.7		
	hydrant ID		Ø pressure [mWC]		Ø pressure [mWC]			Ø pressure [mWC]		
Pérez	HG3933	205	89.46779	89.49433	89.04379	89.20103	89.40798	89.19217	89.32188	89.50220
			89.48105676		89.21760082			89.33875354		
	HG4215	1248	88.55467	88.58539	88.31553	88.32302	88.50181	88.35352	88.44954	88.61276
			88.57002652		88.38012180			88.47194004		
	HG4339b	210	94.55621	94.59845	94.24005	94.29263	94.49472	94.22744	94.41202	94.57072
			94.57733226		94.34246758			94.40339231		
	HG4383	3768	88.40398	88.44550	88.09724	88.14324	88.34056	88.07471	88.25811	88.42454
			88.42473804		88.19367838			88.25245319		
	HG4540	1536	61.25212	61.29819	60.96193	60.99299	61.18446	60.93191	61.10392	61.27122
			61.27515884		61.04646149			61.10234995		
Casillas	HG3420	423	82.39189	82.41319	82.11283	82.11544	82.32863	82.17515	82.29633	82.46404
			82.40254007		82.18563259			82.31184249		
	HG3835	433	87.68945	87.73707	87.38770	87.43515	87.64404	87.44347	87.57511	87.73741
			87.71326005		87.48896341			87.58532926		
	HG3933	205	89.46779	89.49433	89.04379	89.20103	89.40798	89.19217	89.32188	89.50220
			89.48105676		89.21760082			89.33875354		
	HG4215	1248	88.55467	88.58539	88.31553	88.32302	88.50181	88.35352	88.44954	88.61276
			88.57002652		88.38012180			88.47194004		
	HG4383	3768	88.40398	88.44550	88.09724	88.14324	88.34056	88.07471	88.25811	88.42454
			88.42473804		88.19367838			88.25245319		
SPuDU	HG3420	423	82.39189	82.41319	82.11283	82.11544	82.32863	82.17515	82.29633	82.46404
			82.40254007		82.18563259			82.31184249		
	HG3933	205	89.46779	89.49433	89.04379	89.20103	89.40798	89.19217	89.32188	89.50220
			89.48105676		89.21760082			89.33875354		
	HG4162	837	86.00803	86.05235	85.77607	85.76260	85.97866	85.80798	85.92101	86.07456
			86.03019230		85.83910683			85.93451854		
	HG4215	1248	88.55467	88.58539	88.31553	88.32302	88.50181	88.35352	88.44954	88.61276
			88.57002652		88.38012180			88.47194004		
	HG4383	3768	88.40398	88.44550	88.09724	88.14324	88.34056	88.07471	88.25811	88.42454
			88.42473804		88.19367838			88.25245319		

The pressure values are already ordered by sensor placement for further evaluation. Table 4-3 shows the results from the calculations of the mean values of leakage, inflow and pressure for the sensor placements Shannon entropy, Shortest Path 1 and Shortest Path 2 from the leakage simulation at the hydrant HG3880.

Table 4-3: Results from the calculations of the mean values of leakage, inflow and pressures with respect to the different sensor placements (Shannon entropy, Shortest Path1, Shortest Path 2) at HG3880

			0.25/0.33		0.5			0.7		
period 01:00 - 04:00										
date			21.04.2016	22.04.2016	23.04.2016	24.04.2016	25.04.2016	18.04.2016	19.04.2016	20.04.2016
	hydrant ID		Ø pressure [mWC]		Ø pressure [mWC]			Ø pressure [mWC]		
Shannon Entropy	HG3420	423	82.39189	82.41319	82.11283	82.11544	82.32863	82.17515	82.29633	82.46404
			82.40254007		82.18563259			82.31184249		
	HG3933	205	89.46779	89.49433	89.04379	89.20103	89.40798	89.19217	89.32188	89.50220
			89.48105676		89.21760082			89.33875354		
	HG4215	1248	88.55467	88.58539	88.31553	88.32302	88.50181	88.35352	88.44954	88.61276
			88.57002652		88.38012180			88.47194004		
	HG4339b	210	94.55621	94.59845	94.24005	94.29263	94.49472	94.22744	94.41202	94.57072
			94.57733226		94.34246758			94.40339231		
	HG4744	432	31.22968	31.25200	30.95089	30.96525	31.16375	31.00024	31.10153	31.27053
			31.24084306		31.02662864			31.12410008		
Shortest Path 1	HG3445	411	68.56979	68.59933	68.30203	68.29827	68.50570	68.34383	68.45896	68.62897
			68.58456439		68.36866616			68.47725235		
	HG3933	205	89.46779	89.49433	89.04379	89.20103	89.40798	89.19217	89.32188	89.50220
			89.48105676		89.21760082			89.33875354		
	HG4150	206	75.25068	75.28654	74.99437	74.98731	75.19060	75.04499	75.13726	75.32390
			75.26860995		75.05742874			75.16871635		
	HG4339b	210	94.55621	94.59845	94.24005	94.29263	94.49472	94.22744	94.41202	94.57072
			94.57733226		94.34246758			94.40339231		
	HG4744	432	31.22968	31.25200	30.95089	30.96525	31.16375	31.00024	31.10153	31.27053
			31.24084306		31.02662864			31.12410008		
Shortest Path 2	HG3445	411	68.56979	68.59933	68.30203	68.29827	68.50570	68.34383	68.45896	68.62897
			68.58456439		68.36866616			68.47725235		
	HG4150	206	75.25068	75.28654	74.99437	74.98731	75.19060	75.04499	75.13726	75.32390
			75.26860995		75.05742874			75.16871635		
	HG4339b	210	94.55621	94.59845	94.24005	94.29263	94.49472	94.22744	94.41202	94.57072
			94.57733226		94.34246758			94.40339231		
	HG4576	414	30.22241	30.25655	29.93294	29.95892	30.16321	29.89717	30.09304	30.25304
			30.23947678		30.01835502			30.08108426		
	HG4744	432	31.22968	31.25200	30.95089	30.96525	31.16375	31.00024	31.10153	31.27053
			31.24084306		31.02662864			31.12410008		

4.4   Results from the uncalibrated model

The following sections 4.4.1 to 4.4.3 show the results from the calculation with the uncalibrated EPANET model. With the help of the sensor placement methods Casillas, Pérez, and SPuDU the location of the bigger leaks (0.7 l/s and 1.0 l/s) at the hydrants HG3880, HG4504 and HG3164 are calculated. The results of the night measurements can be found in the appendix (A.2). Beside the leak plots also leak histograms, distance histograms, and outflow histograms are shown. In the leak plots the blue cross ✖ displays the actual leak, the filled petrol triangle 🔺 presents the used pressure sensors, and the green dots 🟢 illustrate the calculated leak. A varying degree of intensity in colour represents how often this node has been detected as possible leakages position. The darker the dot, the more often the position was calculated. The leak histogram shows which node is found by the algorithm in which frequency. The distance histogram illustrates how often the leak is found depending on the distance to the actual leak. In the outflow histogram the outflow rate is set on the

x-axis and the percentage of leak found is set on the y-axis. As already explained in section 2, the emitter coefficient c_e characterizes the flow and pressure loss behaviour of nozzles in fluid systems.

4.4.1   0.7 l/s leak at HG3880

In Figure 4.6 the results from the sensor placement methods by Casillas, Pérez and SPuDU for the 0.7 l/s leak at the hydrant HG3880 are shown.
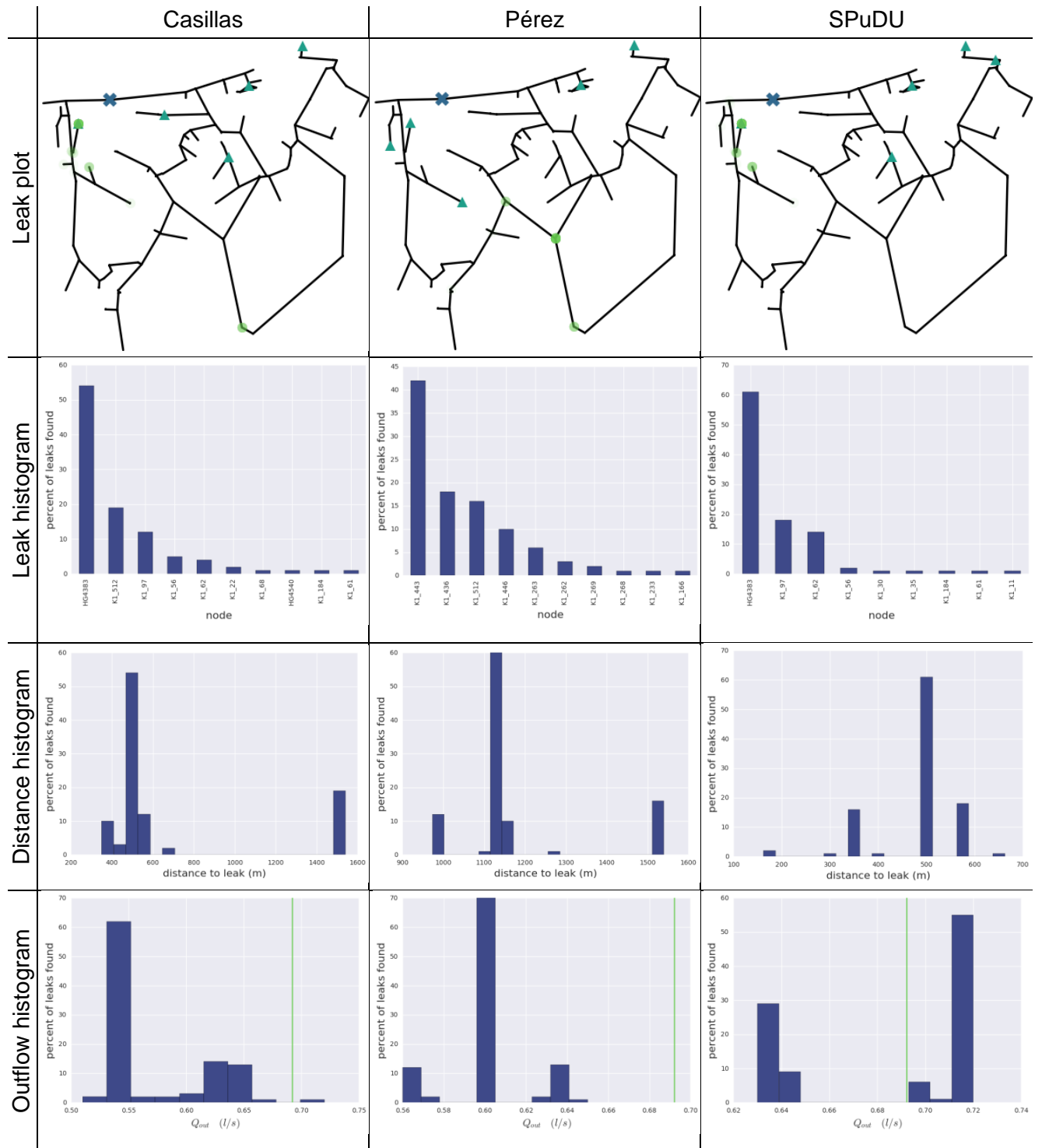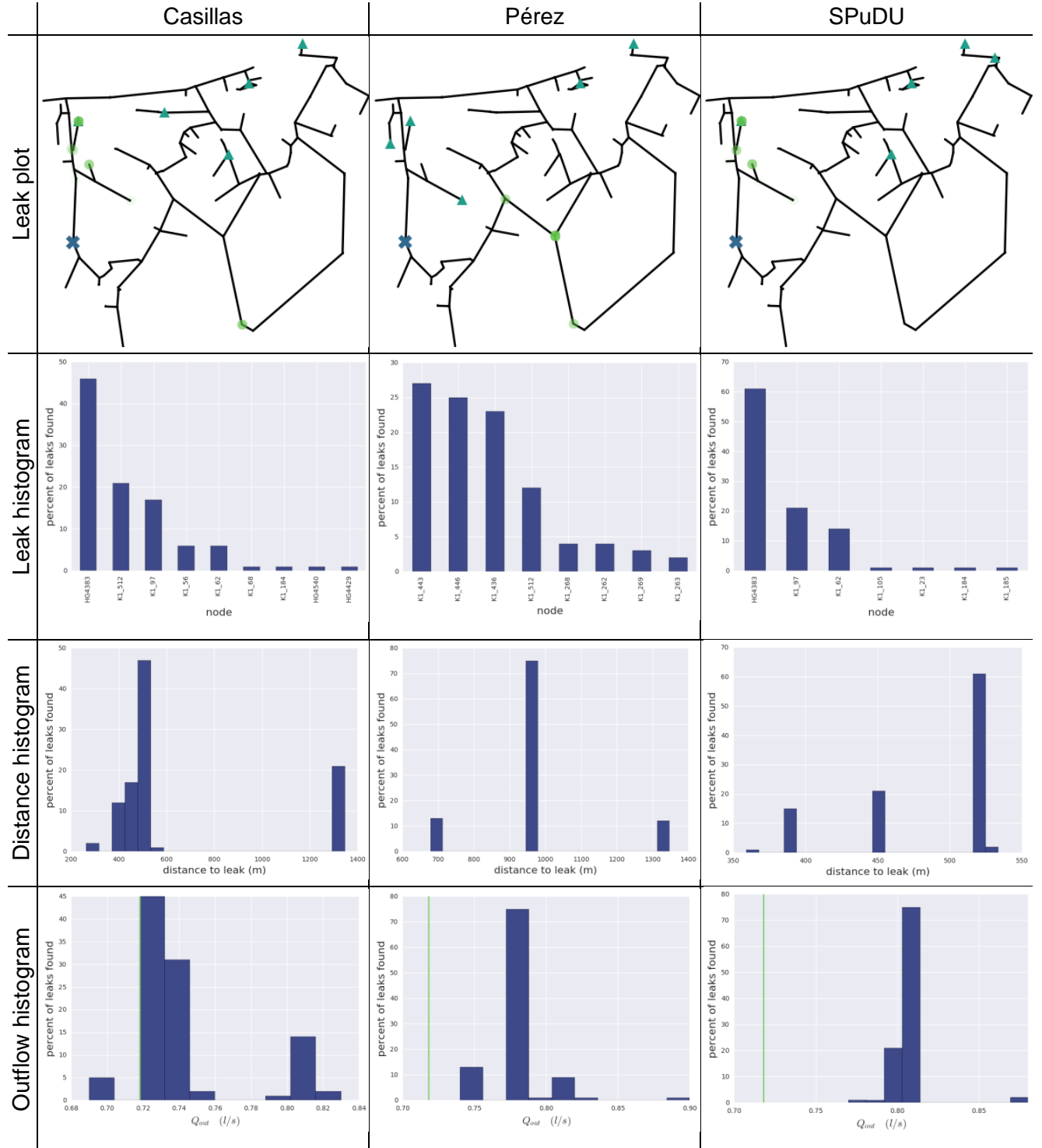

Figure 4.6: Results from the sensor placements Casillas, Pérez and SPuDU (Uncalibrated model, 0.7 l/s leak at HG3880)

55

4.4.2   0.7 l/s leak at HG4504

The results from the sensor placement methods by Casillas, Pérez and SPuDU for the 0.7 l/s leak at the hydrant HG4504 are illustrated in Figure 4.7.

Figure 4.7: Results from the sensor placements Casillas, Pérez and SPuDU (Uncalibrated model, 0.7 l/s leak at HG4504)

4.4.3 1.0 l/s leak at HG3164

In Figure 4.8 leak plots, leakage-, distance- and outflow histograms are shown as a result of the calculations with the sensor placement methods by Casillas, Pérez and SPuDU for the 1.0 l/s leak at the hydrant HG3164.
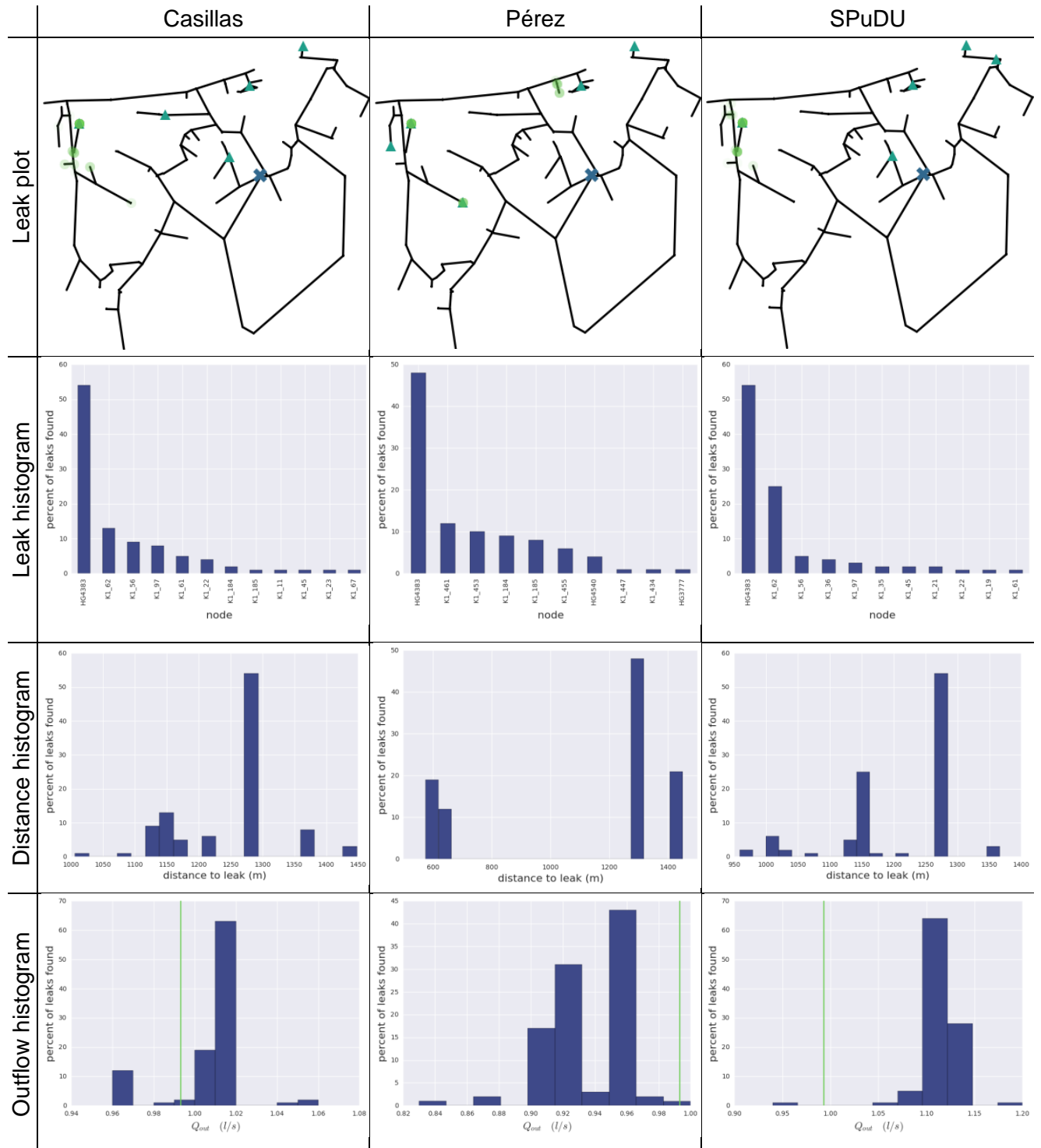
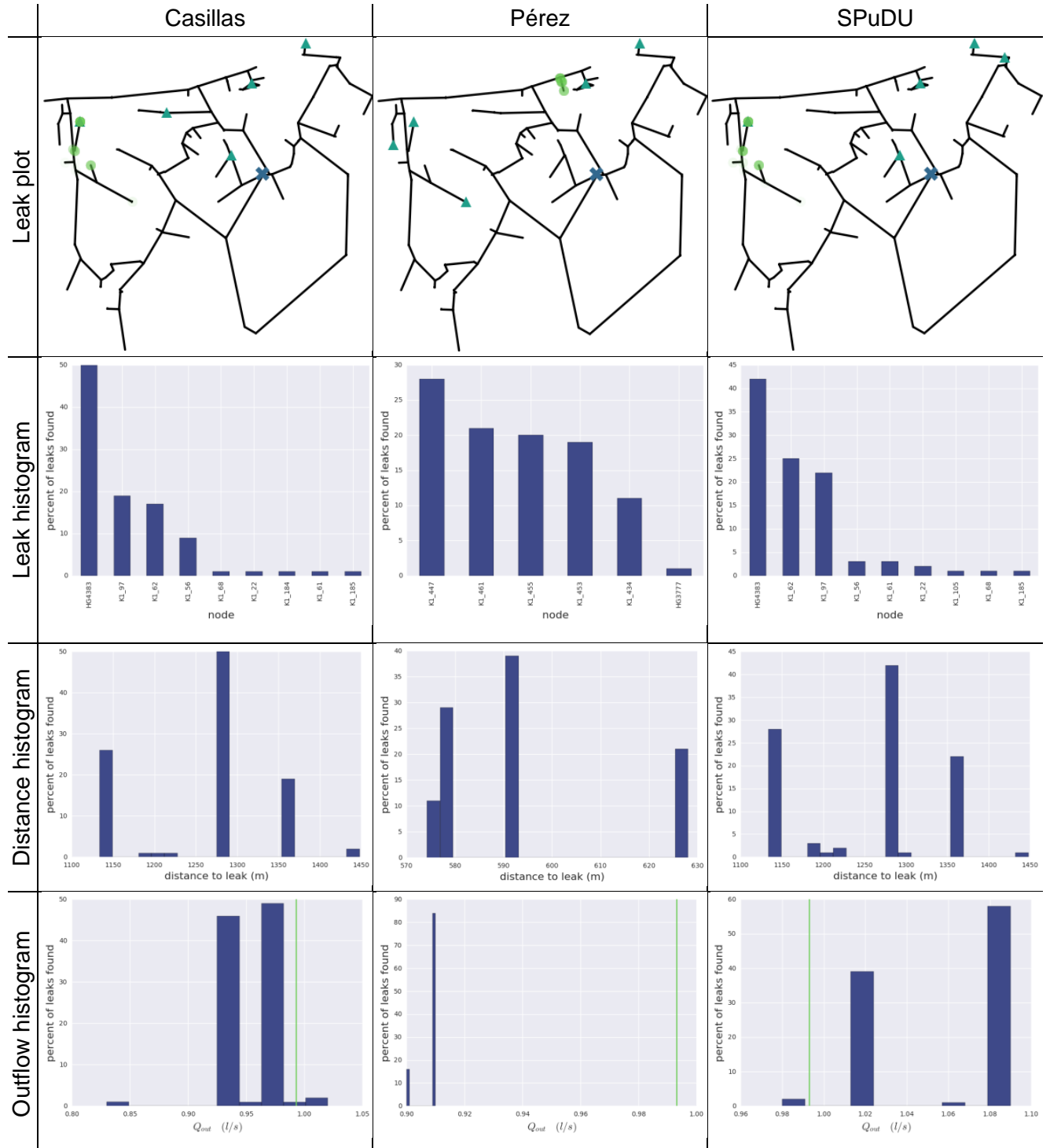**Figure 4.8: Results from the sensor placements Casillas, Pérez and SPuDU (Uncalibrated model, 1.0 l/s leak at HG3164)**

4.5 Results from the calibrated model

The following sections 4.5.1 to 4.5.3 illustrate the results from the calculations with the calibrated EPANET model of the bigger leak sizes. At the hydrants HG3880, HG4504, and HG3164 leaks of 0.7 l/s and 1.0 l/s were simulated and calculated with the sensor placement methods by Casillas, Pérez, SPuDU, Shannon entropy, Shortest Path 1 and 2. Beside the leak plots also leak histograms, distance histograms, and outflow histograms are shown. The results of the night measurements and the small leaks (0.25 l/s, 0.5 l/s) can be found in the appendix (A.3).

A comparison between the uncalibrated and the calibrated model can also be found in the appendix (Figure A - 21).

4.5.1 0.7 l/s leak at HG3880

Figure 4.9 illustrates the results of the calculations with the three sensitivity-based sensor placement algorithms (Casillas, Pérez, SPuDU) with the calibrated model for the 0.7 l/s leak at HG3880.
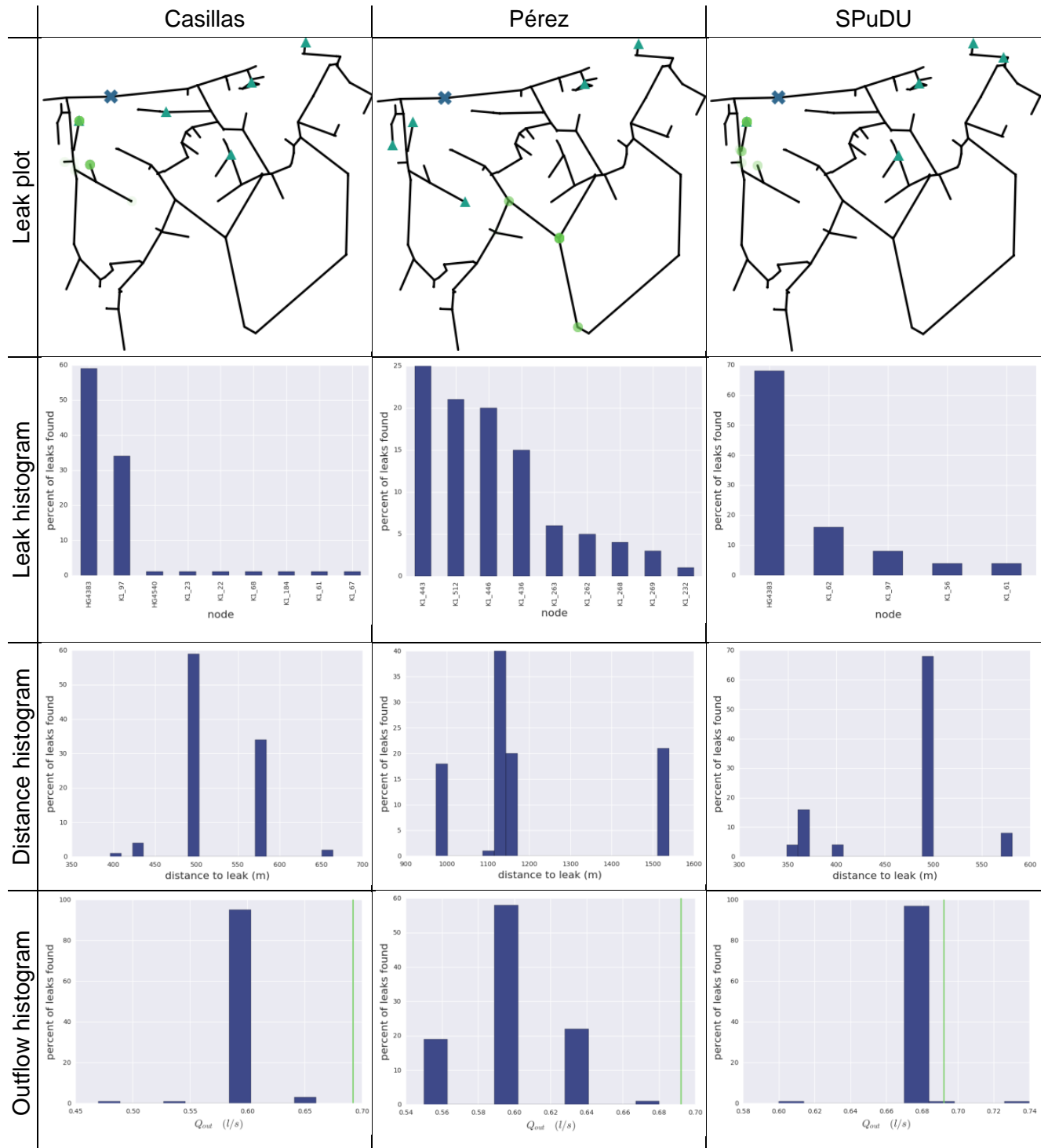
Figure 4.9: Results from the sensor placements Casillas, Pérez and SPuDU (Calibrated model, 0.7 l/s leak at HG3880)

59

In Figure 4.10 the results of the calculations with the sensitivity-based algorithms Shannon entropy and the two topology-based algorithms (Shortest Path 1 and 2) with the calibrated model for the 0.7 l/s leak at HG3880 are shown.
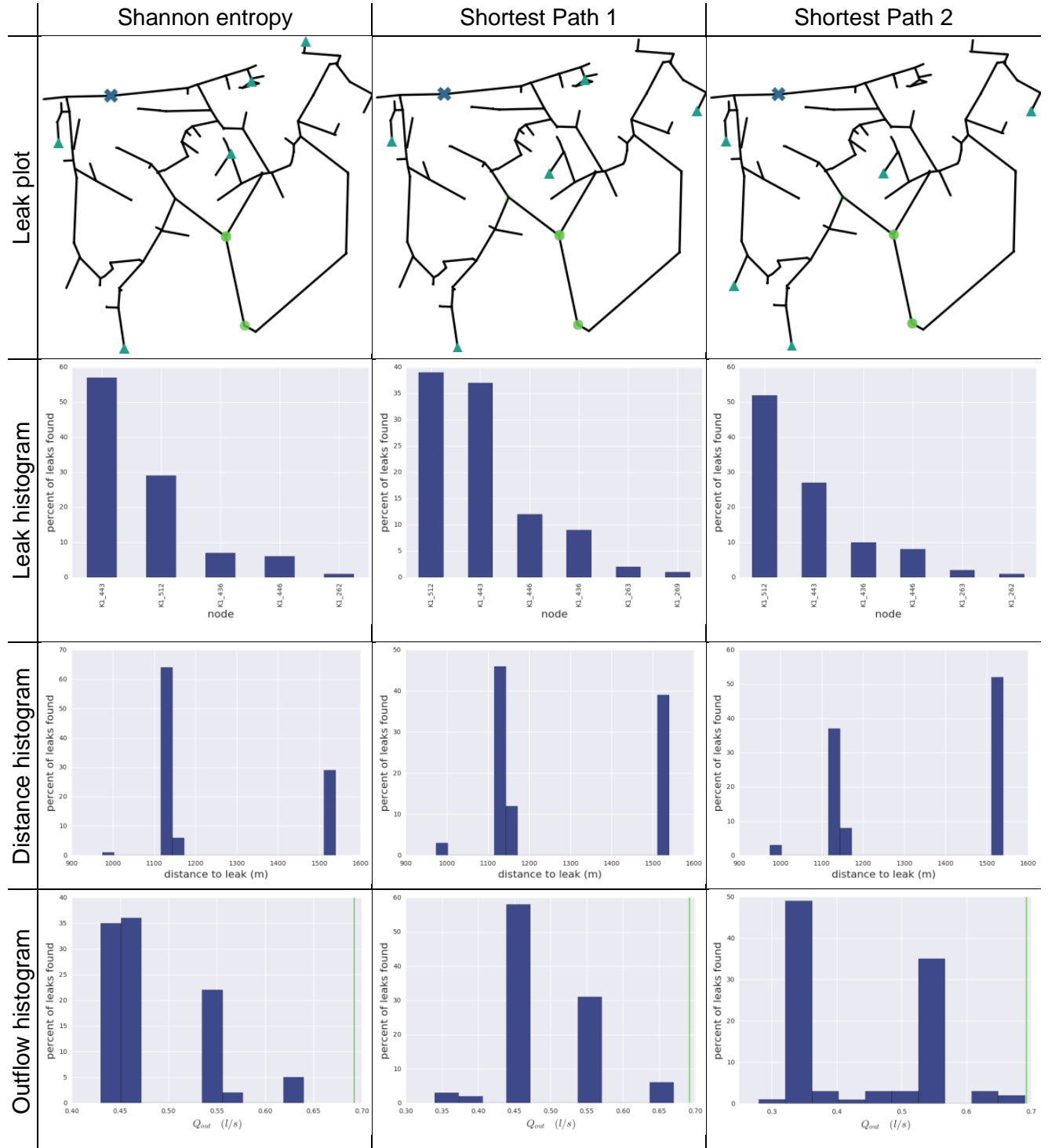
Figure 4.10: Results from the sensor placements Shannon entropy, Shortest Path 1 and Shortest Path 2 (Calibrated model, 0.7 l/s leak at HG3880)

4.5.2   0.7 l/s leak at HG4504

Figure 4.11 illustrates the leak plots, leakage-, distance-, and outflow histograms for the 0.7 l/s leak at the hydrant HG4504 and the sensor placements by Casillas, Pérez and SPuDU.
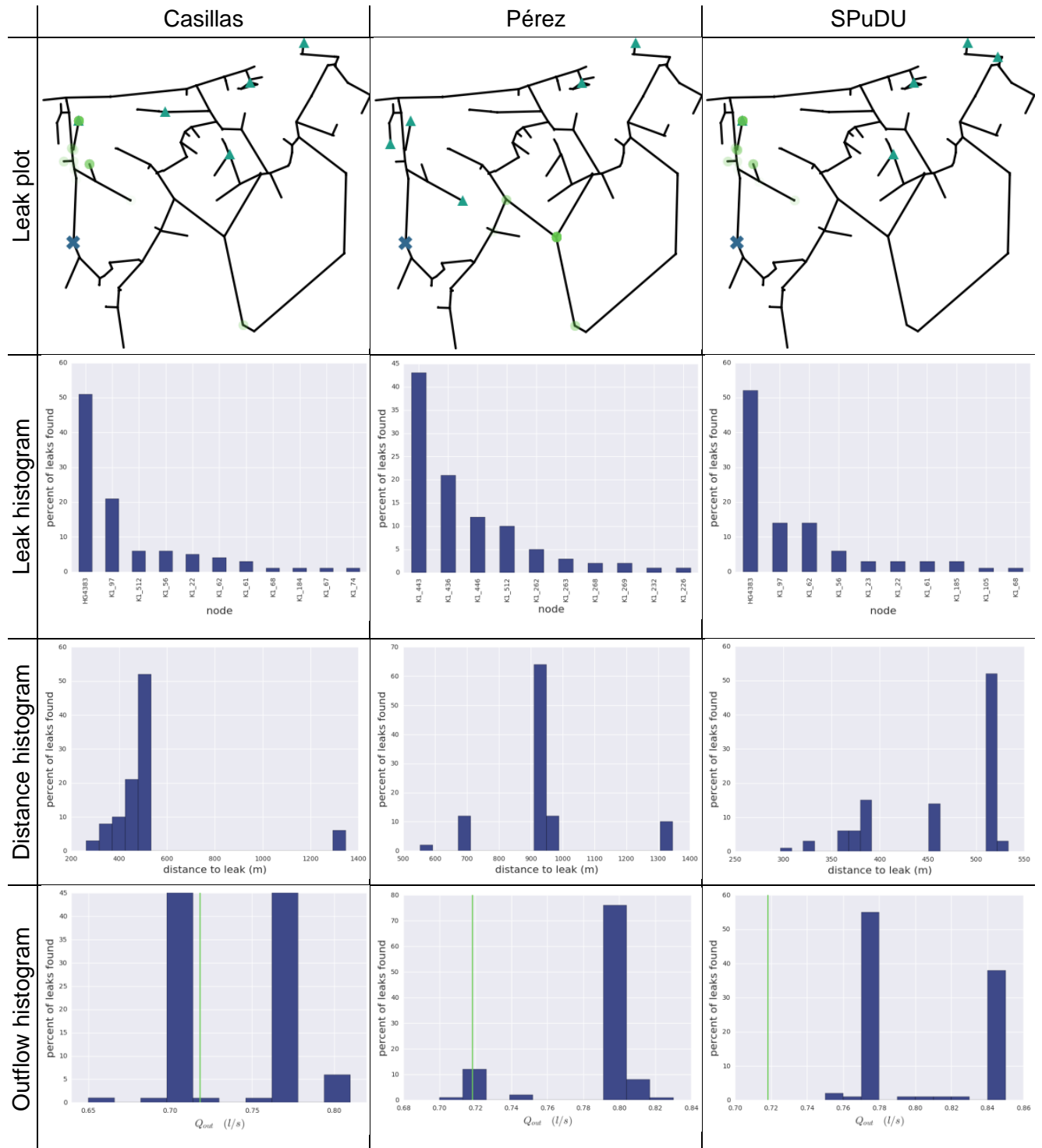
Figure 4.11: Results from the sensor placements Casillas, Pérez and SPuDU (Calibrated model, 0.7 l/s leak at HG4504)

61

The results from the sensor placement methods by Shannon entropy, Shortest Path 1 and 2 for the 0.7 l/s leak at the hydrant HG4504 are shown in Figure 4.12.
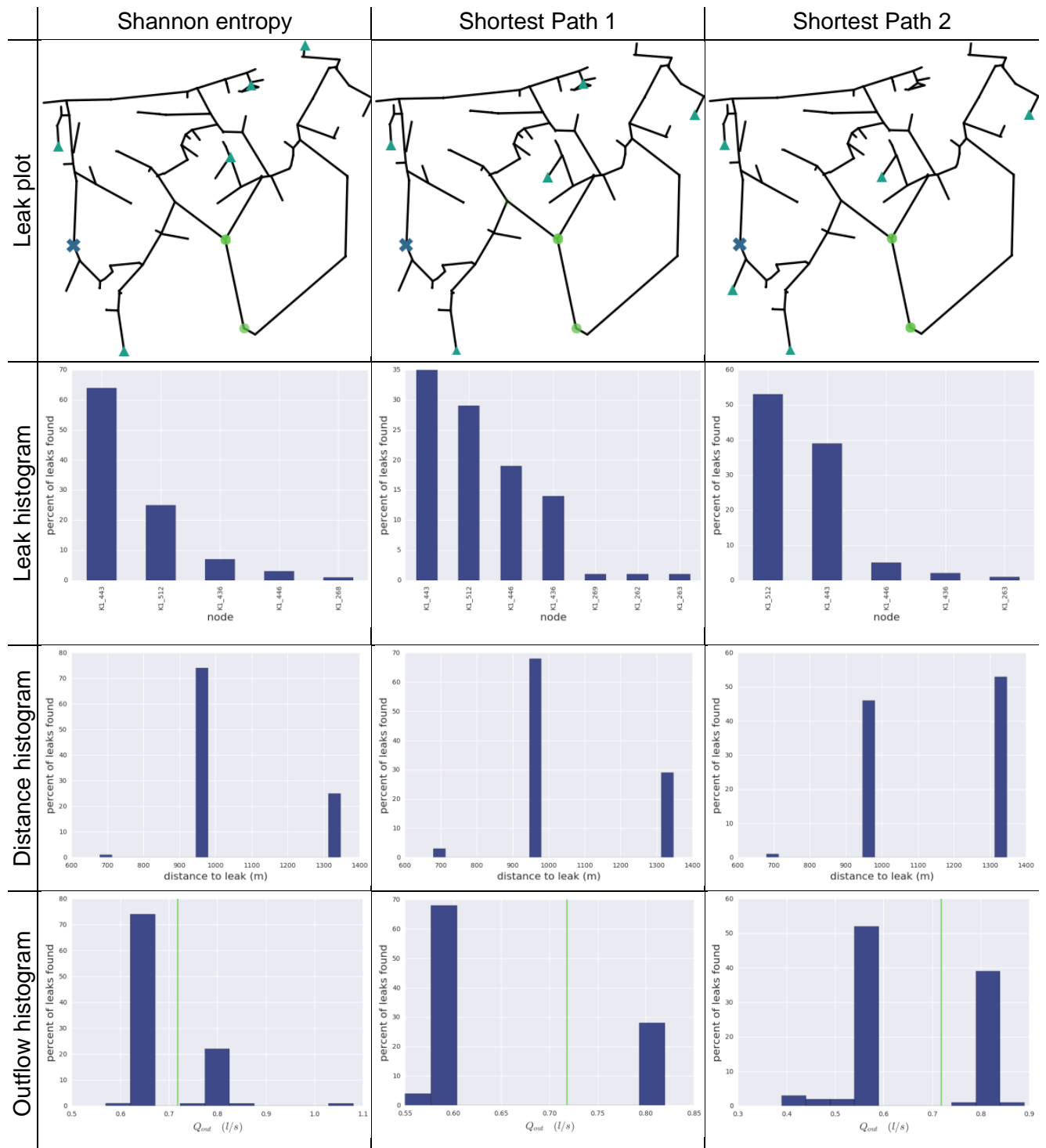
Figure 4.12: Results from the sensor placements Shannon entropy, Shortest Path 1 and Shortest Path 2 (Calibrated model, 0.7 l/s leak at HG4504)

4.5.3   1.0 l/s leak at HG3164

Figure 4.13 depicts the results of the 1.0 l/s leak at HG3164 for the sensor placement algorithms by Casillas, Pérez, and SPuDU.

Figure 4.13: Results from the sensor placements Casillas, Pérez and SPuDU (Calibrated model, 1.0 l/s leak at HG3164)

63

Figure 4.14 shows the results of the calculation with Shannon entropy, Shortest Path 1 and 2 for the 1.0 l/s leak at HG3164 using the calibrated model.
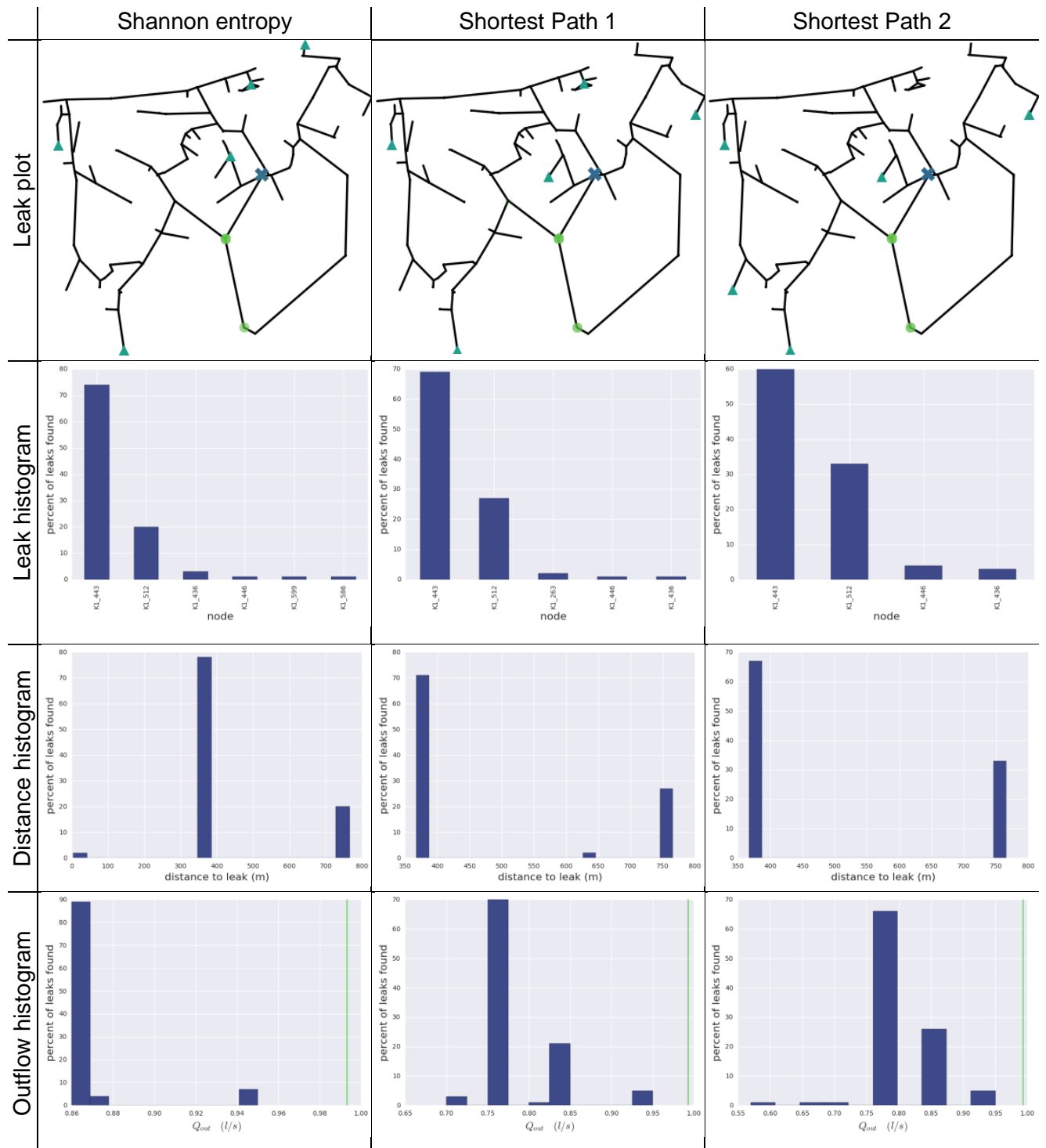
Figure 4.14: Results from the sensor placements Shannon entropy, Shortest Path 1 and Shortest Path 2 (Calibrated model, 1.0 l/s leak at HG3164)

4.6 Results from the recalibrated model

In this section the results from the calculation with the recalibrated EPANET model of the bigger leak sizes are illustrated. At the hydrants HG3880, HG4504, and HG3164 leaks of 0.7 l/s and 1.0 l/s are shown. Here, all twelve sensors are used for the calculations. Beside the leak plots also leak histograms, distance histograms, and outflow histograms are shown.
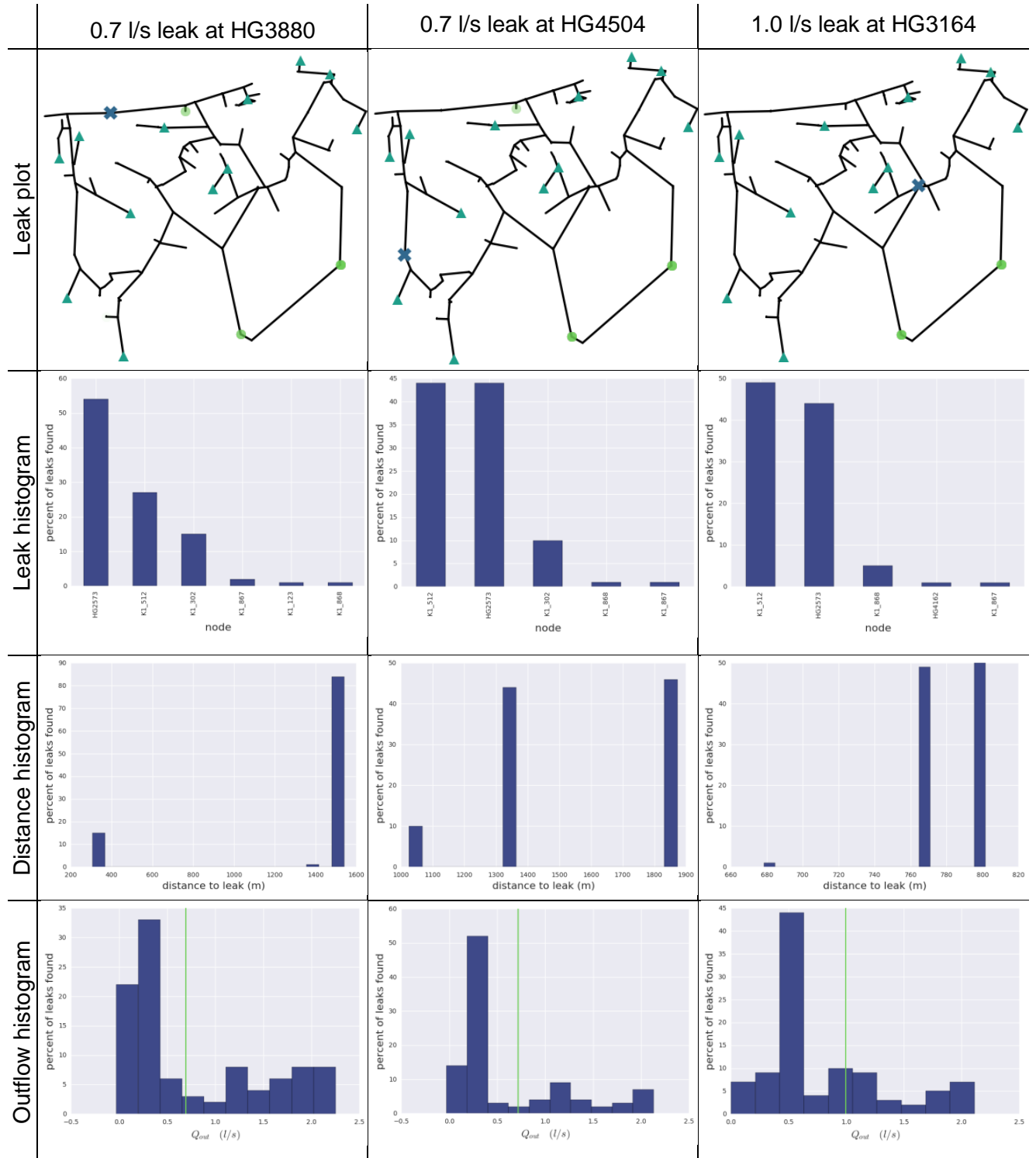
Figure 4.15: Results from the recalibrated model using all sensors (0.7 l/s at HG3880, 0.7 l/s at HG4504, 1.0 l/s at HG3164)

65

5 Discussion of the results

There are many ways to interpret the results and various assessment criteria. In this research the evaluations are based on the distance between the actual leak and the one found by the algorithm. It is not necessary to calculate the exact position of the real leak. Means the leaks found do not have to be within a certain radius but it is important to locate the right corner of the search area. The so-called sectorizing helps the investigator with further pinpointing of the leak. The distance criterion is analyzed for all three leaks and sizes as well as for the night measurements.

In this research six different sensor placement methods were investigated. Four of them chose the monitoring points based on the use of the sensitivity matrix and two selected the monitoring points based on the topology of the search area. The aim was to find out which method works most efficient at leakage localization for this area.

The leakage localization was first calculated with the uncalibrated model and the sensor placements Casillas, Pérez and SPuDU. The calculations were conducted at the hydrants HG3880, HG4504 and HG3164 for the bigger leaks (0.7 and 1.0 l/s) and at the hydrants HG3302, HG3537 and HG3880 for the night measurements (1.0 l/s).

5.1 Uncalibrated model

None of the sensor placement methods was able to localize the exact position of the real leak. For the leaks at the hydrant HG3880 (0.7 and 1.0 l/s) the methods by Casillas and SPuDU provided solid results (see Figure 5.1). The leakages were found within a radius of 500m of the real leak with a probability of 54 % respectively 61%.
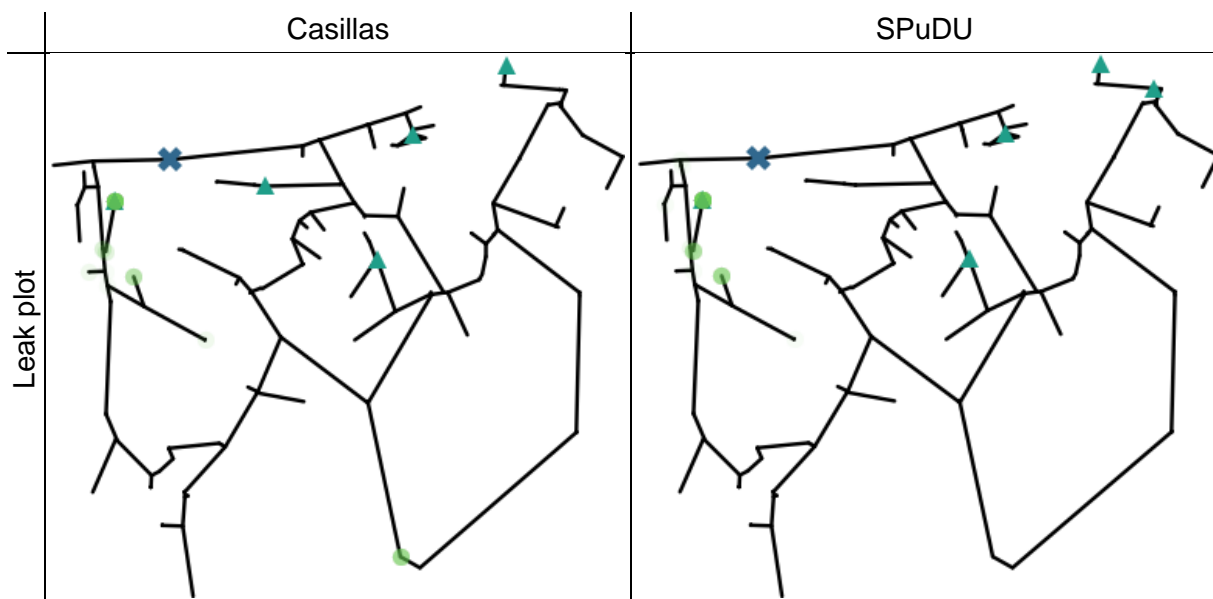
Figure 5.1: Solid results for Casillas and SPuDU (Uncalibrated model, 0.7 l/s leak at HG3880)

In Table 5-1 a statistical evaluation of the 0.7 l/s leak at HG3880 is shown. Regarding the average distance from the found leak to the real one SPuDU provides the best results compared to Pérez and Casillas. The leaks found by Pérez are more than 1.000 m away from the real leak.

Table 5-1: Uncalibrated model, 0.7 l/s leak at HG3880

HG3880 0.7 l/s	Number of nodes found	Most frequently detected leak		Closest leak		Leak furthest away		Average distance to real leak
		[%]	[m]	[%]	[m]	[%]	[m]	[m]
Casillas	10	54	491.67	5	348.90	19	1540.10	689.83
Pérez	10	42	1141.58	1	973.54	16	1540.10	1186.86
SPuDU	9	61	491.67	1	161.93	1	662.93	478.98

Also, for the leak at HG4504 the calculated leak for SPuDU was on the same side of the investigation area as the real leak and the average distance is below 500 m (see Table 5-2). Casillas provides similar results within a radius of 660 m.

Table 5-2: Uncalibrated model, 0.7 l/s leak at HG4504

HG4504 0.7 l/s	Number of nodes found	Most frequently detected leak		Closest leak		Leak furthest away		Average distance to real leak
		[%]	[m]	[%]	[m]	[%]	[m]	[m]
Casillas	9	46	516.57	1	263.23	21	1346.05	658.93
Pérez	8	27	947.53	4	678.84	12	1346.05	961.03
SPuDU	7	61	516.57	1	358.90	1	533.56	482.05

Regarding the average distance to the real leak Table 5-3 shows that the results for the 1.0 l/s leak at HG3164 are not useable for pinpointing a leak in the field.

Table 5-3: Uncalibrated model, 1.0 l/s leak at HG3164

HG3164 1.0 l/s	Number of nodes found	Most frequently detected leak		Closest leak		Leak furthest away		Average distance to real leak
		[%]	[m]	[%]	[m]	[%]	[m]	[m]
Casillas	12	54	1276.46	1	1006.00	1	1447.98	1245.70
Pérez	10	48	1276.46	1	574.19	8	1447.98	1104.15
SPuDU	11	54	1276.46	2	958.75	3	1366.18	1208.38

When looking at the leaks at HG3164 and the night measurements at HG3302 and HG3537 it is noticeable that the algorithm (Casillas and SPuDU) always found the leakage nearly at the same positions as for the leaks at HG3880 (compare Figure 5.1 and Figure 5.2). There, the calculated leak is about 1,300 to 1,500 m away from the actual leak (see Figure 5.2).

These results lead to the conclusion that the optimal results by the sensor placements Casillas and SPuDU at HG3880 are inconsistent. The uncalibrated EPANET model seems to have bigger discrepancies in comparison to the real WDS relating to the roughness values of the pipes.
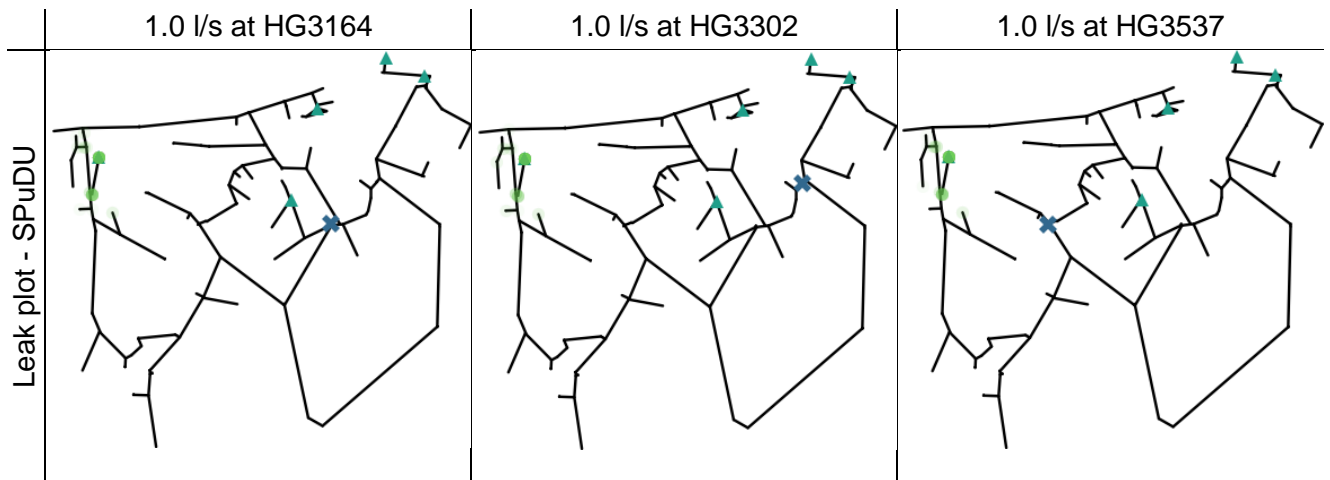
Figure 5.2: Leak plot - SPuDU 1.0 l/s leak at HG3164, HG3302 and HG3537

The sensor placement by Pérez provides different results for the different leaks but regarding to the distances, the results are useless for leakage localization (see Figure 5.3). The leak is found in a different area of the WDS and the average distances are approximately 1,000 m (see Table 5-1 to Table 5-3). If a repairing company takes these results they would probably not find the leak.
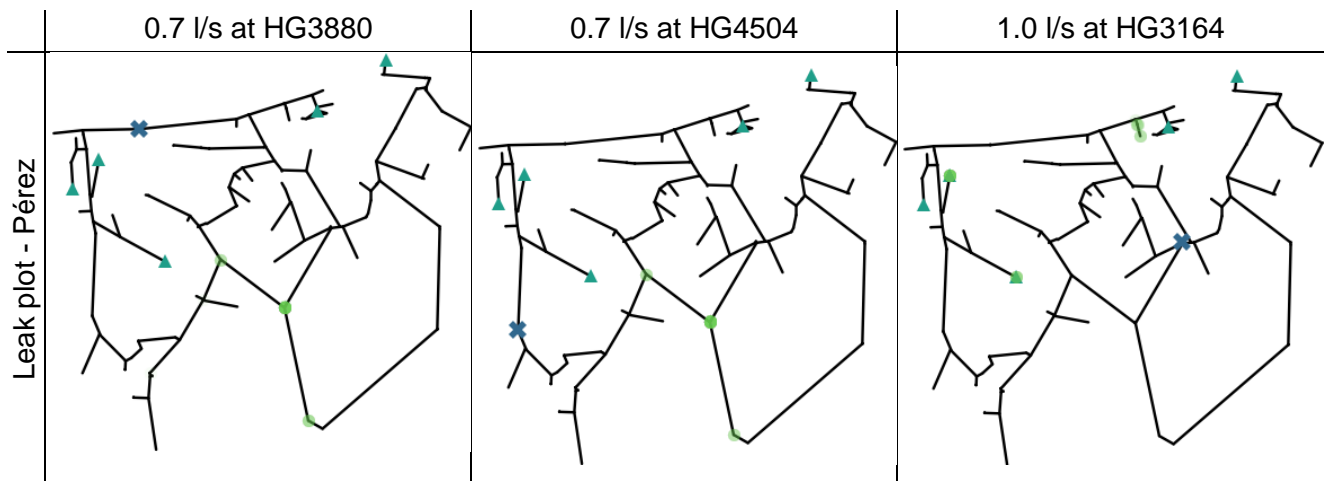
Figure 5.3: Leak plot - Pérez: 0.7 l/s leak at HG3880 and HG4504, 1.0 l/s leak at HG3537

Besides the 1.0 l/s leak at HG3880 the night measurements do not provide any usable results. Figure 5.4 shows these conclusions with respect to the example of the sensor placement SPuDU. The found leaks are approximately 1,000 m away from the real leak (Table A - 5 and Table A - 6).
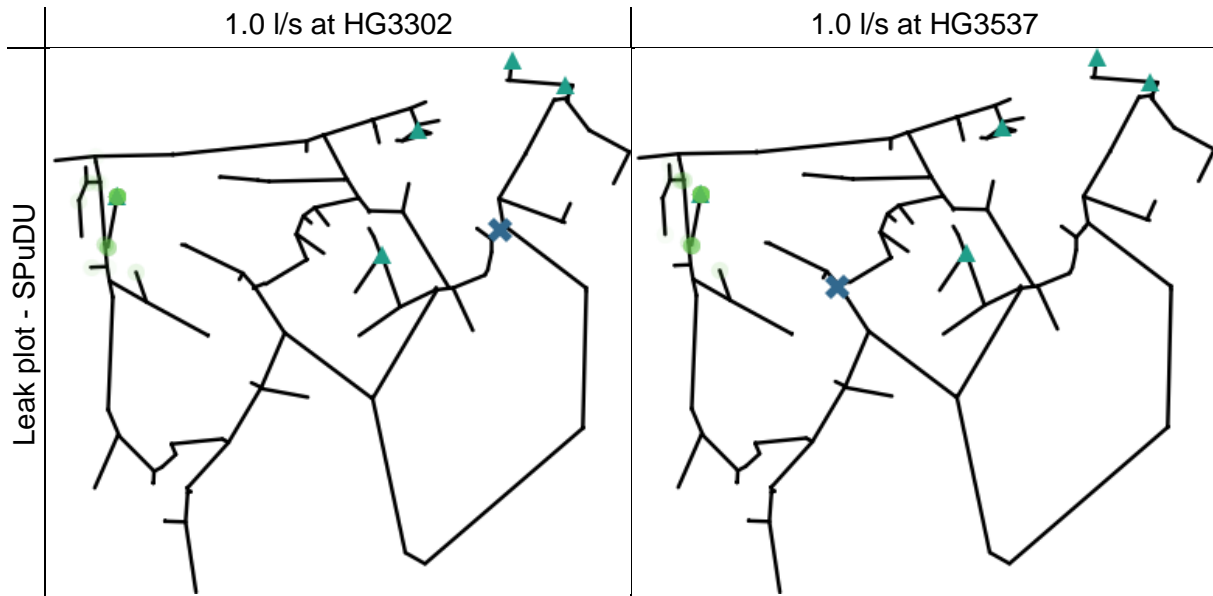
Figure 5.4: Leak plot - SPuDU: 1.0 l/s leak at HG3302 and HG3537

Due to the fact that the results are not that good the behavior of the pressure in case of a leak was analyzed in the hydraulic model. Therefore, a pressure drop of 0.7 l/s and 1.0 l/s was simulated in the EPANET model at HG3880, HG4504 and HG3164 (base demand of 0.7 or 1.0). In Table 5-4 the pressure drop caused by the big leakages using the uncalibrated model at the nodes where the pressure sensors were installed is illustrated. The pressure loss at the nodes where the leak was simulated is highlighted in grey. The pressure drop caused by the leakage is recognizable at each hydrant even if it is very small (between 7 and 17 cm).

The pressure difference of the 1.0 l/s leak at the node HG3164 accounts to 16 cm and is small compared to the other leaks at HG3880 and HG4504 (regarding that the size of the leak is bigger). The pressure loss at the node where the leak was simulated accounts to 14 – 17 cm. The surrounding nodes show a lower pressure drop. These slight differences make it hard to find the approximate position of the real leak.

These results of the pressure loss also reflect the results of the leak plots of the leakage at HG3164. None of the pressure measurements could provide solid solutions for this leakage.

Table 5-4: Pressure loss for 0.7 l/s and 1.0 l/s using the uncalibrated model

Uncalibrated model	0.7 l/s leak at HG3880	0.7 l/s leak at HG4504	1.0 l/s leak at HG3164
	Pressure loss [m]		
Node ID			
HG3164			0.16
HG3420	0.08	0.07	0.14
HG3445	0.08	0.07	0.14
HG3835	0.11	0.10	0.13
HG3880	0.17		
HG3933	0.14	0.12	0.13
HG4150	0.08	0.08	0.14
HG4162	0.08	0.08	0.14
HG4215	0.08	0.08	0.14
HG4339b	0.15	0.13	0.12
HG4383	0.15	0.14	0.13
HG4504		0.14	
HG4540	0.14	0.14	0.12
HG4576	0.11	0.13	0.11
HG4744	0.10	0.10	0.12

5.2 Calibrated model

The leakage localization with the calibrated model was conducted for all sensor placements and all leak sizes (0.25, 0.5 and 0.7 or 1.0 l/s) at the hydrants HG3880, HG4504 and HG3164 and for the night measurements at the hydrants HG3302 (1.0 and 9.0 l/s), HG3537 (1.0 l/s) and HG3880 (1.0 l/s).

Casillas and SPuDU provide solid results for the bigger leaks (0.5 - 1.0 l/s) at HG3880 and HG4504 (see Figure 5.5). The leaks were detected within a radius of 500 m (Table 5-5 and Table 5-7). The positions of the found leaks are similar to the results of the uncalibrated system.

The calibration of the EPANET model has an insignificant effect on the results in this research. The simulations with the calibrated model only detected a few more points closer to the real leak.
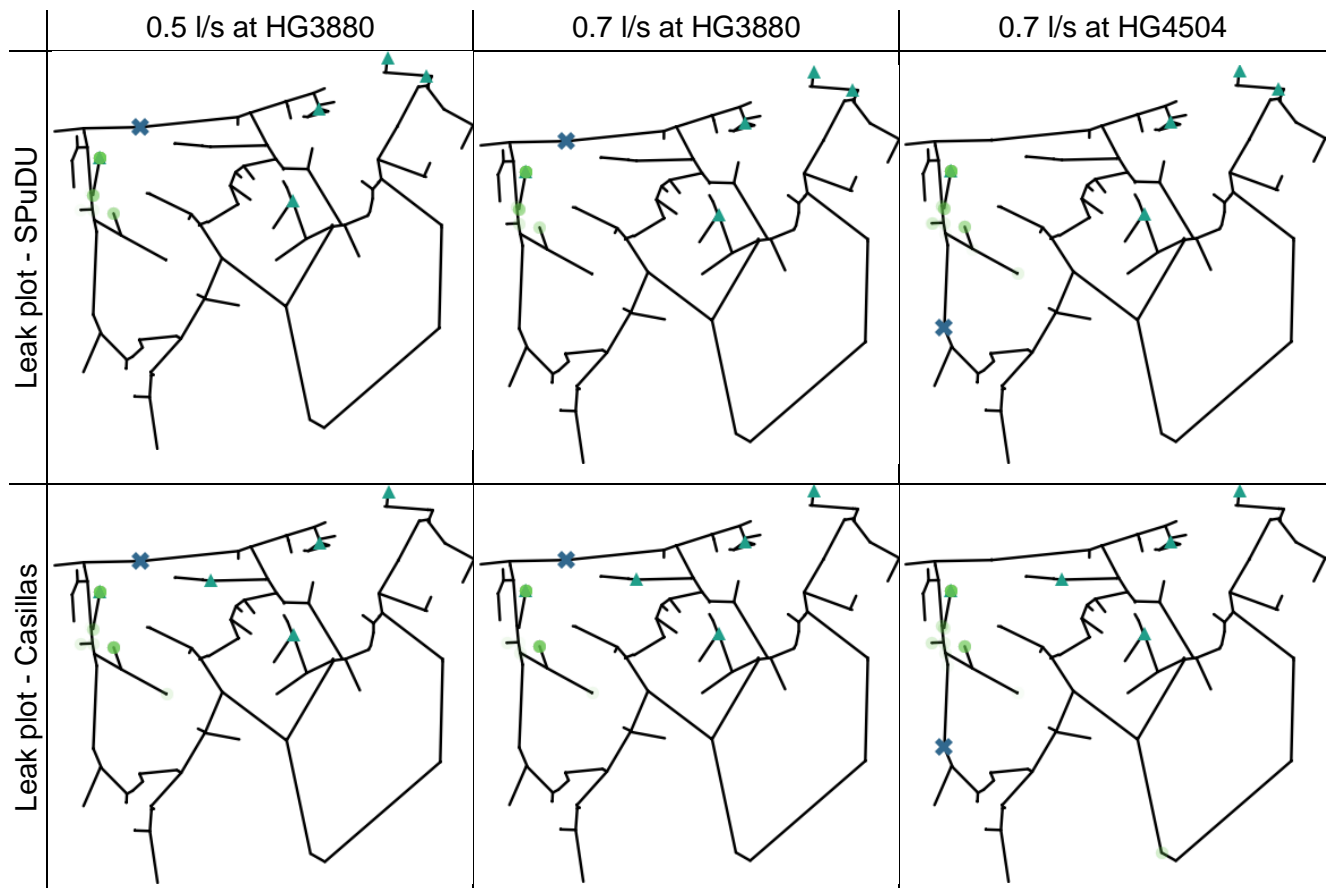
Figure 5.5: Solid results for Casillas and SPuDU for the bigger leaks at HG3880 and HG4504

The sensor placements Shannon entropy, Shortest Path 1 and 2 could not provide any useable solutions for the leaks at HG3880 and HG4504, not even for the bigger ones (0.7 l/s and 1.0 l/s). The found leaks are on the opposite side of the investigation area and more than 1,000 m away from the real leak (e.g. Figure 5.6).
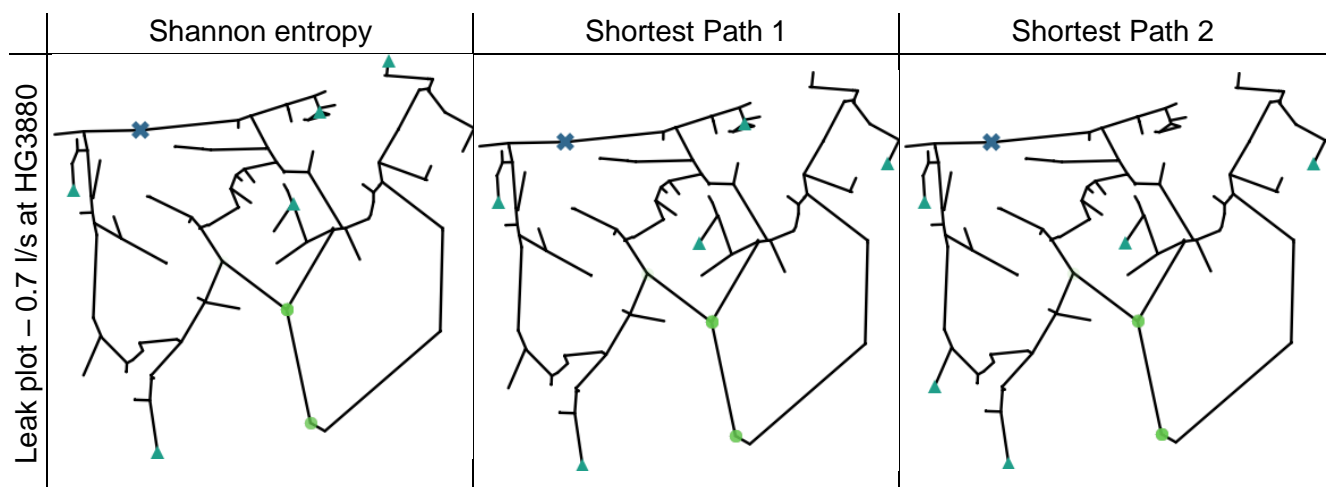
Figure 5.6: Solution for Shannon entropy, Shortest Path 1 and 2 for 0.7 l/s at HG3880

The sensor placement method by Pérez provides similar results within a radius of 1,000 m for the leaks at HG3880 and HG4504. Only the simulation for the 0.5 l/s leak at the hydrant HG3880 could reach results within 660 m (see Table 5-5).

At Table 5-5 the statistical values for the leakage at HG3880 (most frequently detected leak, closest leak, leak furthest away from the actual leak, average distance to the real leak) are shown.

Table 5-5: Calibrated model - 0.7, 0.5 and 0.25 l/s leak at HG3880

HG3880	Number of nodes found	Most frequently detected leak		Closest leak		Leak furthest away		Average distance to real leak
0.7 l/s		[%]	[m]	[%]	[m]	[%]	[m]	[m]
Casillas	9	59	491.67	1	396.14	1	664.28	522.09
Pérez	9	25	1141.58	4	973.54	21	1540.10	1195.96
SPuDU	5	68	491.67	4	348.90	8	581.38	468.33
Shannon	5	57	1141.58	1	974.83	29	1540.10	1255.88
SP 1	6	39	1540.10	1	973.94	39	1540.10	1292.73
SP 2	6	52	1540.10	2	974.59	52	1540.10	1344.34
0.5 l/s		[%]	[m]	[%]	[m]	[%]	[m]	[m]
Casillas	8	52	491.67	1	348.90	1	664.28	509.27
Pérez	5	54	664.28	1	515.01	54	664.28	656.51
SPuDU	6	67	491.67	1	348.90	13	581.38	478.38
Shannon	4	62	1141.58	62	1141.58	23	1540.10	1233.58
SP 1	7	52	1141.58	1	973.94	28	1540.10	1248.64
SP 2	5	43	1540.10	1	973.94	43	1540.10	1311.82
0.25 l/s		[%]	[m]	[%]	[m]	[%]	[m]	[m]
Casillas	17	38	1540.10	1	973.54	38	1540.10	1281.35
Pérez	9	41	1146.94	2	973.54	17	1540.10	1194.49
SPuDU	8	65	491.67	1	1.96	5	1540.10	542.76
Shannon	12	34	1540.10	4	781.54	8	1554.46	1252.70
SP 1	19	29	1540.10	1	559.83	10	1554.46	1334.99
SP 2	11	26	1540.10	1	376.05	19	1554.46	140018

When looking at the leaks at HG3164 it is noticeable that the algorithm always found the leak nearly at the same positions as for the leaks at HG3880 (compare Figure 5.5, Figure 5.6 and Figure 5.7). This could be investigated for all sensor placement methods except for Pérez.

As a result of this the algorithms of SPuDU and Casillas could not provide solid solutions for the leaks at HG3164. The calculated leak is more than 1,000 m away from the actual leak (e.g. Figure 5.7).
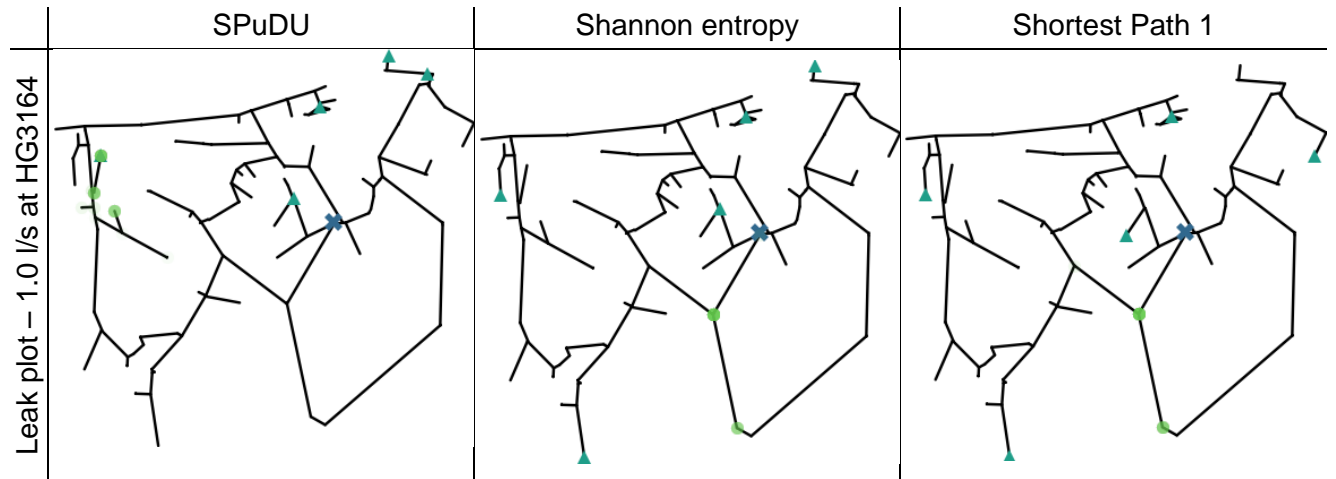
Figure 5.7: Results for 1.0 l/s leak at HG3164 (SPuDU, Shannon entropy and Shortest Path 1)

In Figure 5.7 it is visible that Shannon entropy and the two topology-based algorithms Shortest Path 1 and 2 provide valid solutions for the leak at HG3164 within a radius of 500 m (Table 5-6).

With the sensor placement method by Pérez results within 600 m could be calculated for all leak sizes at HG3164 (Figure 5.8).
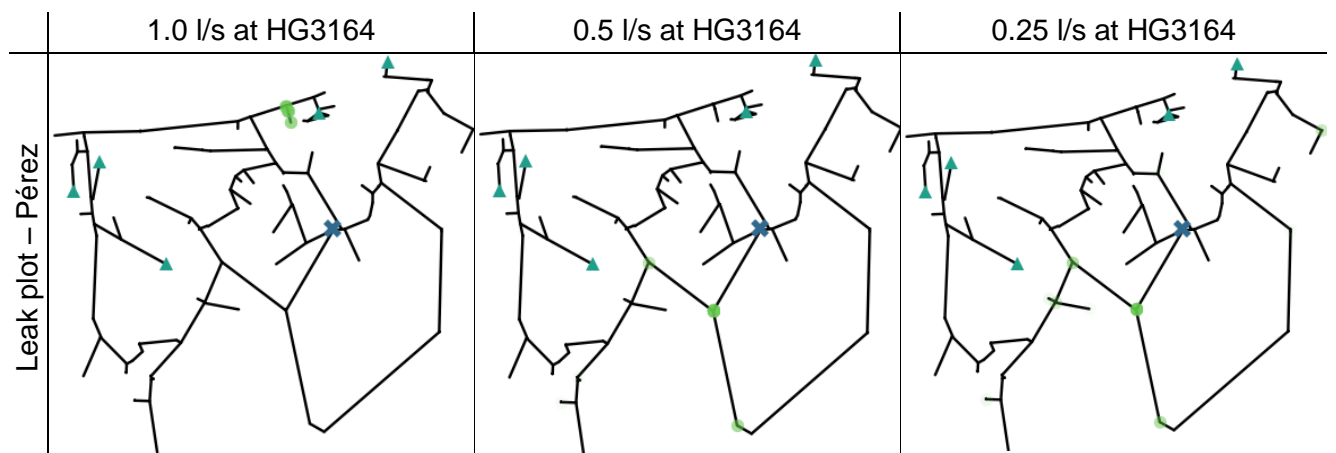
Figure 5.8: Leak plot - Pérez for leaks at HG3164

73

At Table 5-6 the statistical values for the leak at HG3164 (most frequently detected leak, closest leak, leak furthest away from the actual leak, average distance to the real leak) are shown.

Table 5-6: Calibrated model - 0.7, 0.5 and 0.25 l/s leak at HG3164

HG3164	Number of nodes found	Most frequently detected leak		Closest leak		Leak furthest away		Average distance to real leak
1.0 l/s		[%]	[m]	[%]	[m]	[%]	[m]	[m]
Casillas	9	50	1276.46	9	1133.69	1	1447.98	1259.56
Pérez	6	28	577.30	11	574.19	21	628.06	593.32
SPuDU	9	42	1276.46	3	1133.69	1	1447.98	1256.31
Shannon	6	74	367.22	1	4.22	20	765.74	439.78
SP 1	5	69	367.22	69	367.22	27	765.74	480.26
SP 2	4	60	367.22	60	367.22	33	765.74	498.98
0.5 l/s		[%]	[m]	[%]	[m]	[%]	[m]	[m]
Casillas	9	56	1276.46	21	765.74	1	1447.73	1163.73
Pérez	10	29	367.22	29	367.22	1	1147.33	476.47
SPuDU	10	63	1276.46	2	1133.69	1	1449.07	1271.83
Shannon	5	32	765.74	29	367.22	32	765.74	497.01
SP 1	4	35	367.22	35	367.22	27	765.74	475.88
SP 2	14	41	765.74	1	0.00	1	830.31	527.79
0.25 l/s		[%]	[m]	[%]	[m]	[%]	[m]	[m]
Casillas	18	42	765.74	6	367.22	1	1256.26	682.31
Pérez	18	35	372.59	1	218.88	1	1147.67	547.95
SPuDU	26	18	782.00	1	368.34	1	1049.61	866.21
Shannon	11	60	830.31	1	138.26	1	1366.18	794.74
SP 1	10	29	663.02	2	218.88	19	830.31	669.37
SP 2	10	28	663.02	1	218.88	2	1276.46	692.08

It is conspicuous that for the small leaks (0.25 l/s) the algorithms by all sensor placements find a lot of possible leak positions which are widespread over the search area. SPuDU also achieves decent solutions for the small leak sizes (see Figure 5.9).
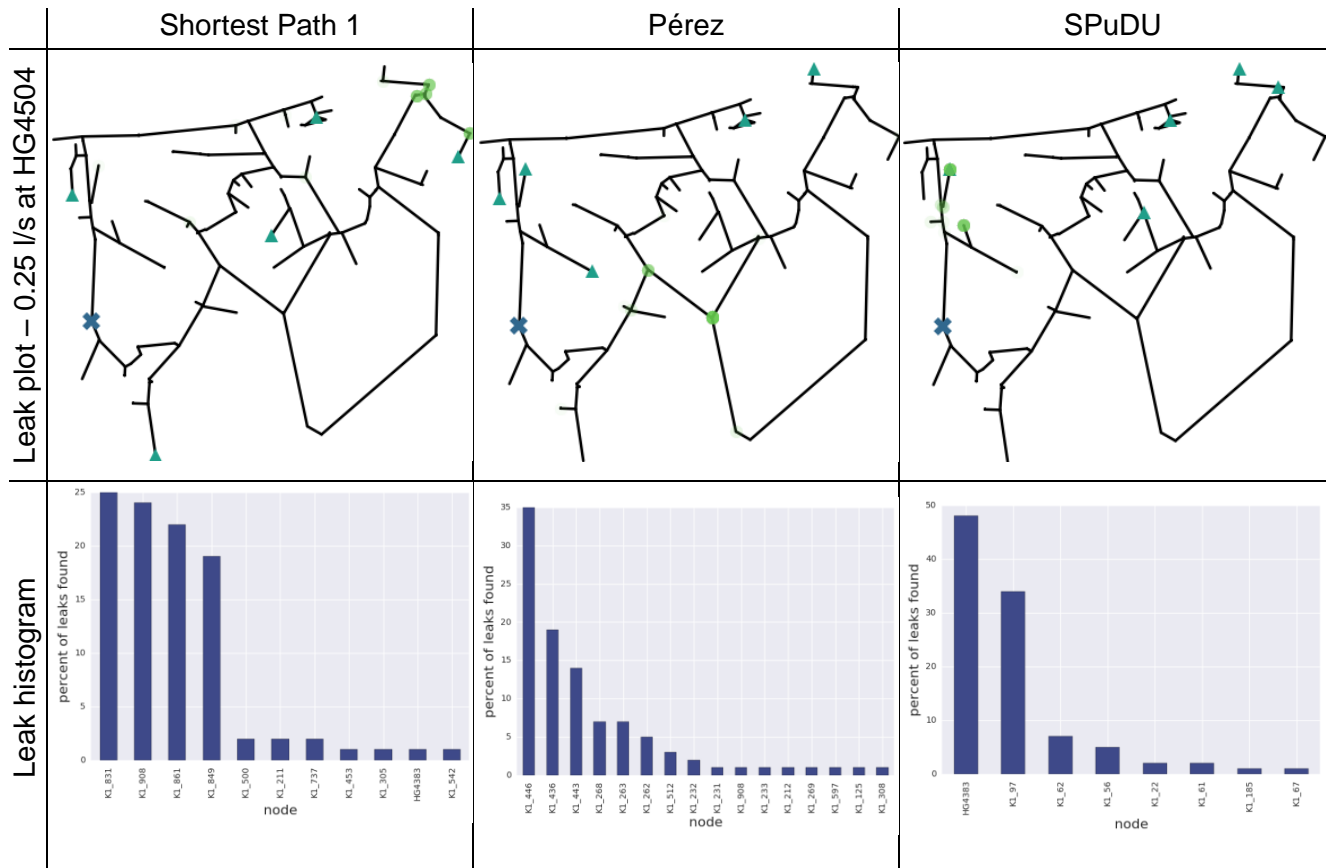
Figure 5.9: Results for the 0.25 l/s leak at HG4504 (Shortest Path 1, Pérez, SPuDU)

The Shannon entropy method and the topology-based algorithms (Shortest Path 1 and 2) only achieved results within 2,000 m (Table 5-7). Regarding that the WDS of Hart is only of 9.55 km length these solutions are not useable for leakage localization. SPuDU also provides results within 500 m for the 0.25 l/s at HG4504 and HG3880.

The most accurate results were achieved with calculations of the bigger leaks (0.7 l/s and 1.0 l/s) at HG3880 and HG4504 by the sensor placement methods SPuDU and Casillas. The solutions of the smaller leaks are not that clear. The conclusion is that the greater the leak, the easier it is to narrow down the area where the actual leak can be located.

From the fact that the methods do not achieve the same results at each leak location with the same leak size, it is difficult to say if one method is better than another. A possible reason for this might be false assumptions for the input parameters in the EPANET model.

In this research none of the six sensor placement methods becomes apparent. It could be seen that the sensitivity-based algorithms (SPuDU, Casillas, Pérez and Shannon entropy) provide better solutions than topology-based algorithms (Shortest Path1 and 2).

75

At Table 5-7 the statistical values for the leak at HG4504 (most frequently detected leak, closest leak, leak furthest away from the actual leak, average distance to the real leak) are shown.

Table 5-7: Calibrated model - 0.7, 0.5 and 0.25 l/s leak at HG4504

HG4504	Number of nodes found	Most frequently detected leak		Closest leak		Leak furthest away		Average distance to real leak
0.7 l/s		[%]	[m]	[%]	[m]	[%]	[m]	[m]
Casillas	11	51	516.57	1	262.55	6	1346.05	518.58
Pérez	10	43	947.53	1	552.57	10	1346.05	947.51
SPuDU	10	52	516.57	1	296.99	3	533.56	462.43
Shannon	5	64	947.53	1	678.84	25	1346.05	1044.49
SP 1	7	35	947.53	1	679.24	29	1346.05	1055.51
SP 2	5	53	1346.05	1	679.89	53	1346.05	1156.20
0.5 l/s		[%]	[m]	[%]	[m]	[%]	[m]	[m]
Casillas	11	59	516.57	1	214.53	18	1346.05	655.29
Pérez	8	34	947.53	3	678.84	18	1346.05	971.31
SPuDU	7	66	516.57	1	326.56	1	534.65	484.40
Shannon	4	35	947.53	12	946.41	29	1346.05	1063.72
SP 1	5	46	1346.05	9	946.41	46	1346.05	1134.95
SP 2	17	30	1346.05	17	946.41	1	1963.41	1156.81
0.25 l/s		[%]	[m]	[%]	[m]	[%]	[m]	[m]
Casillas	18	31	451.76	2	0.00	1	2130.69	637.96
Pérez	16	35	950.65	1	554.89	1	2130.69	900.05
SPuDU	8	48	516.57	1	296.53	1	533.56	469.24
Shannon	12	61	2130.69	1	451.76	1	2135.36	1819.73
SP 1	11	25	1910.57	1	516.57	24	2130.69	1913.19
SP 2	6	27	1963.41	1	998.89	23	2130.69	1965.82

In Table 5-8 the pressure loss at the time of the leakage at HG3880, HG4504 an HG3164 is calculated. The pressure drop caused by the leakage is recognizable at the hydrant where the leak was simulated and the surrounding hydrants.

76

The pressure drop is compared to the one computed with the uncalibrated system a little bit higher. These results show that a leak of 0.25 l/s is very difficult to detect in this WDS of Hart because the pressure loss caused by the leak is very small (4 – 6 cm).

Table 5-8: Pressure loss at leaks HG3880, HG4504 and HG3164

	0.25 l/s leak	0.5 l/s leak	0.7 l/s leak	1.0 l/s leak
	pressure loss [m]			
Node ID				
HG3880	0.06	0.16	0.26	-
HG4504	0.06	0.15	0.24	-
HG3164	0.04	0.08	-	0.19

5.3 Recalibrated model

The calculations of the recalibrated model (change of the tank elevation by 2.5 m in order to further reduce the discrepancies between the measured values and the simulation results) were conducted for the bigger leaks and all twelve sensor positions. With this model the different sensor placement algorithms were not looked at separately.

When looking at the results of the leaks HG3880 and HG4504 (Figure 5.10) the found leaks are more than 1,300 m away from the actual leak. Only the leak at HG3164 and the night measurements at HG3302 and HG3537 achieve results within 1,000 m.
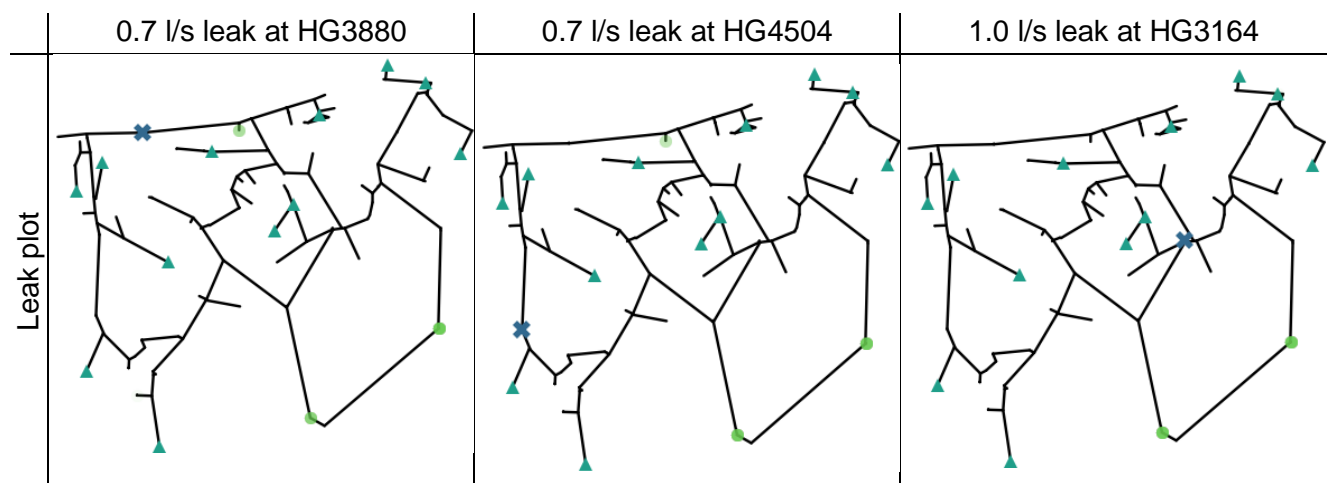
Figure 5.10: Recalibrated model - leak plots

At Table 5-9 the values for the most frequently detected leak, the closest leak and the leak furthest away from the actual leak and the average distance to the real leak are shown.

Table 5-9: Recalibrated model - HG3880, HG4504 and HG3164

	Number of nodes found	Most frequently detected leak		Closest leak		Leak furthest away		Average distance to real leak
		[%]	[m]	[%]	[m]	[%]	[m]	[m]
HG3880 0.7 l/s	6	54	1525.76	15	306.37	27	1540.10	1345.30
HG4504 0.7 l/s	5	44	1346.05	10	1025.14	44	1872.87	1556.29
HG3164 1.0 l/s	5	49	765.74	1	678.43	44	801.60	782.74

The results of the recalibrated model show that the desired improvement of the leakage localization could not be reached with the change of the tank elevation.

In Table 5-10 the pressure loss for the 0.7 l/s and the 1.0 l/s leak using the recalibrated model is illustrated. The pressure drop caused by the leakage is recognizable at the hydrant where the leak was simulated and the surrounding hydrants. The pressure difference for the 0.7 l/s leaks at HG3880 and HG4504 on the position the real leak (grey marked) accounts to 23 cm. At the surrounding hydrants the pressure loss is between 7 and 23 cm. The small differences reflect the results gained by the leak plots.

78

Table 5-10: Pressure loss for 0.7 l/s and 1.0 l/s using the recalibrated model

Recalibrated model	0.7 l/s leak at HG3880	0.7 l/s leak at HG4504	1.0 l/s leak at HG3164
	Pressure loss [m]		
Node ID			
HG3164			0.17
HG3420	0.08	0.08	0.14
HG3445	0.08	0.08	0.14
HG3835	0.13	0.12	0.13
HG3880	0.23		
HG3933	0.16	0.14	0.12
HG4150	0.07	0.07	0.13
HG4162	0.08	0.08	0.14
HG4215	0.07	0.07	0.13
HG4339b	0.22	0.22	0.13
HG4383	0.21	0.23	0.12
HG4504		0.23	
HG4540	0.21	0.23	0.12
HG4576	0.19	0.23	0.12
HG4744	0.09	0.09	0.11

Regarding to the results of the three EPANET models mentioned above none of the sensor placement methods provided excellent solutions for leakage localization. Therefore, it is necessary to have a closer look on possible factors which might have had a negative effect on the measurements.

5.4 Possible influencing factors on leak localization accuracy in Hart near Graz/ Ragnitz

After careful consideration there are several factors which could have had a negative influence on leak localization accuracy in the case study in Hart close to Graz/ Ragnitz:

Different hydraulic systems

It is possible that the conditions at the hydrants, the valves or the pipes changed after the fire flow tests and night measurements which were used for model calibration in a way that these measurements do not longer represent the hydraulic situation in the system. It is also imaginable that the fire flow tests have led to a different system status in case of flow directions and hence to pressure drops that do not represent the

hydraulic status under normal condition. Also, it is not known if the status of valves after the calibration night has changed.

Incorrect Calibration

Based on the points mentioned above it can be that the calibration of the EPANET model does not describe the actual system (normal condition) properly. It can be that for the purpose of model-based leak localization the used fire flow test based calibration is not appropriate.

Inaccurate Algorithm

Another possibility could be that the algorithm used for the leakage localization was incorrect, however this can be excluded in this case. The algorithm was set at 100 cycles. Maybe the results were more precise if the generation size would have been bigger.

The statistical approach was too coarse

The mean values of leakage, inflow and pressures were calculated over three days. Each day the pressure values differed up to 0.4 m. This could have possibly led to further discrepancies. If each day had been looked at separately maybe the results would have been different.

Insufficient time to get familiar with the system

Before starting the leakage measurements only a small data set of the undisturbed system under normal demand conditions existed. The initial state could not be characterized properly. The undisturbed system was only measured between the second and the third leakage measurement. It is unclear how the pressure fluctuates in the undisturbed WDS.

Falsification of the data due to unknown water consumption

There are also unknown demands that could have falsified the data. Due to the fact that the measurements took place during summer additional demands such as filling of swimming pools or other unknown leakages may have been possible.

The tank level might have a greater significance

The influence of the tank filling level could be more significant than thought initially. It is possible that wrong or incorrect data for the filling level and the tank bottom was used for the calculations.

Other measuring errors at pressure loggers and flow meters

Another possible factor that could have influenced the results is a measuring fault at the pressure sensors and or the flow meter. That could have also led to an addition of measuring errors of the different devices.

6 Conclusions

Leak detection in water distribution systems is very important in order to save drinking water and prevent pollution and damage from the surrounding environment. The objective of this research was to compare different sensor placement methods for model-based leak localization of different leak sizes. Therefore, three leaks were simulated in a real-world case study Hart close to Graz.

Model-based leakage localization methods are not really field-tested yet. The six sensor placement methods used in this case study present different sensor positions as results. It was not expected to locate the precise position of the actual leak but to find the most accurate leak location using the algorithm. Results within a radius of 500 m are considered good solutions for this research.

The results of the calibrations with the uncalibrated EPANET model first seem to be solid while analyzing the first simulated leak at HG3880 for the sensor placements Casillas and SPuDU. The leak was found within a radius of 500 m from the actual leak. It turned out later that these results were rather random hits and that the algorithm always found the leak nearly at the same positions for all leak positions.

The first calibration of the EPANET model only has an insignificant effect on the achieved results. Only a few more points closer to the real leak were detected but a significant change was not visible after this calibration. From the fact that the methods do not achieve the same results at each leak location with the same leak size, it is difficult to say if one method is better than another.

The sensor placement method SPuDU developed at the TUGraz achieved valid results for the leaks 0.25 -1.0 l/s at HG3880, 0.25 – 0.7 l/s at HG4504.

In general, it can be said that at bigger leaks (0.7 l/s and 1.0 l/s) the search area can be narrowed down to a smaller radius which makes later pinpointing of the exact position of the leak easier. At the small leaks (0.25 l/s) the leak positions found by the algorithm vary greatly and are widespread over the search area.

Regarding the results of the three EPANET models none of the sensor placement methods provided excellent solutions for leakage localization in this research.

For further studies it is recommended that the general build-up of the artificial leaks should be arranged differently. Considering the varying diameter of a PE-pipe it is better to use a pipe made of stainless steel to avoid measuring inaccuracies.

Further, the undisturbed WDS should be measured over a longer period of time in order to get to know possible variations in the pressure of the system, unusual water consumption or other factors.

List of Tables

List of Figures

References

Almandoz, J., Arregui, F., Cabrera, E. and Cobacho, R. 2005. *Leakage Assessment through Water Distribution Network Simulation.* s.l. : Journal of Water Resources Planning and Management, Vol. 131 (6), 2005. 458-466.

Bodendorfer, U. 2003. *Genetic Algorithms: Theory and Applications.* Linz : Fuzzy Logic Laboratorium Linz-Hagenberg, 2003.

Casillas, M.V., Puig, V., Garza-Castañón, L.E. and Rosich, A. 2013. *Optimal Sensor Placement for Leak Location in Water Distribution Networks Using Genetic Algorithms.* s.l. : Sensors, 2013. 13, 14984-15005.

Dalton, J. 2007. Roulette wheel selection. *Newcastle University.* [Online] 2007. [Cited: 08 09 2016.] http://www.edc.ncl.ac.uk/highlight/rhjanuary2007g02.php.

Darwin, C. November 1859. *On the Origin of Species. Or the Preservation of Favoured Races in the Struggle for Life.* London : s.n., November 1859.

Das Land Steiermark. 2015. [Online] 2015. [Cited: 18 09 2016.] http://www.statistik.steiermark.at.

De Schaetzen, W.B.F., Walters, G.A. and Savic, D.A. 2000. *Optimal sampling design for model calibration using shortest path, genetic and entropy algorithms.* s.l. : Urban Water 2, 2000. 141-152.

Dong, X., Liu, S., Tao, T., Li, S. and Xin, K. 2012. *A comparative study of differential evolution and genetic algorithms for optimizing the design of water distribution systems.* Shanghai, China : Journal of Zhejiang University-SCIENCE A (Applied Physics & Engineering), 2012.

Endress + Hauser. Portable Ultrasonic Flow Measuring System - prosonic flow 92. *Temporary volume flow measurement of liquids.* [Online] [Cited: 30 08 2016.] http://www.ashdale.co.uk/items/products/instrumentation/flow/ultrasonic/pdf/en026v1 _ti060den.pdf.

EPA US Environmental Protection Agency. EPANET. *Software That Models the Hydraulic and Water Quality Behavior of Water Distribution Piping Systems.* [Online] [Cited: 30 08 2016.] https://www.epa.gov/water-research/epanet.

European Union. 2015. *EU Reference document Good Practices on Leakage Management WFD CIS WG PoM.* Luxembourg : Office for Official Publications of the European Communities, 2015. ISBN 978-92-79-45069-3.

Fanner, P. and Lambert, A. March 2009. *Calculating SRELL with Pressure Management, Active Leakage Control and Leak Run-Time Options, with confidence limits.* Cape Town, South Africa : IWA Specialist Conference "Waterloss 2009", March 2009.

Fanner, P., Sturm, R., Thornton, J., Liemberger, R., Davis, S.E. and Hoogerwerf, T. 2007. *Leakage Management Technologies.* s.l. : Awwa Research Foundation (AwwaRF) and the U.S. Environmental Protection Agency (USEPA), 2007.

Farley, M. 2001. *Leakage Management and Control.* s.l. : WHO, 2001.

Farley, M. and Trow, S. 2003. *Losses in Water Distribution Networks – A Practitioner's Guide to Assessment, Monitoring and Control.* London : IWA Publishing, 2003. ISBN 1900222116.

Farley, M. 2003. *Non-revenue water - International best practice for assessment, monitoring and control.* Atlantis, Paradise Island, Bahamas : 12th Annual CWWA Water, Wastewater & Solid Waste Conference, 2003.

Farley, M., Wyeth, G., Ghazali, Z., Istandar, A. and Singh, S. 2008. *The Manager's Non-Revenue Water Handbook.* 2008.

FLEXIM GmbH. Software FluxData. [Online] [Cited: 01 09 2016.] http://www.flexim.ro/ultrasonicflowmeterpro_software.php.htm.

FLEXIM GmbH Specifications FLUXUS ADM 6725. *The Portable Flowmeter.* [Online] [Cited: 06 07 2016.] http://www.mimos.si/FLEXIM/AMD6725.pdf.

FLEXIM GmbH 2008. Technical Specifications FLUXUS ADM 6725. [Online] 01 06 2008. [Cited: 06 07 2016.] http://www.flexim.com/sites/default/files/public_downloas/tsfluxus_f6725v1-0en.pdf.

FLEXIM GmbH 2006. Tragbares Ultraschall-Durchflussmessgerät FLUXUS ADM 6725. *Firmware V5.xx.* [Online] 2006. [Cited: 06 07 2016.] http://www.sigrist-ag.ch/tb/turbinenbau/pdf_ultraschall/Bedienungsanleitung%20ADM6725.pdf.

Frauendorfer, R. and Liemberger, R. 2010. *The Issues and Challenges of Reducing Non-Revenue Water.* Philippines : Asian Development Bank, 2010. ISBN 978-92-9092-398-5.

Goldberg, D.E. 1989. *Genetic Algorithm in Search, Optimization, and Machine Learning.* Boston, MA, USA : Addison-Wesley Longman Publishing Co., Inc., 1989. ISBN:0201157675.

Grefenstette, J.J. 1986. *Optimization of Control Parameters for Genetic Algorithms.* s.l. : IEEE Transactions on Systems, Man, and Cybernetics, SMC-16 No.1, 1986. 122-128.

Grunwell, D. and Ratcliffe, B. 1981. *Location of underground leaks using the leak noise correlator.* s.l. : Water Research Center. Technical Report 157, 1981.

Hamilton, S. and Charalambous, B. 2013. *Leak Detection - Technology and Implementation.* London : IWA Publishing, 2013. ISBN 9781780404714.

Hunaidi, O., Wang, A., Bracken, M., Gambino, T. and Fricke, C. 2004. *Acoustic methods for locating leaks in municipal water pipe networks.* Dead Sea, Jordan : International Conference on Water Demand Management, 2004. 1-44.

Kapala, J.M. 2016. *Influence of hydraulic water distribution network calibration on model based leak localisation problems.* Università di Bologna : s.n., 2016.

Kaya, Y., Uyar, M. and Tekin, R. 2011. A Novel Crossover Operator for Genetic Algorithms: Ring Crossover. [Online] 2011. [Cited: 08 09 2016.] https://arxiv.org/ftp/arxiv/papers/1105/1105.0355.pdf.

Keller AG für Druckmesstechnik. 2014. Logger 5.1 Manual. [Online] 2014. [Cited: 01 09 2016.] http://www.keller-druck2.ch/swupdate/InstallerLogger5/manual/logger5_E_en.pdf.

Lambert, A. 2002. *A Water losses management and techniques.* s.l. : Water Science and Technology:Water Supply, 2 (4), 2002. 1-20.

Lambert, A. and Hirner, W. 2000. Losses from water supply systems: Standard terminology and recommended performance measures. [Online] 2000. [Cited: 21 08 2009.] www.iwahq.org.

Lambert, A. 1993. *Background and Burst Estimates (BABE).* 1993.

Lambert, A. May 2000. *What do we know about pressure: Leakage relationships in distribution systems?* Brno, Czech Republik : IWA Conference "System Approach to Leakage Control and Water Distribution Systems Management", May 2000.

Lambert, A.O. and Lalonde, A. 2005. *Using practical predictions of Economic Intervention Frequency to calculate Short-run Economic Leakage Level, with or without Pressure Management .* Halifax, Nova Scotia, Canada : Proceedings of IWA Specialised Conference "Leakage 2005", 2005.

Landuyt, L. 2015. *Calibration of a hydraulic network model in a Styrian water distribution company.* Universiteit Gent : s.n., 2015.

Liemberger, R. and Farley, M. 2004. *Developing a non-revenue water reduction strategy Part 1: Investigating and assessing water losses.* Marrakech, Morocco : Proceeding of IWA WWC 2004 Conference, 2004.

Malhotra, R., Singh, N. and Singh, Y. March 2011. *Genetic Algorithms: Concepts, Design for Optimization of Process.* Punjab Technical University, Jalandhar, Punjab, India : Computer and Information Science, March 2011. Vol. 4, No. 2.

Mamlook, R. and Al-Jayyous, O. 2003. *Fuzzy sets analysis for leak detection in infrastructure systems: a proposed methodology.* s.l. : Cleaning Techniques and Environmental Policy, 6 (1), 2003. 26-31.

Mashford, J., Silva, D. De, Marney, D. and Burn, S. 2009. *An Approach to Leak Detection in Pipe Networks Using Analysis of Monitored Pressure Values by Support Vector Machine.* Gold Coast, Queensland, Australia : Third International Conference on Network and System Security, 2009. 534-539.

Meseguer, J., Mirats-Tur, J.M., Cembrano, G. and Puig, V. 2015. Spain : 13th Computer Control for Water Industry Conference, CCWI 2015, 2015.

Mitchell, M. 1996. *An Introduction to Genetic Algorithm.* Massachusetts : Massachusetts Institute of Technology, 1996.

Moors, J. 2016. *Model-based leak localization in small water supply networks.* s.l. : Delft University of Technology, 2016.

Pérez, R., Puig, V., Pascual, J., Peralta, A., Landeros, E. and Jordanas, Ll. 2009. *Pressure sensor distribution for leak detection in Barcelona water distribution network.* s.l. : Water Science & Technology: Water Supply - WSTWS, Vol. 9, No. 6, pp 715-721, 2009.

Pérez, R., Puig, V., Pascual, J., Quevedo, J., Landeros, E. and Peralta, A. 2011. *Methodology for leakage isolation using pressure sensitivity analysis in water distribution.* s.l. : Control Engineering Practice, Vol. 19, No. 10, 2011. 1157-1167.

Pérez, R., Sanz, G., Puig, V., Quevedo, J., Cugueró, M.A., Nejjari, F., Meseguer, J., Cembrano, G., Mirats, J.M. and Sarrate, R. 2013. *Leakage Localization in Water Networks - A model-based methodology using pressure sensors applied to a real case in Barcelona network.* s.l. : IEEE Control Systems, Vol. 34, 2013. 24-36.

Pilcher, R., Hamilton, S., Chapman, H., Field, D., Ristovski, B. and Stapely, S. March 2007. *Leak Location and Repair guidance notes.* Bucharest, Romania : International Water Association. Water Loss Task Forces, March 2007.

Pudar, R. S. and Liggett, J. A. 1992. *Leaks in pipe networks.* s.l. : Journal of Hydraulic Engineering. 118 (7), 1031-1046, 1992.

Pure Technologies. SmartBall® Technology. [Online] [Cited: 07 10 2016.] https://www.puretechltd.com/technologies-brands/smartball.

Puust, R., Kapelan, Z., Savic, D.A. and Koppel, T. February 2010. *A review of methods for leakage management in pipe networks.* s.l. : Urban Water Journal Vol. 7, No. 1, February 2010. 25-45.

Python. 2016. *Programming language.* [Online] Python Software Foundation (US), 2016. [Cited: 13 9 2016.] https://www.python.org/. Python.

Quevedo, J., Cugueró, M., Pérez, R., Nejjari, F., Puig, V. and Mirats, J. 2011. *Leakage Location in Water Distribution Networks based on Correlation Measurement of Pressure Sensors.* San Sebastián : 8th IWA Symposium on Systems Analysis and Integrated Assessment, 2011.

Ragot, J. and Maquin, D. 2006. *Fault measurement detection in a urban water supply network.* s.l. : Journal of Process Control, Vol. 16, No. 9, 2006. 887-902.

Razali, N.M. and Geraghty, J. July 6-8, 2011. *Genetic Algorithm Performance with Different Selection Strategies in Solving TSP.* London, U.K. : Proceedings of the World Congress on Enigneering 2011 Vol II, July 6-8, 2011.

RLE Technologies. Early Leak Detection : An Ounce of Prevention. [Online] [Cited: 06 10 2016.] http://rletech.com/blog/early-leak-detection-ounce-prevention/.

Rosich, A. and Puig, V. 2013. *Model-based leakage localization in drinking water distribution networks using structured residuals.* s.l. : Control Conference (ECC), 2013 European, 2013.

Rossman, L. 2000. *EPANET 2 User´s Manual.* Washington, DC, USA : United States Environmental Protection Agency, 2000.

Sastry, K. and Goldberg, D.E. 2002. *Analysis of Mixing in Genetic Algorithms: A survey.* Illinois : IlliGAL report No. 2002012, 2002.

Schrotter, S. 2010. *Ermittlung des wirtschaftlich optimalen Leckortungsturnusses von Wasserleitungen.* Graz : Institut für Siedlungswasserwirtschaft und Landschaftswasserbau, Technischen Universität Gr, 2010.

SETEC Engineering. SEWAD 30. *Pressure sensors.* [Online] [Cited: 06 07 2016.] http://www.setec.at/en/100.html.

SEWERIN. Technologies for leak detection. [Online] [Cited: 07 10 2016.] http://www.sewerin.co.uk/products/water-leak-location/secorrphon/.

Shannon, C. E. July, October 1948. *A Mathematical Theory of Communication.* s.l. : The Bell System Technical Journal, July, October 1948. Vol. 27, pp. 379-423, 623-656.

Steffelbauer, D., Günther, M., Neumayer, M. and Fuchs-Hanusch, D. 2014. *Sensor Placement and Leakage Isolation with Differential Evolution.* s.l. : World Environmental and Water Resources Congress 2014: Water without Borders ASCE 2014, 2014. 408-416.

Steffelbauer, D., Günther, M., Neumayer, M. and Fuchs-Hanusch, D. 2014. *Sensor Placement and Leakage Localization considering Demand Uncertainties.* s.l. : 16th Conference on Water Distribution System Analysis, WDSA 2014, Procedia Engineering 89 (2014), 2014. 1160-1167.

Steffelbauer, D.B., Günther, M. and Fuchs-Hanusch, D. 2016. *Leakage Localization with Differential Evolution: A Closer Look on Distance Metrics.* Graz, Austria : XVIII International Conference on Water Distribution Systems, WDSA2016, 2016.

Stenberg, R. 1982. *Leak detection in water supply systems.* Stockholm, Sweden : The Swedish Water and Waste Water Works Association, 1982.

Storn, R. and Price, K. 1997. *Differential Evolution – A simple and efficient heuristic for global optimization over continuous spaces.* s.l. : Journal of Global Optimization, 11, 1997. 341-359.

Thornton, J., Sturm, R. and Kunkel, G. 2008. *Water Loss Control.* s.l. : McGraw-Hill, 2008.

Tutorialspoint. *Genetic Algorithms Tutorial.* [Online] [Cited: 08 09 2016.] https://www.tutorialspoint.com/genetic_algorithms/index.htm.

Worksmart, Inc. 2012. Advanced Subsurface Imaging. [Online] 2012. [Cited: 07 10 2016.] http://www.worksmartinc.net/.

Wu, Z.Y. and Sage, P. 2006. *Water Loss detection via genetic algorithm optimization-based model calibration.* Cincinnati, Ohio : ASCE 8th Annual International Symposium on Water Distribution System Analysis, 2006.

Appendix

In the following all calculated data during this research for example the mean values and the results from the uncalibrated and calibrated model is shown.

A.1   Mean values of leakage at HG4504 and HG3164

Table A - 1: Results of the calculations of the mean values of leakage, inflow and pressures with respect to the different sensor placements (Pérez, Casillas, SPuDU) at HG4504

			leak 2 - HG4504
period	01:00 - 04:00										
date			26.04.2016	27.04.2016	28.04.2016	29.04.2016	30.04.2016	01.05.2016	02.05.2016	03.05.2016	04.05.2016
				0.25			0.5			0.7	
	hydrant ID			Ø pressure [mWC]			Ø pressure [mWC]			Ø pressure [mWC]	
Pérez	HG3933	205	89.33604	89.39038	89.55793	89.41917	89.38657	89.47967	89.37371	89.34943	89.34766
				89.42811604			89.42847278			89.35693011	
	HG4215	1248	88.44395	88.48468	88.57383	88.46898	88.46160	88.57867	88.37150	88.44640	88.43376
				88.50081904			88.50308551			88.41722254	
	HG4339b	210	94.42460	94.46854	94.64033	94.49723	94.46591	94.56605	94.41437	94.40265	94.38649
				94.51115924			94.50973168			94.40117243	
	HG4383	3768	88.28096	88.30359	88.47616	88.33535	88.28334	88.39686	88.26973	88.23717	88.22150
				88.35356872			88.33851744			88.24279926	
	HG4540	1536	61.12533	61.15153	61.36028	61.18927	61.16500	61.23595	61.09505	61.09545	61.08206
				61.21238130			61.19674127			61.09085468	
Casillas	HG3420	423	82.26196	82.28570	82.50204	82.37920	82.28359	82.37345	82.28939	82.31629	82.25479
				82.34989796			82.34541372			82.28682451	
	HG3835	433	87.57356	87.60752	87.79545	87.63600	87.60704	87.69971	87.60715	87.55475	87.53210
				87.65884159			87.64758599			87.56466808	
	HG3933	205	89.33604	89.39038	89.55793	89.41917	89.38657	89.47967	89.37371	89.34943	89.34766
				89.42811604			89.42847278			89.35693011	
	HG4215	1248	88.44395	88.48468	88.57383	88.46898	88.46160	88.57867	88.37150	88.44640	88.43376
				88.50081904			88.50308551			88.41722254	
	HG4383	3768	88.28096	88.30359	88.47616	88.33535	88.28334	88.39686	88.26973	88.23717	88.22150
				88.35356872			88.33851744			88.24279926	
SPuDU	HG3420	423	82.26196	82.28570	82.50204	82.37920	82.28359	82.37345	82.28939	82.31629	82.25479
				82.34989796			82.34541372			82.28682451	
	HG3933	205	89.33604	89.39038	89.55793	89.41917	89.38657	89.47967	89.37371	89.34943	89.34766
				89.42811604			89.42847278			89.35693011	
	HG4162	837	85.88589	85.95738	86.04148	85.94381	85.93028	86.05640	85.86694	85.90752	85.91199
				85.96158597			85.97683252			85.89548370	
	HG4215	1248	88.44395	88.48468	88.57383	88.46898	88.46160	88.57867	88.37150	88.44640	88.43376
				88.50081904			88.50308551			88.41722254	
	HG4383	3768	88.28096	88.30359	88.47616	88.33535	88.28334	88.39686	88.26973	88.23717	88.22150
				88.35356872			88.33851744			88.24279926	

Table A - 2: Results of the calculations of the mean values of leakage, inflow and pressures with respect to the different sensor placements (Shannon entropy, Shortest Path 1, Shortest Path 2) at HG4504

period	01:00 - 04:00		leak 2 - HG4504							
date			26.04.2016	27.04.2016	28.04.2016	29.04.2016	30.04.2016	01.05.2016	02.05.2016	03.05.2016	04.05.2016
				0.25			0.5			0.7	
	hydrant ID			Ø pressure [mWC]			Ø pressure [mWC]			Ø pressure [mWC]	
Shannon Entropy	HG3420	423	82.26196	82.28570	82.50204	82.37920	82.28359	82.37345	82.28939	82.31629	82.25479
				82.34989796			82.34541372			82.28682451	
	HG3933	205	89.33604	89.39038	89.55793	89.41917	89.38657	89.47967	89.37371	89.34943	89.34766
				89.42811604			89.42847278			89.35693011	
	HG4215	1248	88.44395	88.48468	88.57383	88.46898	88.46160	88.57867	88.37150	88.44640	88.43376
				88.50081904			88.50308551			88.41722254	
	HG4339b	210	94.42460	94.46854	94.64033	94.49723	94.46591	94.56605	94.41437	94.40265	94.38649
				94.51115924			94.50973168			94.40117243	
	HG4744	432	31.07882	31.12682	31.30354	31.17670	31.12523	31.19585	31.09977	31.09631	31.09863
				31.16972853			31.16592547			31.09823726	
Shortest Path 1	HG3445	411	68.43617	68.45508	68.64544	68.56487	68.48811	68.55724	68.45996	68.46674	68.44773
				68.51222898			68.53673880			68.45814171	
	HG3933	205	89.33604	89.39038	89.55793	89.41917	89.38657	89.47967	89.37371	89.34943	89.34766
				89.42811604			89.42847278			89.35693011	
	HG4150	206	75.13700	75.19074	75.29250	75.19203	75.15533	75.23694	75.06909	75.13006	75.10956
				75.20674409			75.19477061			75.10290326	
	HG4339b	210	94.42460	94.46854	94.64033	94.49723	94.46591	94.56605	94.41437	94.40265	94.38649
				94.51115924			94.50973168			94.40117243	
	HG4744	432	31.07882	31.12682	31.30354	31.17670	31.12523	31.19585	31.09977	31.09631	31.09863
				31.16972853			31.16592547			31.09823726	
Shortest Path 2	HG3445	411	68.43617	68.45508	68.64544	68.56487	68.48811	68.55724	68.45996	68.46674	68.44773
				68.51222898			68.53673880			68.45814171	
	HG4150	206	75.13700	75.19074	75.29250	75.19203	75.15533	75.23694	75.06909	75.13006	75.10956
				75.20674409			75.19477061			75.10290326	
	HG4339b	210	94.42460	94.46854	94.64033	94.49723	94.46591	94.56605	94.41437	94.40265	94.38649
				94.51115924			94.50973168			94.40117243	
	HG4576	414	30.08191	30.11620	30.28459	30.16005	30.09319	30.20602	30.07271	30.06495	30.01569
				30.16089801			30.15308477			30.05111764	
	HG4744	432	31.07882	31.12682	31.30354	31.17670	31.12523	31.19585	31.09977	31.09631	31.09863
				31.16972853			31.16592547			31.09823726	

Table A - 3: Results of the calculations of the mean values of leakage, inflow and pressures with respect to the different sensor placements (Pérez, Casillas, SPuDU) at HG3164

period	01:00 - 04:00		leak 3 - HG3164							
date			16.05.2016	17.05.2016	18.05.2016	10.05.2016	11.05.2016	12.05.2016	13.05.2016	14.05.2016	15.05.2016
			0.25			0.5			1.0		
	hydrant ID		Ø pressure [mWC]			Ø pressure [mWC]			Ø pressure [mWC]		
Pérez	HG3933	205	89.50338	89.57882	89.52474	89.43127	89.51718	89.33542	89.09687	89.18793	89.18734
				89.53564716			89.42796007			89.15737783	
	HG4215	1248	88.56552	88.65503	88.59103	88.42687	88.55296	88.38183	88.12256	88.21164	88.23528
				88.60385764			88.45388843			88.18982541	
	HG4339b	210	94.56288	94.61810	94.58585	94.48225	94.61083	94.41931	94.16790	94.24357	94.25758
				94.58894497			94.50412941			94.22301676	
	HG4383	3768	88.42552	88.51522	88.46015	88.31830	88.41160	88.26999	88.03360	88.11711	88.09158
				88.46696357			88.33329755			88.08076252	
	HG4540	1536	61.26162	61.38523	61.33326	61.17704	61.31482	61.10571	60.87041	60.95368	60.97873
				61.32670427			61.19918921			60.93427199	
Casillas	HG3420	423	82.37190	82.45225	82.38126	82.23822	82.34082	82.18399	81.92341	82.00733	82.00623
				82.40180411			82.25434411			81.97899116	
	HG3835	433	87.70887	87.79970	87.74093	87.61963	87.71252	87.57215	87.30011	87.39128	87.41371
				87.74983274			87.63476757			87.36837099	
	HG3933	205	89.50338	89.57882	89.52474	89.43127	89.51718	89.33542	89.09687	89.18793	89.18734
				89.53564716			89.42796007			89.15737783	
	HG4215	1248	88.56552	88.65503	88.59103	88.42687	88.55296	88.38183	88.12256	88.21164	88.23528
				88.60385764			88.45388843			88.18982541	
	HG4383	3768	88.42552	88.51522	88.46015	88.31830	88.41160	88.26999	88.03360	88.11711	88.09158
				88.46696357			88.33329755			88.08076252	
SPuDU	HG3420	423	82.37190	82.45225	82.38126	82.23822	82.34082	82.18399	81.92341	82.00733	82.00623
				82.40180411			82.25434411			81.97899116	
	HG3933	205	89.50338	89.57882	89.52474	89.43127	89.51718	89.33542	89.09687	89.18793	89.18734
				89.53564716			89.42796007			89.15737783	
	HG4162	837	86.00745	86.07288	86.03044	85.89921	86.05275	85.82320	85.59274	85.63536	85.69324
				86.03692333			85.92505042			85.64044453	
	HG4215	1248	88.56552	88.65503	88.59103	88.42687	88.55296	88.38183	88.12256	88.21164	88.23528
				88.60385764			88.45388843			88.18982541	
	HG4383	3768	88.42552	88.51522	88.46015	88.31830	88.41160	88.26999	88.03360	88.11711	88.09158
				88.46696357			88.33329755			88.08076252	

Table A - 4: Results of the calculations of the mean values of leakage, inflow and pressures with respect to the different sensor placements (Shannon entropy, Shortest Path 1, Shortest Path 2) at HG3164

			leak 3 - HG3164								
period	01:00 - 04:00										
date			16.05.2016	17.05.2016	18.05.2016	10.05.2016	11.05.2016	12.05.2016	13.05.2016	14.05.2016	15.05.2016
			0.25			0.5			1.0		
	hydrant ID		Ø pressure [mWC]			Ø pressure [mWC]			Ø pressure [mWC]		
Shannon Entropy	HG3420	423	82.37190	82.45225	82.38126	82.23822	82.34082	82.18399	81.92341	82.00733	82.00623
				82.40180411			82.25434411			81.97899116	
	HG3933	205	89.50338	89.57882	89.52474	89.43127	89.51718	89.33542	89.09687	89.18793	89.18734
				89.53564716			89.42796007			89.15737783	
	HG4215	1248	88.56552	88.65503	88.59103	88.42687	88.55296	88.38183	88.12256	88.21164	88.23528
				88.60385764			88.45388843			88.18982541	
	HG4339b	210	94.56288	94.61810	94.58585	94.48225	94.61083	94.41931	94.16790	94.24357	94.25758
				94.58894497			94.50412941			94.22301676	
	HG4744	432	31.26417	31.31853	31.25382	31.13684	31.25063	31.06308	30.82616	30.94893	30.95983
				31.27884273			31.15018525			30.91164162	
Shortest Path 1	HG3445	411	68.56442	68.62535	68.59352	68.46118	68.55043	68.38622	68.12423	68.20268	68.23878
				68.59443129			68.46594057			68.18856424	
	HG3933	205	89.50338	89.57882	89.52474	89.43127	89.51718	89.33542	89.09687	89.18793	89.18734
				89.53564716			89.42796007			89.15737783	
	HG4150	206	75.23025	75.33275	75.27483	75.13427	75.20960	75.09760	74.84123	74.87836	74.94870
				75.27927343			75.14715639			74.88943319	
	HG4339b	210	94.56288	94.61810	94.58585	94.48225	94.61083	94.41931	94.16790	94.24357	94.25758
				94.58894497			94.50412941			94.22301676	
	HG4744	432	31.26417	31.31853	31.25382	31.13684	31.25063	31.06308	30.82616	30.94893	30.95983
				31.27884273			31.15018525			30.91164162	
Shortest Path 2	HG3445	411	68.56442	68.62535	68.59352	68.46118	68.55043	68.38622	68.12423	68.20268	68.23878
				68.59443129			68.46594057			68.18856424	
	HG4150	206	75.23025	75.33275	75.27483	75.13427	75.20960	75.09760	74.84123	74.87836	74.94870
				75.27927343			75.14715639			74.88943319	
	HG4339b	210	94.56288	94.61810	94.58585	94.48225	94.61083	94.41931	94.16790	94.24357	94.25758
				94.58894497			94.50412941			94.22301676	
	HG4576	414	30.22314	30.30554	30.25974	30.14115	30.26554	30.04610	29.84840	29.90185	29.93643
				30.26280394			30.15093007			29.89556053	
	HG4744	432	31.26417	31.31853	31.25382	31.13684	31.25063	31.06308	30.82616	30.94893	30.95983
				31.27884273			31.15018525			30.91164162	

A.2 Results from the night measurements with the uncalibrated model

This section illustrates the results from the calculation with the uncalibrated EPANET model from the night measurements. At the hydrants HG3302, HG3537, and HG3880 leaks of 1.0 l/s were simulated and calculated with the sensor placement methods by Casillas, Pérez, and SPuDU. Beside the leak plots also leak histograms, distance histograms, and outflow histograms are shown.

A.2.1 **Statistical evaluations**

Table A - 5: Uncalibrated model, night measurement - 1.0 l/s leak at HG3302

HG3302 1.0 l/s	Number of nodes found	Most frequently detected leak		Closest leak		Leak furthest away		Average distance to real leak
		[%]	[m]	[%]	[m]	[%]	[m]	[m]
Casillas	7	56	1461.65	13	1318.87	11	1551.36	1429.16
Pérez	12	30	1461.65	10	554.79	30	1461.65	903.94
SPuDU	12	66	1461.65	1	1131.91	3	1551.36	1414.06

Table A - 6: Uncalibrated model, night measurement - 1.0 l/s leak at HG3537

HG3537 1.0 l/s	Number of nodes found	Most frequently detected leak		Closest leak		Leak furthest away		Average distance to real leak
		[%]	[m]	[%]	[m]	[%]	[m]	[m]
Casillas	12	61	1313.98	2	1078.68	61	1313.98	1255.95
Pérez	5	44	1313.98	20	1249.17	9	1332.06	1307.20
SPuDU	9	59	1313.98	5	1078.68	59	1313.98	1250.97

Table A - 7: Uncalibrated model, night measurement - 1.0 l/s leak at HG3880

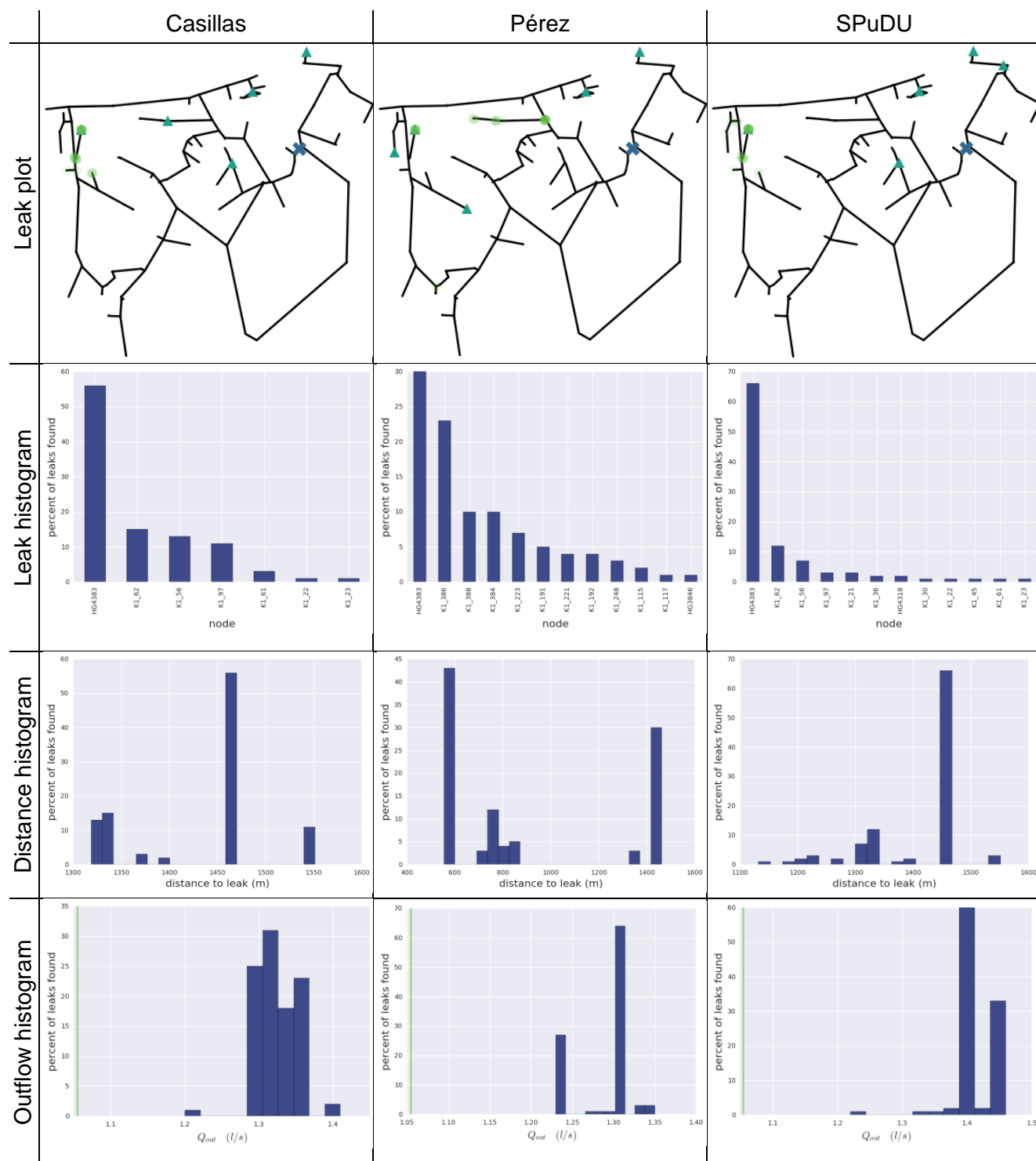| HG3880 1.0 l/s	Number of nodes found	Most frequently detected leak		Closest leak		Leak furthest away		Average distance to real leak
		[%]	[m]	[%]	[m]	[%]	[m]	[m]
Casillas	10	62	491.67	1	228.19	3	581.38	445.22
Pérez	5	46	491.67	46	491.67	11	664.28	577.81
SPuDU	8	64	491.67	2	221.21	1	581.38	443.90

A.2.2   **1.0 l/s leak at HG3302**

Figure 6.1: Results from the sensor placements Casillas, Pérez and SPuDU (Uncalibrated model, 1.0 l/s leak at HG3302)
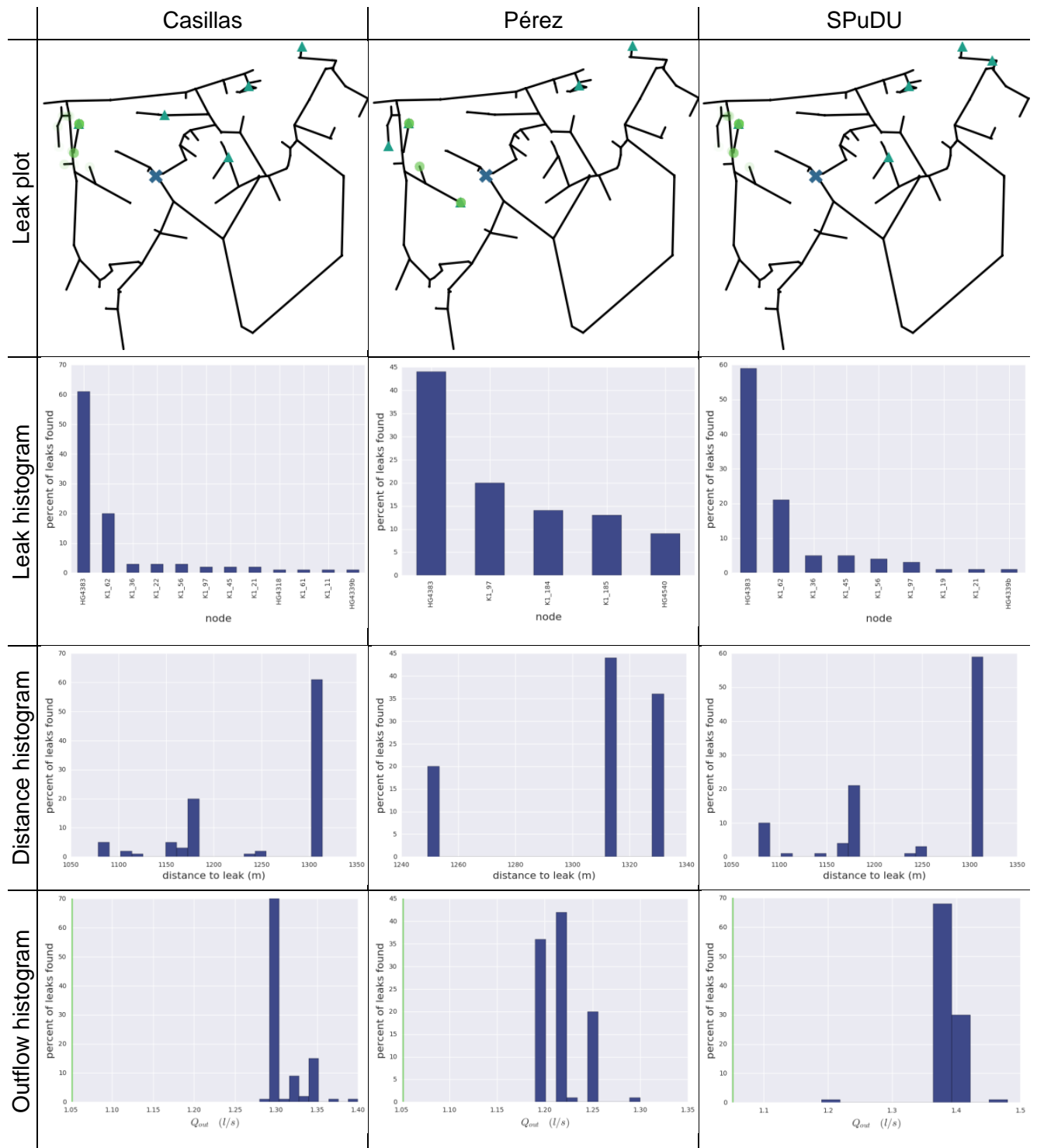
A.2.3 **1.0 l/s leak at HG3537**

Figure 6.2: Results from the sensor placements Casillas, Pérez and SPuDU (Uncalibrated model, 1.0 l/s leak at HG3537)
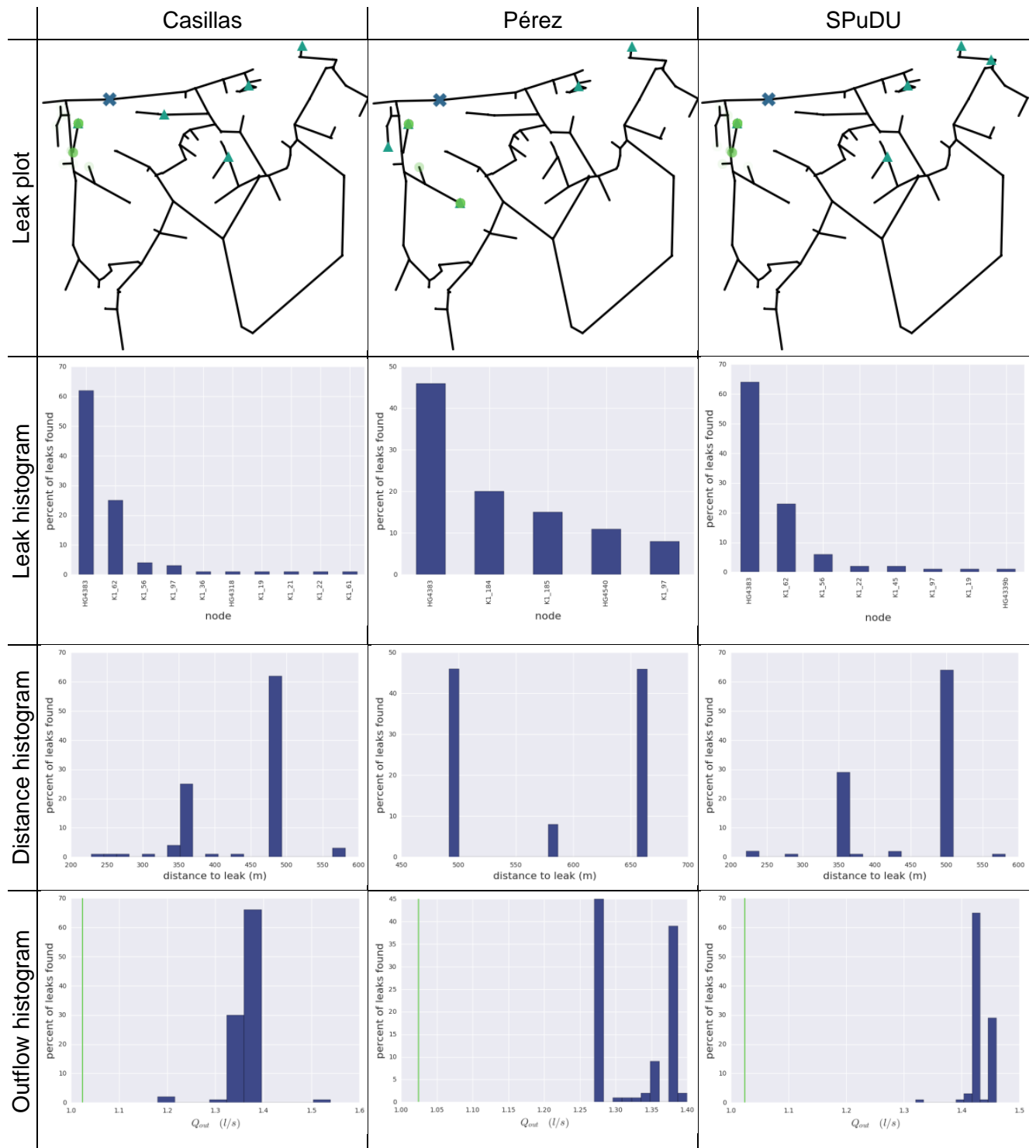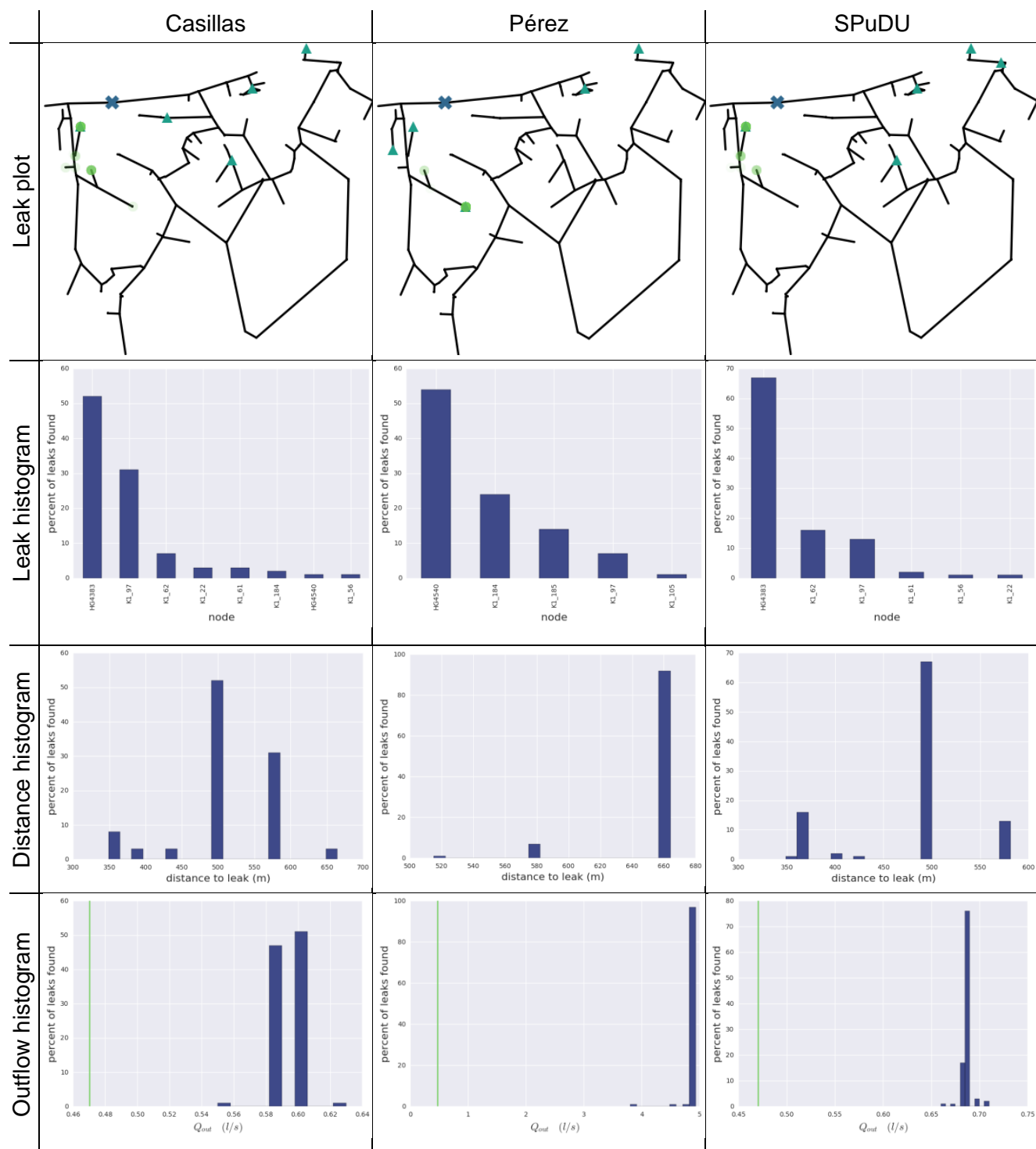
A.2.4   **1.0 l/s leak at HG3880**

Figure 6.3: Results from the sensor placements Casillas, Pérez and SPuDU (Uncalibrated model, 1.0 l/s leak at HG3880)

A.3 Results from the calibrated model

A.3.1 **Statistical evaluations**

Table 6-1: Calibrated model - 1.0 and 9.0 l/s leak at HG3302

HG3302	Number of nodes found	Most frequently detected leakage		Closest leakage		Leakage furthest away	
1.0 l/s		[%]	[m]	[%]	[m]	[%]	[m]
Casillas	8	61	1551.36	9	1318.87	1	1634.25
Pérez	22	23	557.57	2	507.57	1	1147.4
SPuDU	16	27	1131.99	17	1131.91	2	1633.17
Shannon	3	75	602.60	75	602.60	22	1001.13
SP 1	4	72	602.60	72	602.60	26	1001.13
SP 2	4	64	602.60	64	602.60	33	1001.13
9.0 l/s		[%]	[m]	[%]	[m]	[%]	[m]
Casillas	3	97	404.06	97	404.06	1	476.24
Pérez	3	77	473.07	77	473.07	2	507.97
SPuDU	1	100	242.76	100	242.76	-	-
Shannon	2	94	404.06	6	242.76	94	404.76
SP 1	2	97	404.06	3	242.76	97	404.76
SP 2	2	86	404.06	14	242.76	86	404.06

Table 6-2: Calibrated model - 1.0 leak at HG3537

HG3537 1.0 l/s	Number of nodes found	Most frequently detected leakage		Closest leakage		Leakage furthest away	
		[%]	[m]	[%]	[m]	[%]	[m]
Casillas	7	49	1313.98	5	1123.97	1	1330.72
Pérez	7	23	649.98	15	646.87	9	1313.98
SPuDU	7	40	1313.98	6	1123.97	40	1313.98
Shannon	5	79	389.32	3	388.20	15	787.85
SP 1	5	80	389.32	80	389.32	2	820.80
SP 2	4	65	389.32	6	388.20	28	787.85

Table 6-3: Calibrated model - 1.0 leak at HG3880

HG3880 1.0 l/s	Number of nodes found	Most frequently detected leakage		Closest leakage		Leakage furthest away	
		[%]	[m]	[%]	[m]	[%]	[m]
Casillas	10	49	491.67	3	348.90	1	664.28
Pérez	6	47	491.67	47	491.67	5	664.28
SPuDU	7	49	491.67	4	348.90	11	581.38
Shannon	2	64	559.83	64	559.83	36	594.19
SP 1	3	60	559.83	60	559.83	14	1540.10
SP 2	4	66	1141.58	2	974.59	28	1540.10

Table A - 8: Pressure loss at the leaks HG3880

HG3880	0.25 l/s leak	0.5 l/s leak	0.7 l/s leak	1.0 l/s leak
	pressure loss [m]			
Node ID				
HG3420	0.02	0.05	0.07	0.11
HG3445	0.02	0.05	0.07	0.11
HG3835	0.05	0.09	0.13	0.20
HG3880	0.06	0.16	0.26	0.44
HG3933	0.05	0.10	0.15	0.24
HG4150	0.02	0.05	0.07	0.11
HG4162	0.02	0.05	0.07	0.11
HG4215	0.02	0.05	0.07	0.11
HG4339b	0.06	0.15	0.23	0.38
HG4383	0.06	0.15	0.22	0.36
HG4540	0.06	0.14	0.22	0.35
HG4576	0.06	0.13	0.19	0.30
HG4744	0.03	0.06	0.09	0.14

Table A - 9: Pressure loss at the leaks HG4504

HG4504	0.25 l/s leak	0.5 l/s leak	0.7 l/s leak
	pressure loss [m]		
Node ID			
HG3420	0.02	0.05	0.07
HG3445	0.02	0.05	0.07
HG3835	0.04	0.08	0.12
HG3933	0.05	0.09	0.13
HG4150	0.02	0.05	0.07
HG4162	0.02	0.05	0.07
HG4215	0.02	0.05	0.07
HG4339b	0.06	0.15	0.24
HG4383	0.06	0.15	0.24
HG4504	0.06	0.15	0.24
HG4540	0.06	0.15	0.24
HG4576	0.06	0.15	0.24
HG4744	0.03	0.06	0.10

Table A - 10: Pressure loss at the leaks HG3164

HG3164	0.25 l/s leak	0.5 l/s leak	0.7 l/s leak	1.0 l/s leak
	pressure loss [m]			
Node ID				
HG3164	0.04	0.08	0.12	0.19
HG3420	0.03	0.07	0.10	0.16
HG3445	0.03	0.07	0.10	0.16
HG3835	0.03	0.07	0.10	0.15
HG3933	0.03	0.06	0.09	0.14
HG4150	0.03	0.07	0.10	0.16
HG4162	0.03	0.07	0.10	0.16
HG4215	0.03	0.07	0.10	0.16
HG4339b	0.03	0.06	0.09	0.14
HG4383	0.03	0.06	0.09	0.14
HG4540	0.03	0.06	0.09	0.13
HG4576	0.03	0.06	0.09	0.13
HG4744	0.02	0.05	0.07	0.11

A.3.2   0.5 l/s leak at HG3880

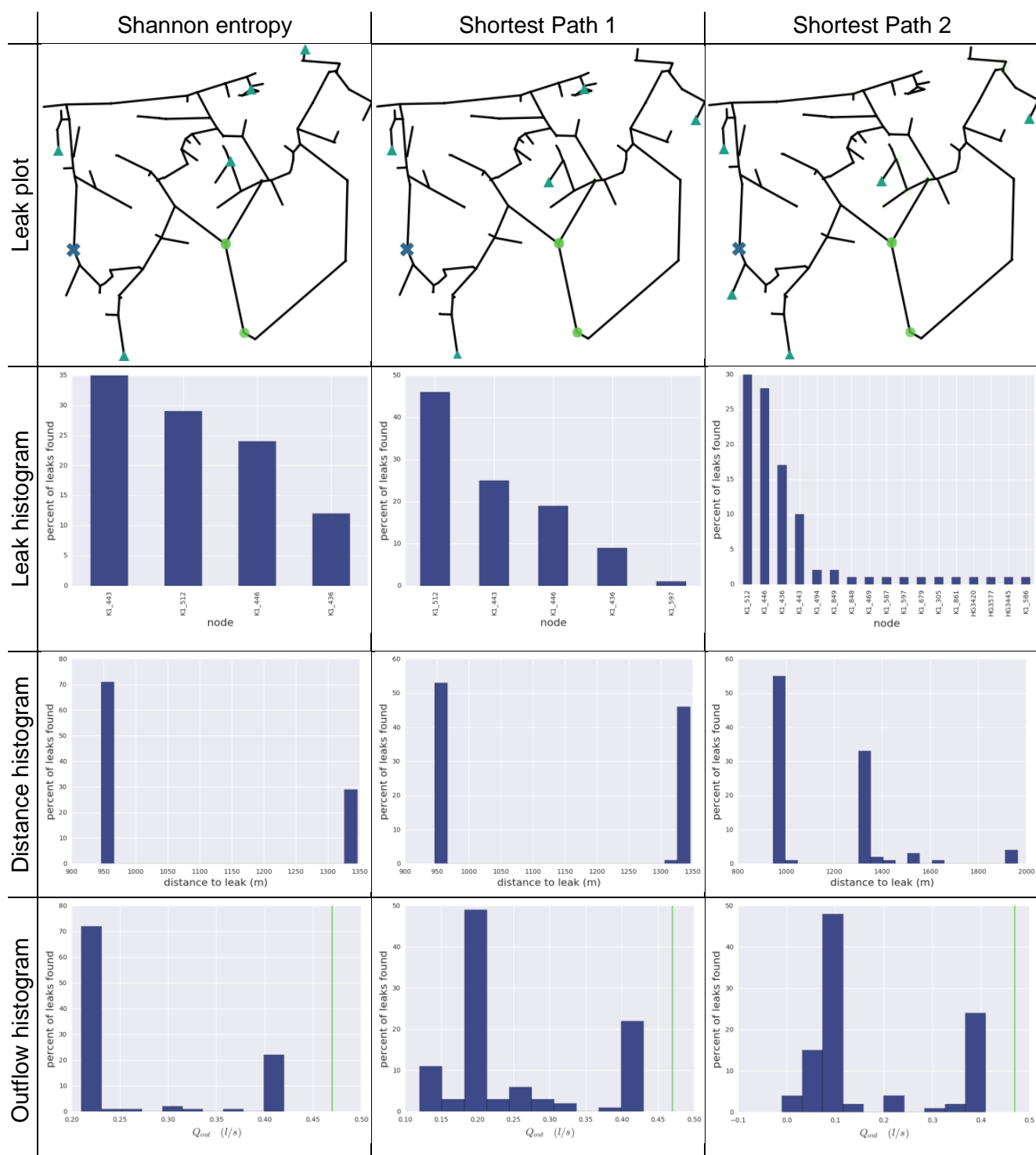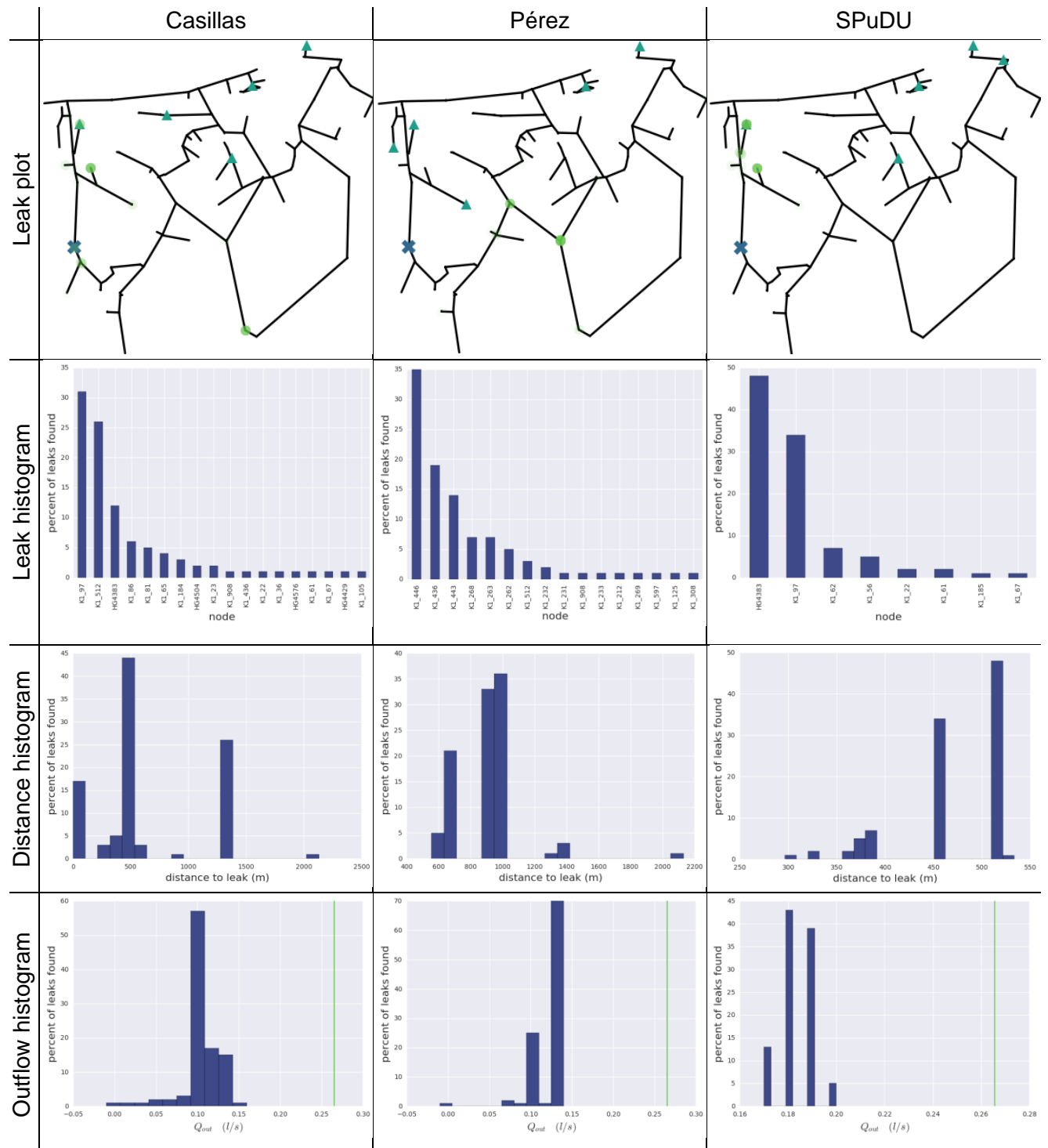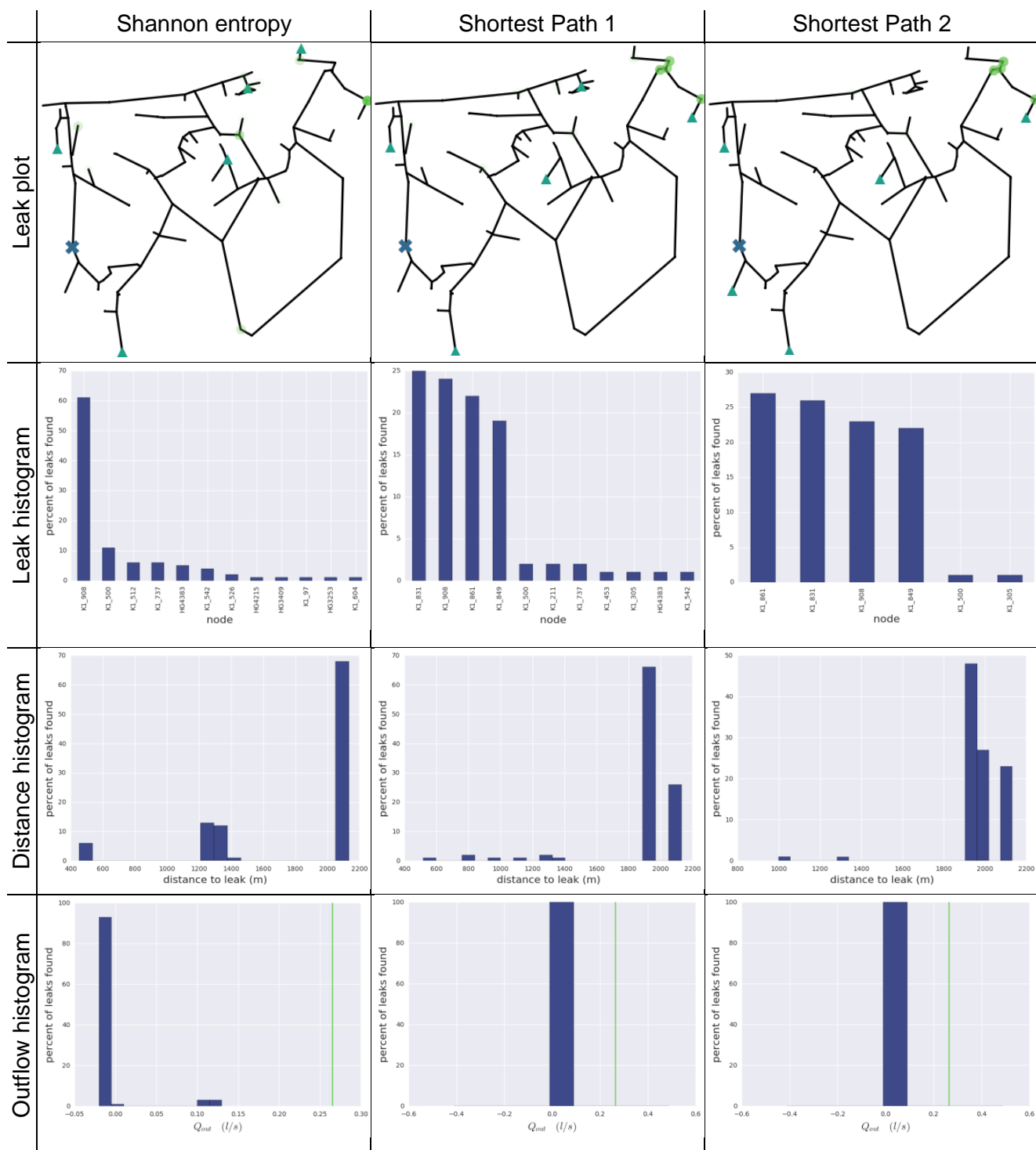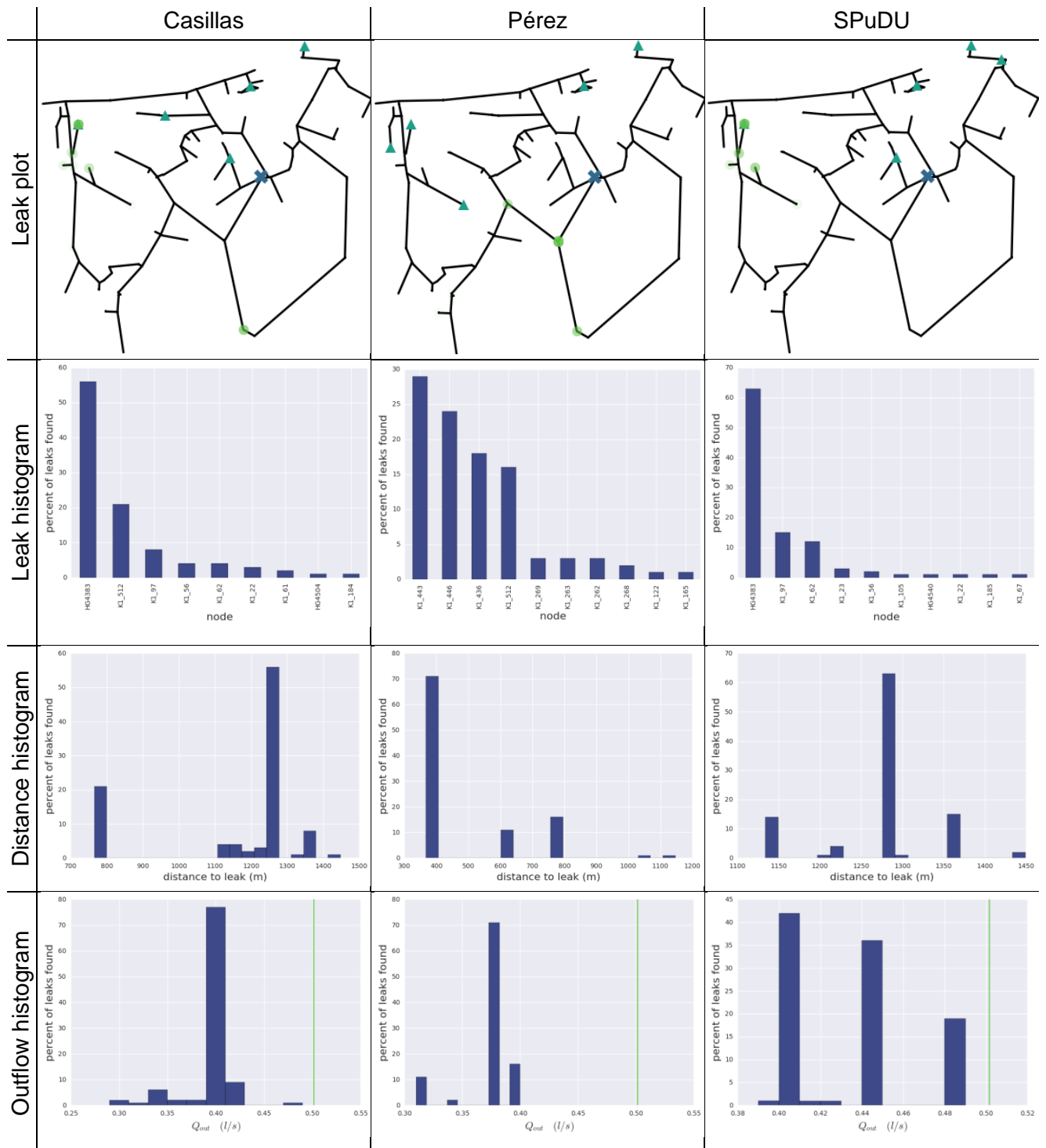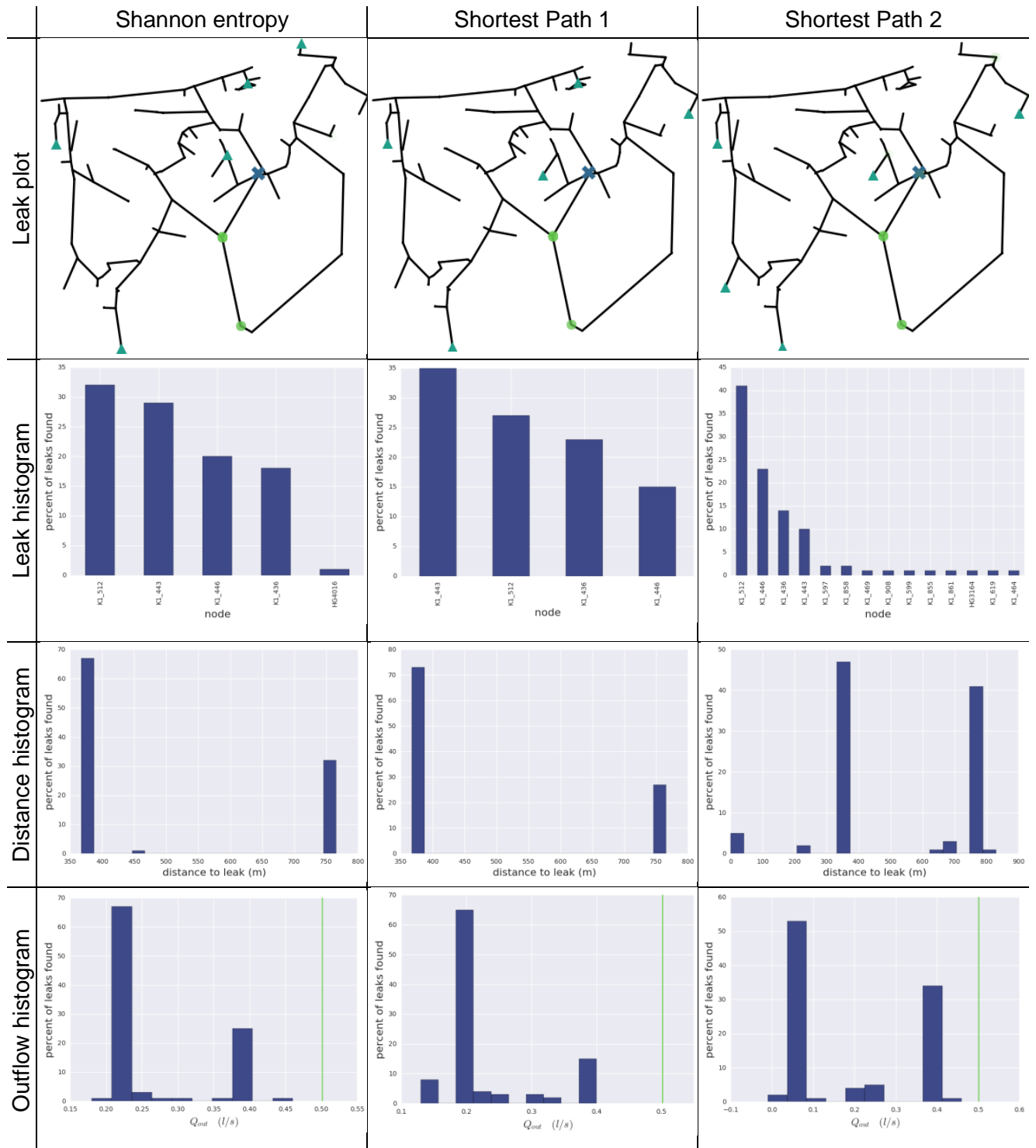**Figure A - 1: Results from the sensor placements Casillas, Pérez and SPuDU (Calibrated model, 0.5 l/s leak at HG3880)**
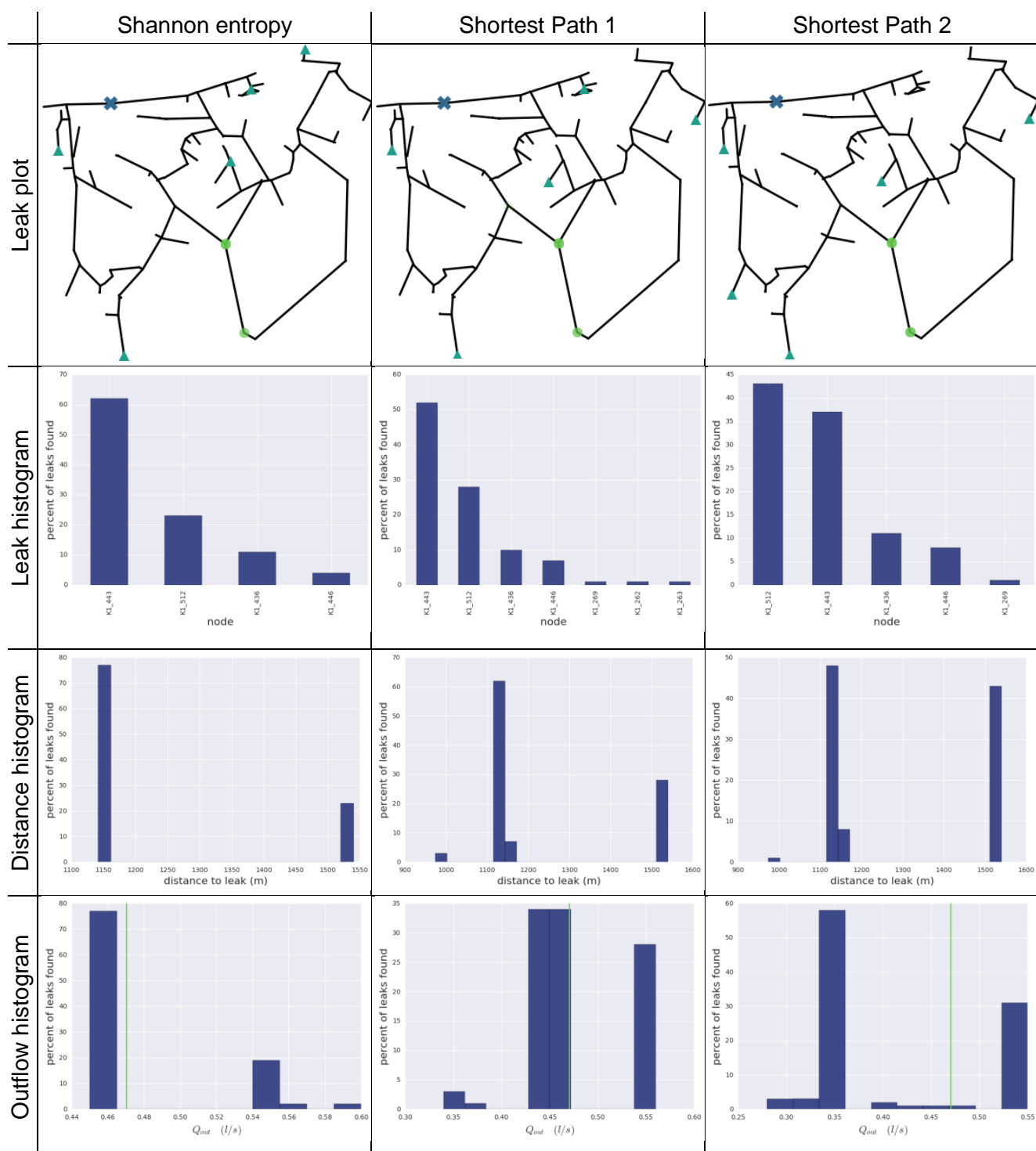
Figure A - 2: Results from the sensor placements Shannon entropy, Shortest Path 1 and Shortest Path 2 (Calibrated model, 0.5 l/s leak at HG3880)
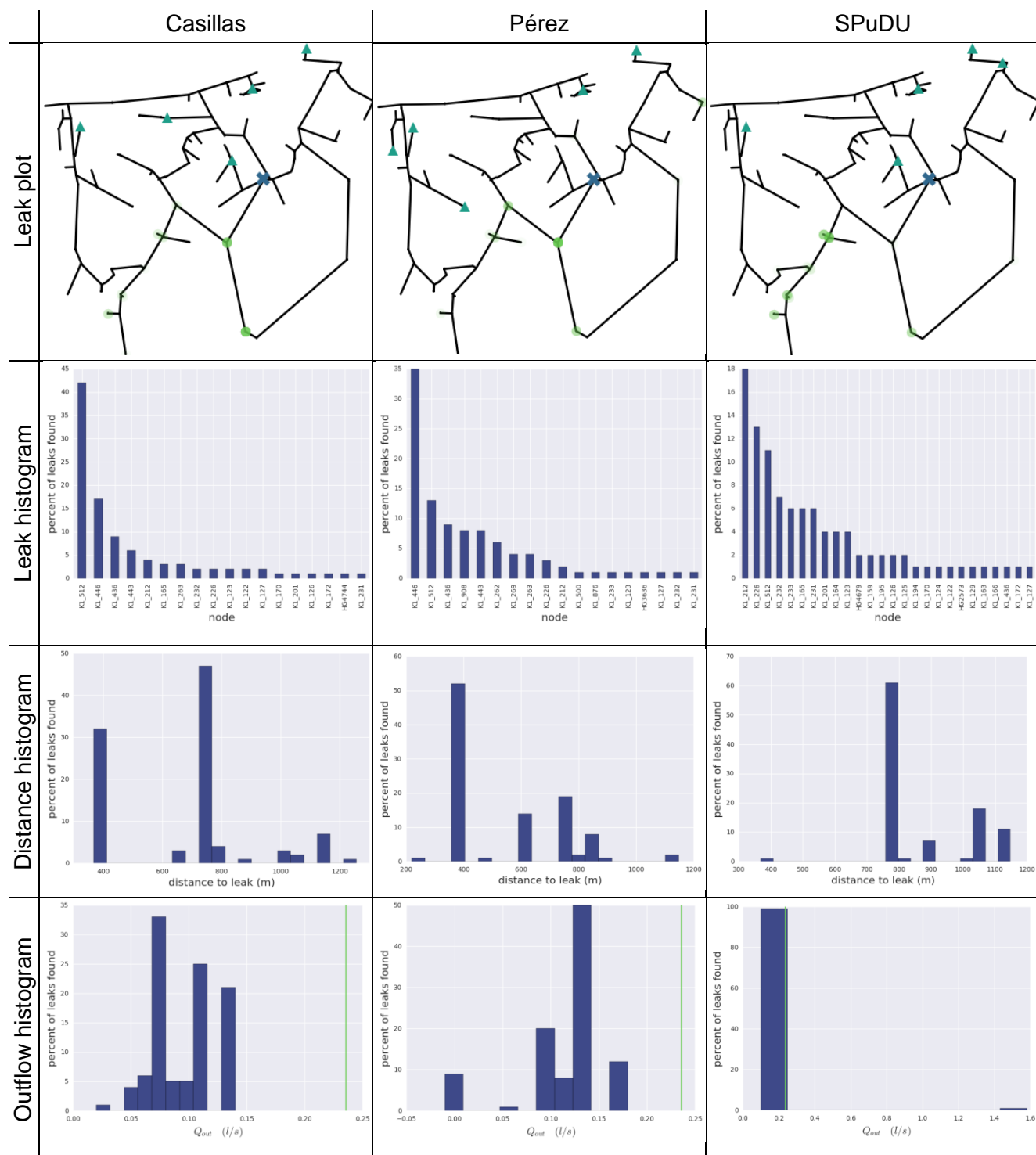
A.3.3 **0.25 l/s leak at HG3880**
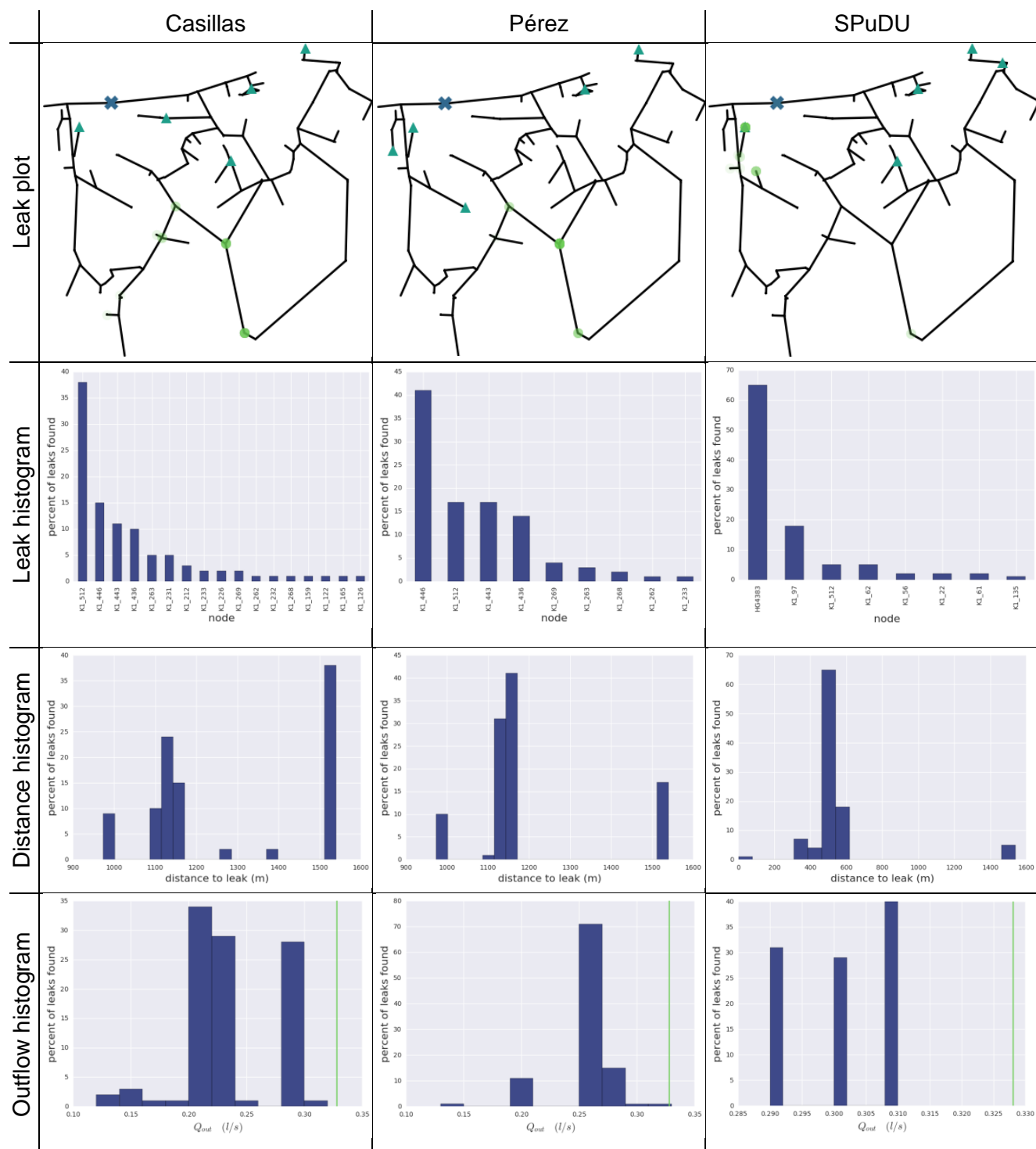
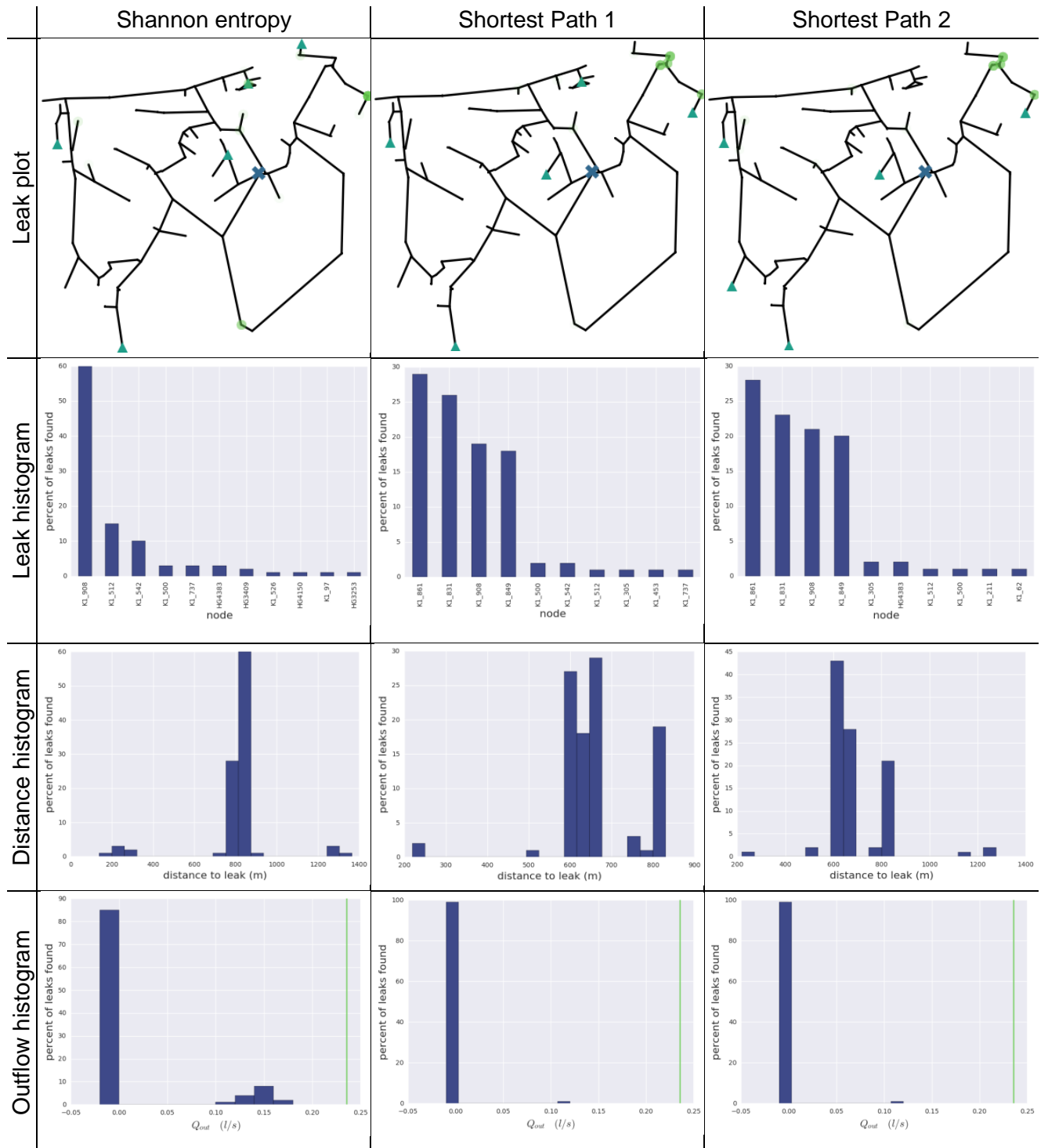**Figure A - 3: Results from the sensor placements Casillas, Pérez and SPuDU (Calibrated model, 0.25 l/s leak at HG3880)**
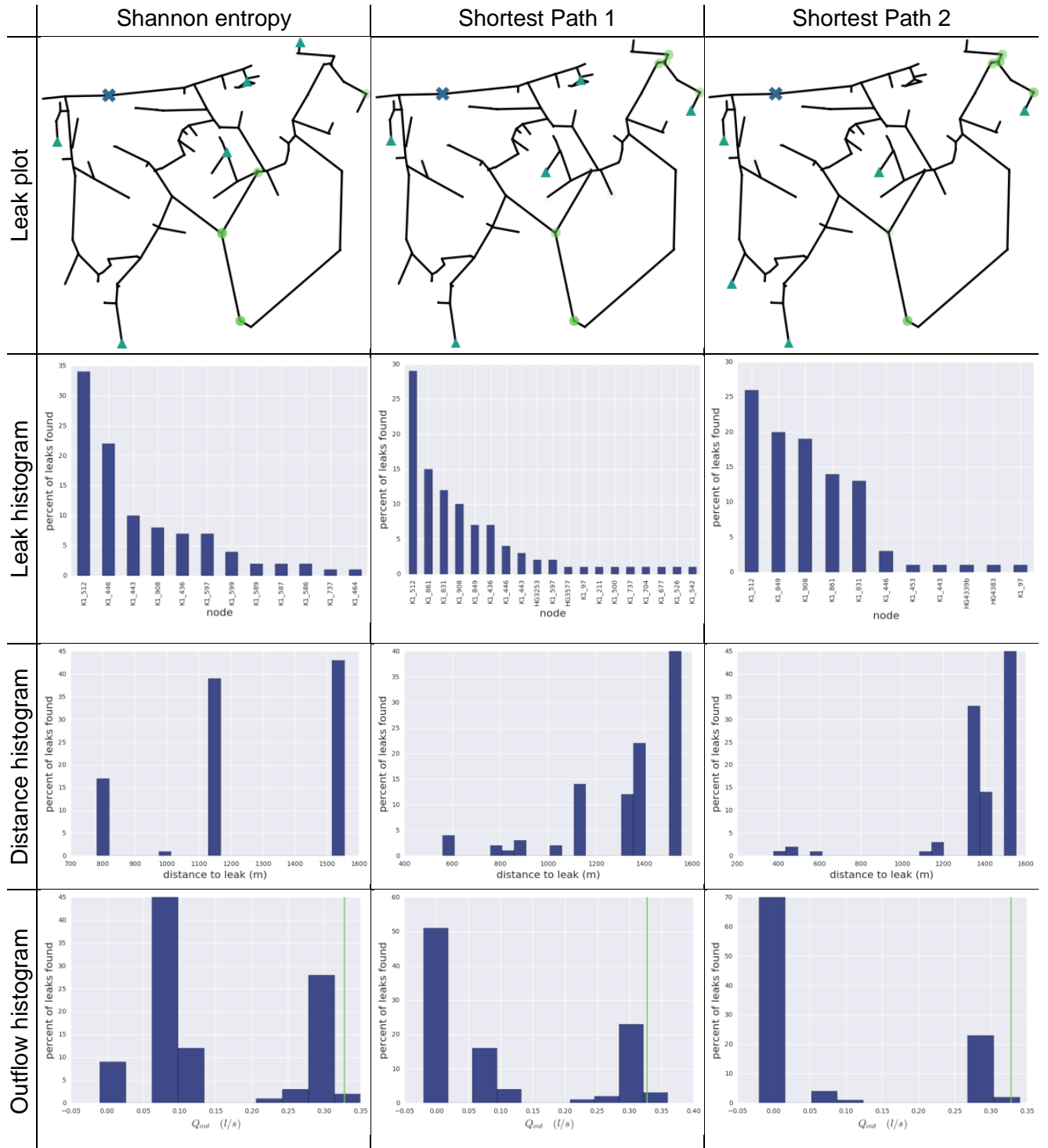
Figure A - 4: Results from the sensor placements Shannon entropy, Shortest Path 1 and Shortest Path 2 (Calibrated model, 0.25 l/s leak at HG3880)

A.3.4   **0.5 l/s leak at HG4504**
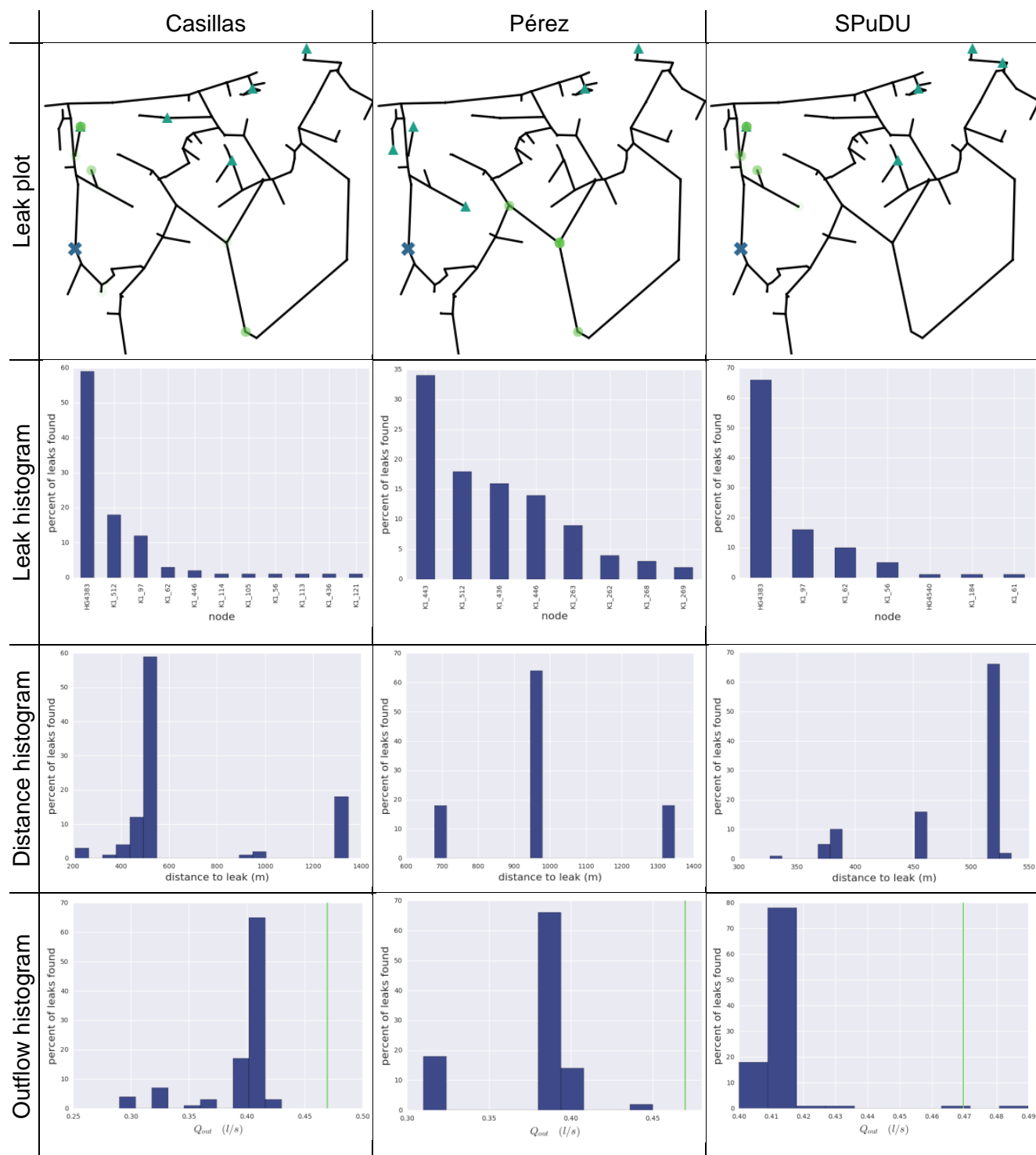
Figure A - 5: Results from the sensor placements Casillas, Pérez and SPuDU (Calibrated model, 0.5 l/s leak at HG4504)

Figure A - 6: Results from the sensor placements Shannon entropy, Shortest Path 1 and Shortest Path 2 (Calibrated model, 0.5 l/s leak at HG4504)
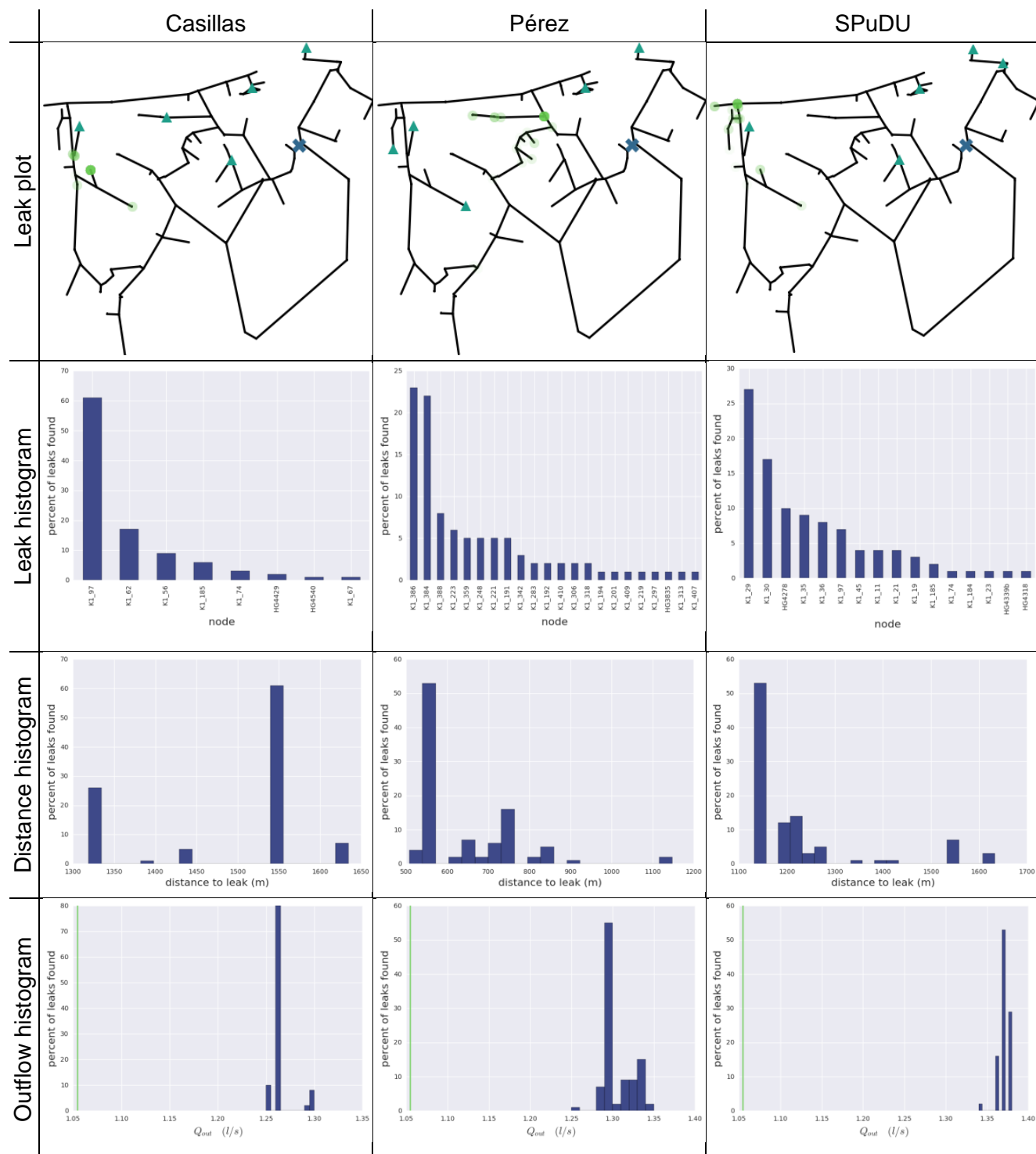
A.3.5　　**0.25 l/s leak at HG4504**

Figure A - 7: Results from the sensor placements Casillas, Pérez and SPuDU (Calibrated model, 0.25 l/s leak at HG4504)
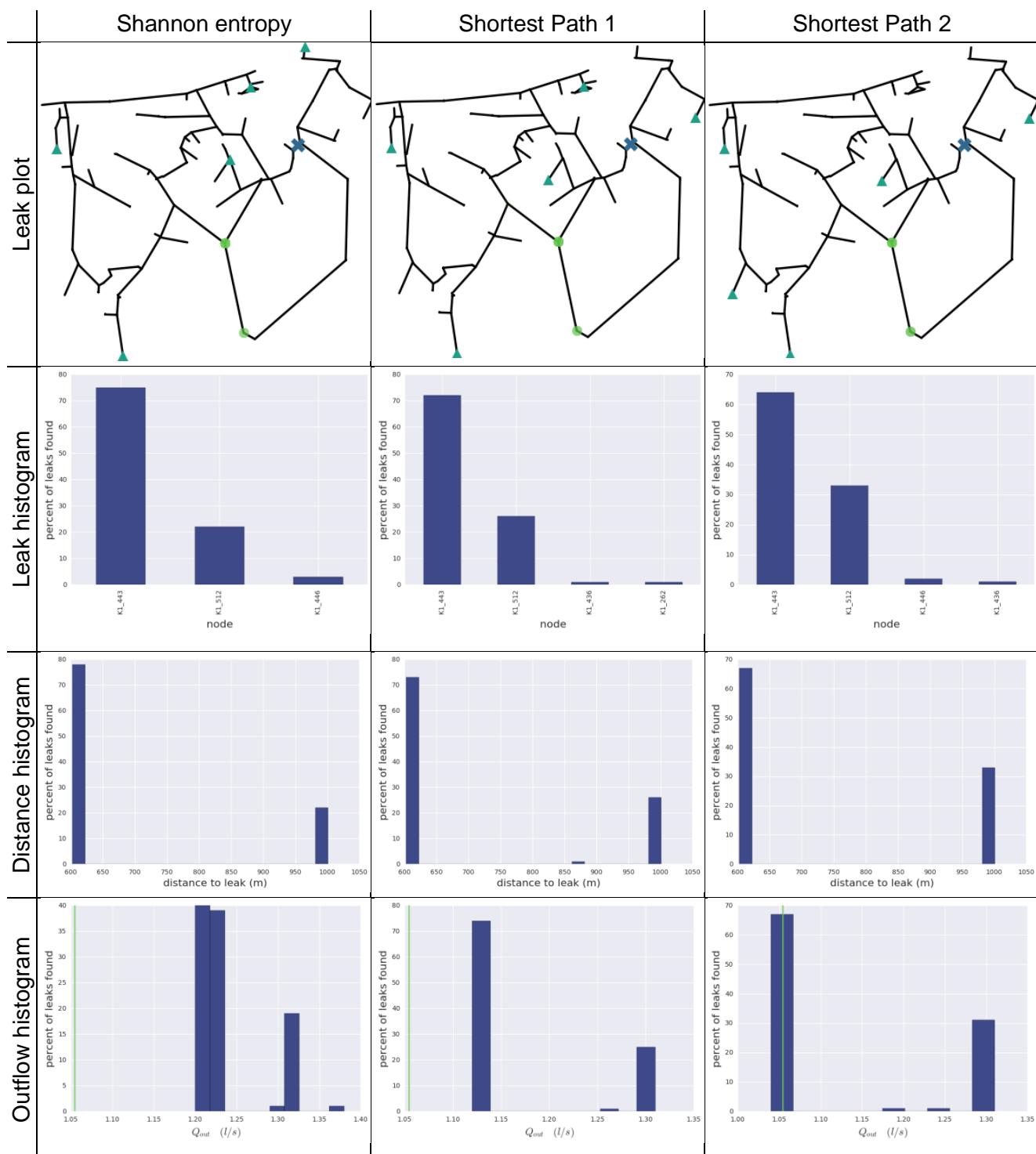
Figure A - 8: Results from the sensor placements Shannon entropy, Shortest Path 1 and Shortest Path 2 (Calibrated model, 0.25 l/s leak at HG4504)

A.3.6 **0.5 l/s leak at HG3164**

Figure A - 9: Results from the sensor placements Casillas, Pérez and SPuDU (Calibrated model, 0.5 l/s leak at HG3164)

Figure A - 10: Results from the sensor placements Shannon entropy, Shortest Path 1 and Shortest Path 2 (Calibrated model, 0.5 l/s leak at HG3164)
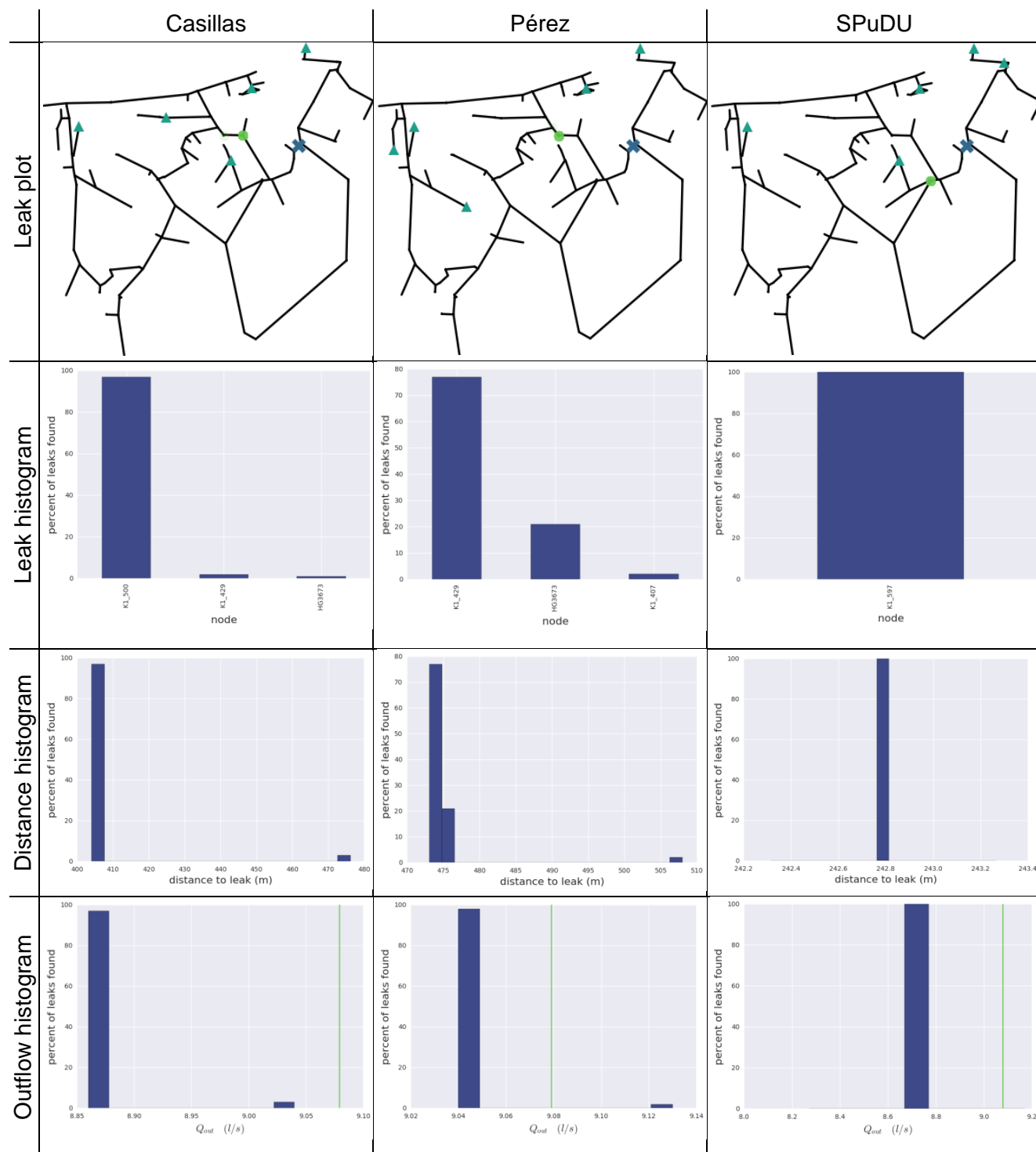
A.3.7 **0.25 l/s leak at HG3164**

Figure A - 11: Results from the sensor placements Casillas, Pérez and SPuDU (Calibrated model, 0.25 l/s leak at HG3164)

Figure A - 12: Results from the sensor placements Shannon entropy, Shortest Path 1 and Shortest Path 2 (Calibrated model, 0.25 l/s leak at HG3164)

A.3.8 **Night measurements**

A.3.8.1 **1.0 l/s leak at HG3302**

Figure A - 13: Results from the sensor placements Casillas, Pérez and SPuDU (Calibrated model, 1.0 l/s leak at HG3302)
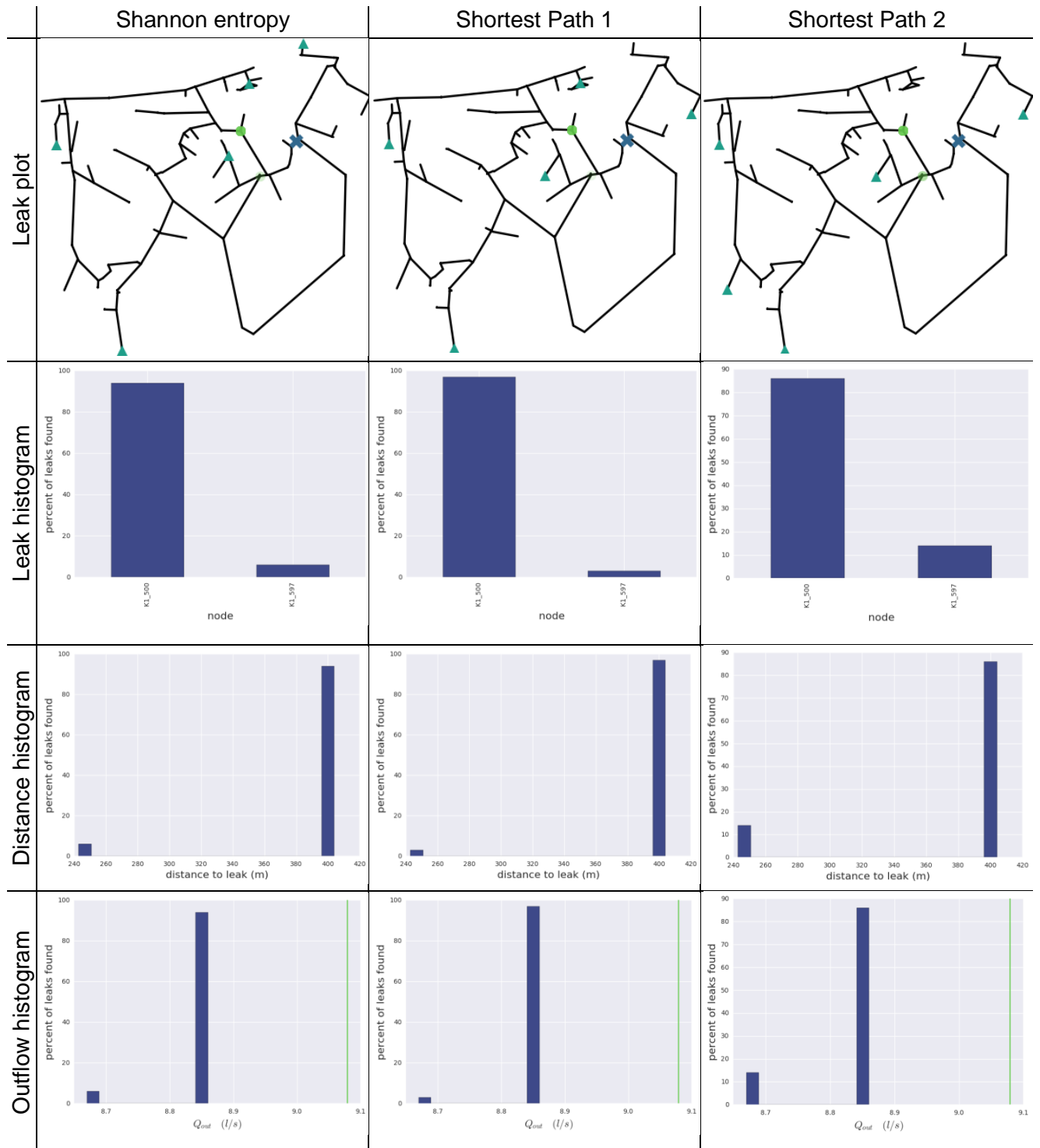
Figure A - 14: Results from the sensor placements Shannon entropy, Shortest Path 1 and Shortest Path 2 (Calibrated model, 1.0 l/s leak at HG3302)

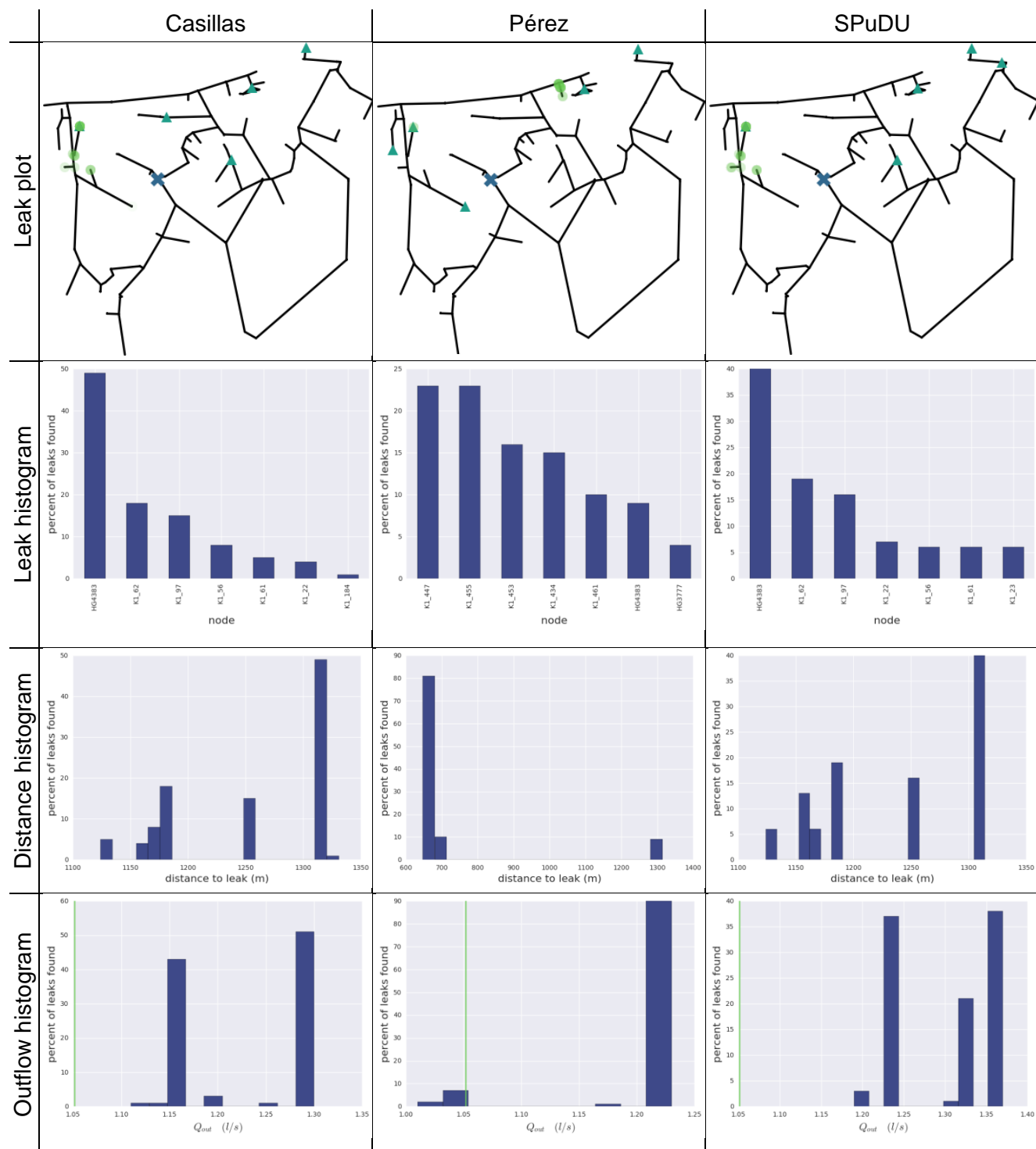A.3.8.2   **9.0 l/s leak at HG3302**

Figure A - 15: Results from the sensor placements Casillas, Pérez and SPuDU (Calibrated model, 9.0 l/s leak at HG3302)

Figure A - 16: Results from the sensor placements Shannon entropy, Shortest Path 1 and Shortest Path 2 (Calibrated model, 9.0 l/s leak at HG3302)

A.3.8.3 **1.0 l/s leak at HG3537**

Figure A - 17: Results from the sensor placements Casillas, Pérez and SPuDU (Calibrated model, 1.0 l/s leak at HG3537)
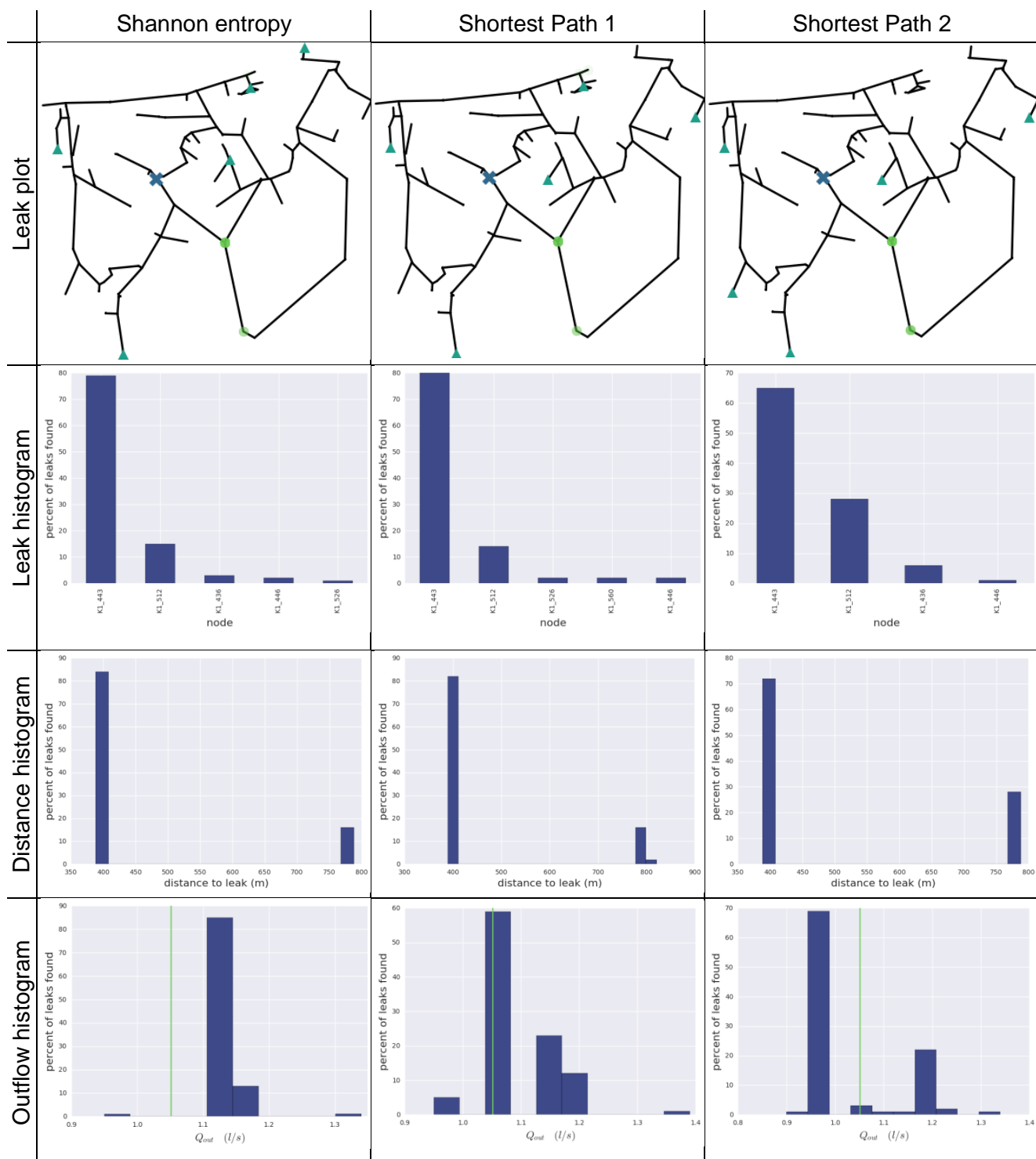
Figure A - 18: Results from the sensor placements Shannon entropy, Shortest Path 1 and Shortest Path 2 (Calibrated model, 1.0 l/s leak at HG3537)

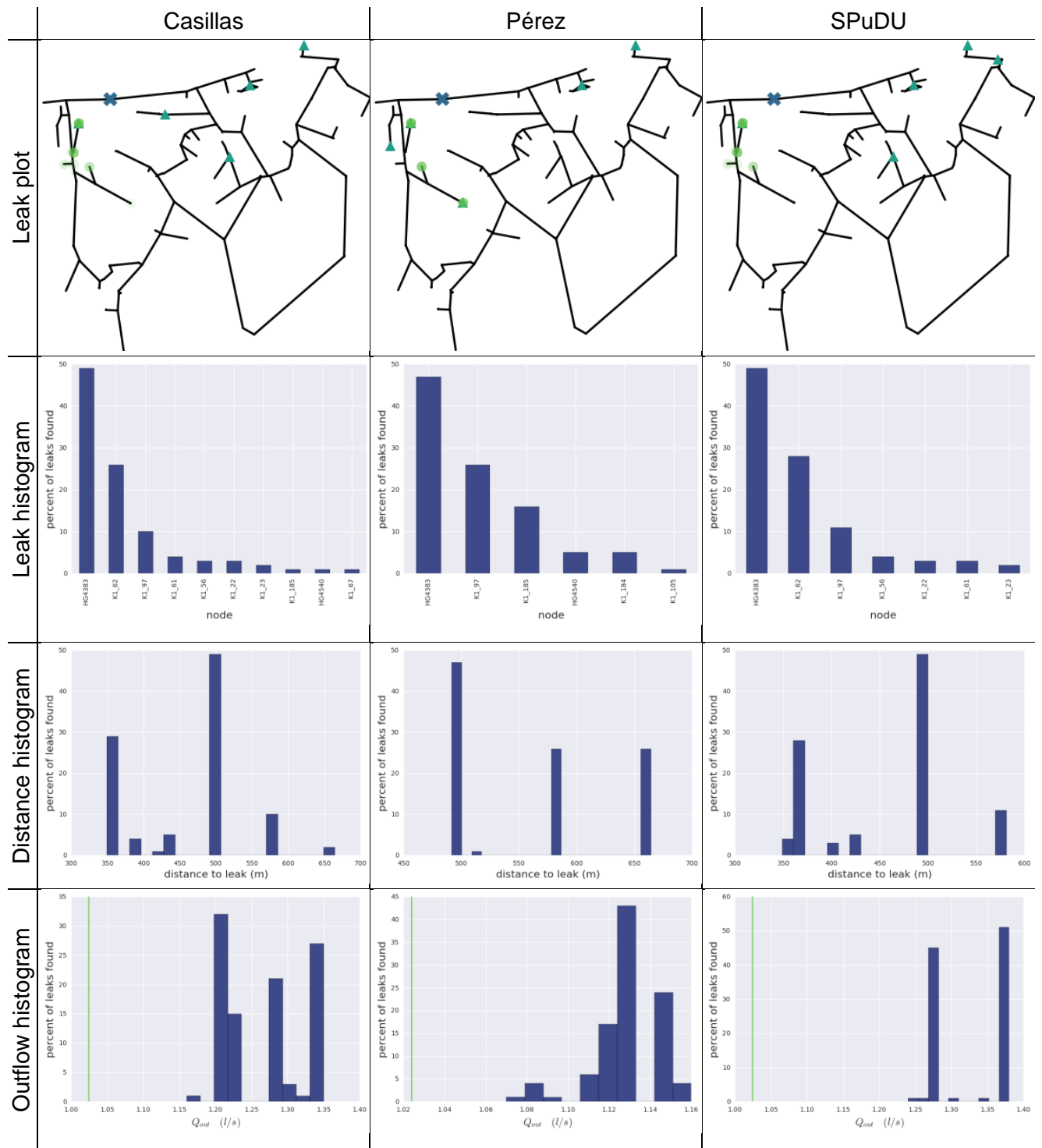### A.3.8.4 **1.0 l/s leak at HG3880**

Figure A - 19: Results from the sensor placements Casillas, Pérez and SPuDU (Calibrated model, 1.0 l/s leak at HG3880)
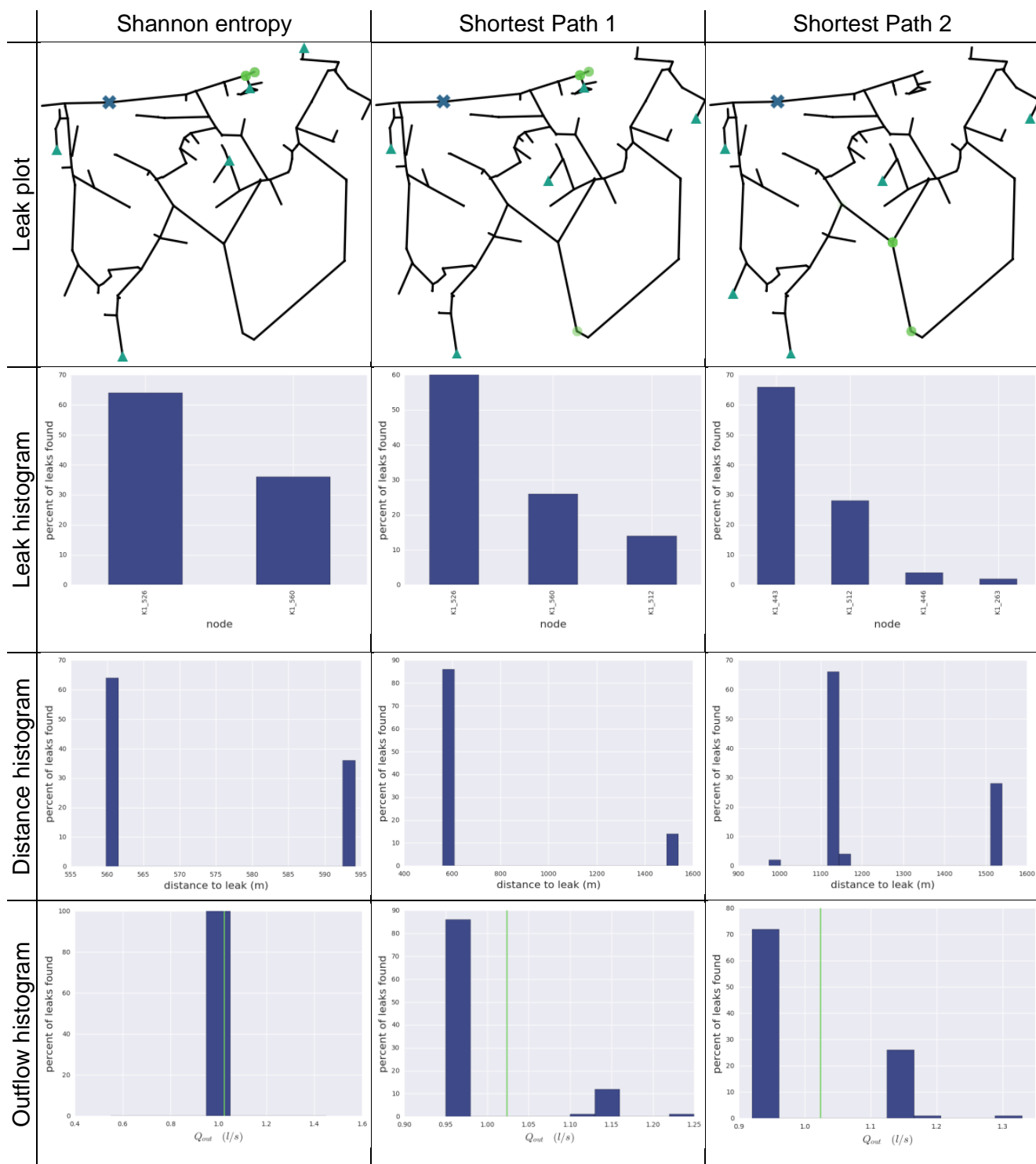
Figure A - 20: Results from the sensor placements Shannon entropy, Shortest Path 1 and Shortest Path 2 (Calibrated model, 1.0 l/s leak at HG3880)

A.4 Results from the recalibrated model

Table A - 11: Recalibrated model - HG3302, HG3537 and HG3880

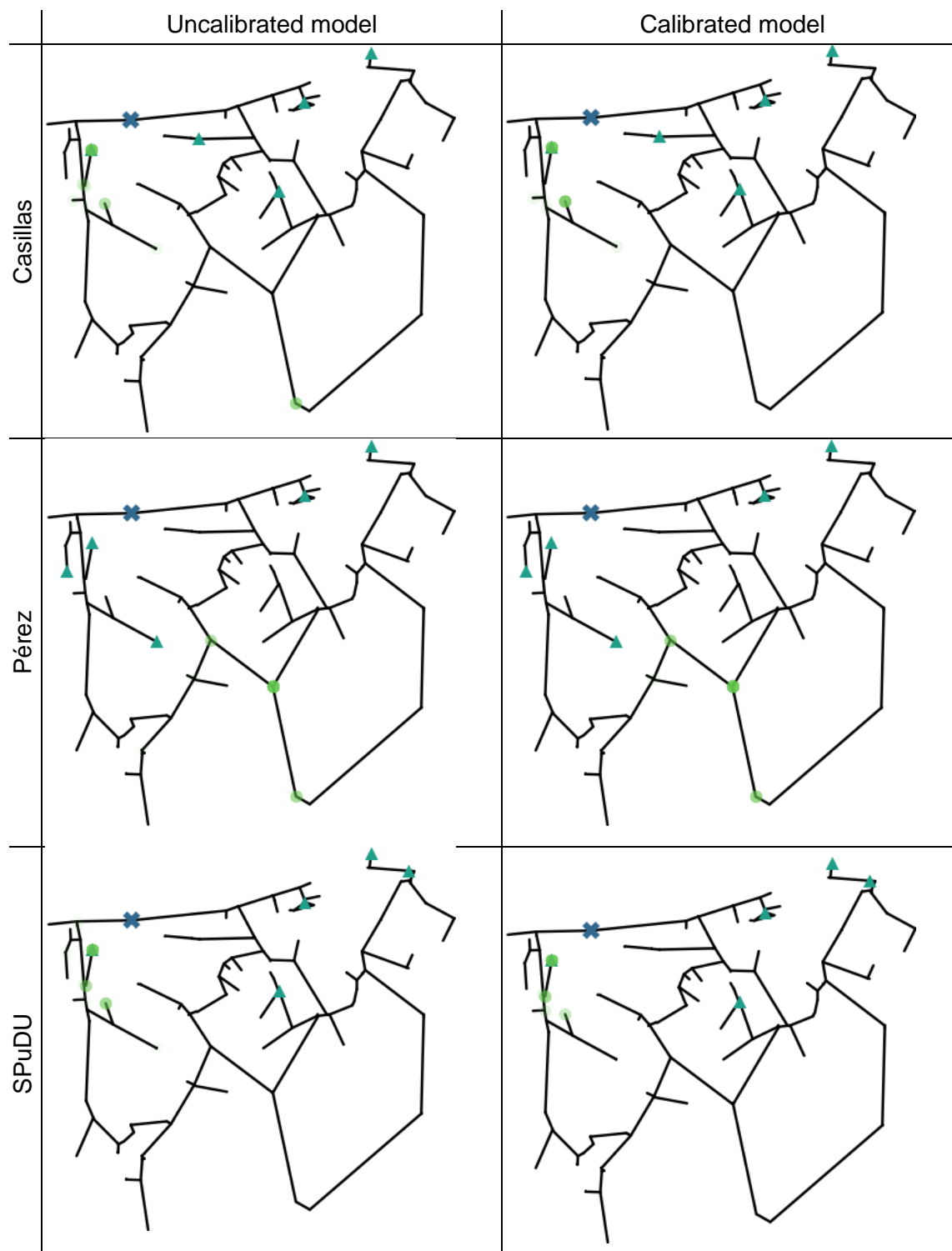|	Number of nodes found	Most frequently detected leakage		Closest leakage		Leakage furthest away	
		[%]	[m]	[%]	[m]	[%]	[m]
HG3302 1.0 l/s	4	50	554.95	1	553.33	48	1001.13
HG3537 1.0 l/s	3	50	1314.67	48	787.85	2	1313.70
HG3880 1.0 l/s	6	49	1540.10	1	1359.96	49	1540.10

A.5 Comparison between uncalibrated and calibrated model

Figure A - 21: Comparison of leak plots of uncalibrated, calibrated and recalibrated model (0.7 l/s leak at HG3880)